Development of Short-Range Laminar Aircraft

Conceptual Design with Integrated System Sizing

Petr Martínek

TU Delft

DLR Deutsches Zentrum für Luft- und Raumfahrt
German Aerospace Center

Development of Short-Range Laminar Aircraft

Conceptual Design with Integrated System Sizing

by

Petr Martínek

to obtain the degree of

Master of Science
in Aerospace Engineering

at the Delft University of Technology,
to be defended publicly on Thursday January 30, 2025 at 10:00 AM.

Thesis committee:	Dr.ir. M. Hoogreef	TU Delft	Supervisor
	Dr.ir. G. la Rocca	TU Delft	Chair
	L.T. Lima Pereira	TU Delft	Examiner
	B. Fröhler	DLR	Supervisor

Cover: Airbus A340 Laminar Flow BLADE Demonstrator. Available at `https://www.airbus.com`, Accessed on 23.01.2025, Modified

TU Delft

DLR Deutsches Zentrum für Luft- und Raumfahrt
German Aerospace Center

Acknowledgements

This master thesis represents the final step in the most challenging and the most exciting chapter of my life so far, which has been studying Aerospace Engineering at Delft University of Technology. Looking back at all the milestones and obstacles I encountered along the way, it is hard to believe how far I have come and how much I have learned. However, one thing is absolutely clear. I would never have been able to fulfill my dream of becoming an aerospace engineer without the incredible people who supported me, made this dream possible, and to whom I will forever remain grateful.

I would first like to thank my colleagues at DLR, especially in the Overall Aircraft Design Group, for warmly welcoming me into their amazing collective, for their help, and for sharing their experience and insights, which have expanded my knowledge of aircraft design to a whole new level.

I am especially grateful to my supervisor, Benjamin Fröhler, not only for giving me the opportunity to join DLR in the first place but, most importantly, for being the best mentor I could have wished for. His help, ideas, and feedback have not only significantly improved the quality of my work but also helped me grow as an engineer.

I would also like to thank my TU Delft supervisor, Maurice Hoogreef, for his guidance and support throughout the seven months I spent working on this thesis.

A special thanks also goes to my friend and colleague from TU Delft, Ángel Garmilla Manzano, with whom I had the pleasure of sharing this journey at DLR from the very beginning. He was my closest companion throughout the entire journey and always lifted my spirits whenever times were tough.

I will never be able to fully express my gratitude to the Redeker family for their unbelievable hospitality during my year with them as an exchange student in the United States, and especially to Stacey. It was her determination and energy that made it possible for me to even begin this journey.

Ich werde auch immer meiner lieben Tante Sylva und meinem lieben Onkel Péťa dankbar sein, die mir mein Studium ermöglicht und mich während meines Studiums immer unterstützt haben.

Nakonec bych rád poděkoval mé nejbližší rodině za její podporu, lásku a trpělivost. Vím, že to se mnou bylo často k nevydržení, ale to, co mi dodávalo sílu, výdrž a odhodlání i v těch nejtěžších časech, bylo vědomí, že jsem se vždy mohl vracet domů k rodině, která mě bezpodmínečně podporovala ve všem, co jsem dělal, a nikdy nepochybovala o tom, že nakonec zvládnu všechno, co jsem si předsevzal. Bez její opory bych nikdy nebyl schopen ustát tlak, který tato výzva obnášela.

Tuto práci bych rád věnoval své babičce Vendule, která mi předala základy zvídavosti, lásky k vědomostem, kritického myšlení a schopnosti učit se, což byl vklad, který mě provázel po celé mé cestě k tomu, stát se inženýrem.

The support of all those who have believed in me throughout the years now motivates me to keep pushing myself and to further build on this incredible privilege they have given me. I promise to make the most of it.

Thank you so much, vielen Dank a děkuju.

Petr Martínek
Delft, January 2025

Abstract

The aviation industry is currently facing significant pressure to enhance its sustainability by increasing aircraft energy efficiency and reducing its climate impact. A promising approach to fulfilling these demands is to improve the aircraft's aerodynamic performance through drag reduction by implementing laminar flow technologies, particularly Natural Laminar Flow (NLF) or Hybrid Laminar Flow Control (HLFC). Prior works assessing laminar flow technologies have mostly focused on evaluating their aerodynamic performance and, in the case of the HLFC, on the influence of system design. The impact of these technologies on the overall aircraft performance has received only limited consideration, with the majority of studies focusing on long-range aircraft, utilizing simplified models for HLFC systems, and considering only one laminar flow technology at a time. This study adopts a holistic approach to assess the potential fuel savings that could be achieved by combined application of NLF and HLFC technologies on the various components of a short-to-medium range aircraft concept, with an intended entry into service in 2035. To achieve this objective, a conceptual aircraft design process is employed. This process captures the aerodynamic effects of laminar flow technologies and fully integrates the HLFC system design to provide an accurate estimate of aircraft performance. The findings of this study reveal a potential for fuel savings of 5.9% on the design mission through the combined application of NLF and HLFC, compared to a turbulent aircraft with an equivalent technology level. Additionally, the results indicate that strategic combination of the two technologies on a single component can significantly reduce complexity while further enhancing fuel savings. A failure analysis also provides an initial estimate of the impact of various failure scenarios on the aircraft's performance. These findings demonstrate that, despite the aircraft's short range, the combined implementation of the two laminar flow technologies offers a potential for fuel savings with reduced complexity, motivating further research in their application to this aircraft category.

Keywords: Hybrid Laminar Flow Control, Natural Laminar Flow, Conceptual Aircraft Design

Contents

Part I

Scientific Paper

Development of Short-Range Laminar Aircraft: Conceptual Design with Integrated System Sizing

Petr Martínek
Delft University of Technology, Delft, Netherlands

The aviation industry is currently facing significant pressure to enhance its sustainability by increasing aircraft energy efficiency and reducing its climate impact. A promising approach to fulfilling these demands is to improve the aircraft's aerodynamic performance through drag reduction by implementing laminar flow technologies, particularly Natural Laminar Flow (NLF) or Hybrid Laminar Flow Control (HLFC). Prior works assessing laminar flow technologies have mostly focused on evaluating their aerodynamic performance and, in the case of the HLFC, on the influence of system design. The impact of these technologies on the overall aircraft performance has received only limited consideration, with the majority of studies focusing on long-range aircraft, utilizing simplified models for HLFC systems, and considering only one laminar flow technology at a time. This study adopts a holistic approach to assess the potential fuel savings that could be achieved by combined application of NLF and HLFC technologies on the various components of a short-to-medium range aircraft concept, with an intended entry into service in 2035. To achieve this objective, a conceptual aircraft design process is employed. This process captures the aerodynamic effects of laminar flow technologies and fully integrates the HLFC system design to provide an accurate estimate of aircraft performance. The findings of this study reveal a potential for fuel savings of 5.9% on the design mission through the combined application of NLF and HLFC, compared to a turbulent aircraft with an equivalent technology level. Additionally, the results indicate that strategic combination of the two technologies on a single component can significantly reduce complexity while further enhancing fuel savings. A failure analysis also provides an initial estimate of the impact of various failure scenarios on the aircraft's performance. These findings demonstrate that, despite the aircraft's short range, the combined implementation of the two laminar flow technologies offers a potential for fuel savings with reduced complexity, motivating further research in their application to this aircraft category.

Keywords: Hybrid Laminar Flow Control, Natural Laminar Flow, Conceptual Aircraft Design

Nomenclature

Acronyms

BF	Block Fuel
DM	Design Mission
EM	Evaluation Mission
$HLFC$	Hybrid Laminar Flow Control
HTP	Horizontal Tailplane
NLF	Natural Laminar Flow
$TLAR$	Top-Level Aircraft Requirement
VTP	Vertical Tailplane

Latin Symbols

C_f	Skin friction coefficient [-]
$\dot{m}$	Mass flow [kg/s]
$nLam$	Extent of laminar flow [-]
P	Power [W]
PR	Pressure ratio [W]
R	Universal gas constant [J/(kg · K)]
Re	Reynolds number [-]
S	Surface area [m^2]
T	Temperature [K]
v	Velocity [m/s]
x_t	Distance to the leading-edge[m]
Y	Specific energy [J/kg]

Greek Symbols

γ	Heat capacity ratio [-]
μ	Dynamic viscosity [N · s/m^2]

Subscripts and Superscripts

t	Transition point

1 Introduction

The primary objective of today's aviation industry is undoubtedly the reduction of its global climate impact. This is driven by the ambitious goals set by governments around the world in order to address the ongoing climate crisis. In Europe, such plans have already manifested in the form of the Green Deal, which is complemented by the Flightpath 2050, a specific strategy for the aviation industry developed by the European Commission. These declarations set the goal of achieving climate neutrality by 2050 and exert an increasing pressure on the industry to reduce its climate impact by improving energy efficiency.

Nevertheless, the motivation to enhance fuel efficiency also arises from within the industry itself. A reduction in fuel consumption would not only result in decreased operational costs but would also improve the sector's economic sustainability and resilience by reducing its high sensitivity to fuel prices, which are projected to increase in the future.

The necessity for enhanced energy efficiency and reduced fuel consumption draws attention to innovative technologies that could be capable of delivering such benefits and that could be utilized in the upcoming generation of passenger aircraft. Two such priming technologies are natural laminar flow (NLF) and hybrid laminar flow control (HLFC), which belong to the category of laminar flow technologies.

A number of previous studies have evaluated the effect of NLF [1–6] and HLFC [7–11] on aircraft design and performance. These studies have employed a variety of methodologies, including retrofitting the technology to an existing aircraft and considering it in the conceptual aircraft design. Nevertheless, there are certain areas of interest with regard that still require further investigation.

First, although previous studies have demonstrated the potential benefits of each individual technology, there has been very limited investigation into the possibility of utilizing them simultaneously on a single aircraft or even a single component. By combining the NLF and HLFC, it may be possible to leverage their respective advantages and enhance the overall benefit on the aircraft level.

A second room for further investigation is a consequence of a common practice observed in the majority of previous works. The design process typically initiates with a set of top-level aircraft requirements (TLARs), which are based on an existing aircraft that the new developed concept is intended to replace in the corresponding market sector. However, as the design progresses, these TLARs are often varied in order to maximize the benefit obtained from the utilization of laminar technologies. To illustrate, the cruise Mach number is frequently reduced in order to permit the use of a wing with a lower sweep angle to postpone transition. However, in practice, key performance requirements are traditionally derived from market analysis, and their variation can pose challenges to meeting customer expectations. Therefore, a more conservative approach involves utilizing the TLARs applicable to aircraft operating in the considered market sector today. These TLARs should then be treated as fixed and not varied as part of the conceptual design process.

The next challenge in assessing the benefits of an HLFC system on a specific aircraft component is accurately estimating the mass and power consumption of the suction system. Although, sensitivity analyses were previously conducted ([12, 13]), in which the two values in question were the varied inputs provided to establish a range of potential benefits, such an approach is not applicable in the conceptual aircraft design process, which aims to produce a fully defined aircraft concept.

The most elaborate method for a preliminary estimation of the mass and power requirements of HLFC systems was introduced by Pe and Thielecke [14], which was subsequently used in modified forms in additional studies [15, 16]. These studies, however, approached the sizing of the HLFC system for a given component as a standalone problem, rather than integrating the methodology into a larger aircraft design process.

A unique study was conducted by Risse [17], who integrated the aforementioned methodology with aircraft sizing tools and high-fidelity aerodynamic simulations to create an integrated preliminary aircraft sizing process. This process was then used to assess the potential of the HLFC technology when applied to the wing and empennage of a long-range passenger aircraft.

Finally, many of the existing studies have examined laminar flow technologies primarily in the context of medium-to-long range aircraft [8, 13, 17–20]. However, more than half of total CO_2 emissions are currently produced by the short-to-medium range aircraft category, with the highest emissions observed in the short-range segment [21]. Demonstrating that the laminar flow technologies could achieve meaningful fuel savings when applied to this aircraft category would therefore represent a significant step toward achieving the discussed sustainability goals.

In light of these observations, this paper aims to contribute to the ongoing assessment of laminar technologies by conducting a conceptual design of a short-to-medium range aircraft equipped with both NLF and HLFC, with the sizing process accounting for the effects of both technologies. For HLFC, this will be achieved by employing an approach analogous to that introduced by Risse [17]. Specifically, the HLFC system design and evaluation will be integrated into the preliminary aircraft sizing process using the methodology proposed by Pe and Thielecke [14]. Additionally, the

aircraft will be designed for a short-to-medium range with a fixed set of TLARs, based on an existing aircraft currently operating in this market sector. The design process will also leverage the advantages of NLF and HLFC by considering their combined application at both the aircraft and component levels. The components considered for the application of these technologies will include the wing, vertical tailplane (VTP), and horizontal tailplane (HTP).
Based on these goals, the ultimate objective of this paper is to answer to the following research question:

What fuel savings can be expected from the application of laminar flow technologies to a short-to-medium range aircraft with a fixed set of top-level requirements, when considering a realistic laminar flow system design in the aircraft sizing process?

The discussion in this paper is structured as follows: after the introduction, the methodology used is presented in Chapter 2, including the description of the utilized tools and their fundamental working principles. Chapter 3 provides a detailed discussion of the aircraft configurations, including descriptions of the reference and baseline aircraft and insights into the integrated HLFC subsystem configuration. Chapter 4 then presents and discusses the obtained results. Finally, a conclusion summarizing the key design decisions and outlining possible directions for further research is provided in Chapter 5.

2 Methodology

This chapter provides a description of the methods and software utilized in this study and their integration into a larger conceptual aircraft sizing process. Furthermore, more detailed information is provided regarding the calculations performed by the software for sizing and analysis of HLFC systems. Finally, the modelling of the laminar regions for both HLFC and NLF is explained.

2.1 Software integration environment

The aircraft concepts presented in this paper were developed using an integrated collection of aircraft design and analysis tools, all of which were developed internally by the DLR. This collection of tools, further referred to as the "workflow," was created and hosted in a software integration platform, RCE [22], also developed by DLR.
RCE (Remote Component Environment) is an open-source software that enables the integration of discrete calculation tools into larger workflows. The transfer of data between the various tools and workflows is facilitated by the CPACS data format.
CPACS (Common Parametric Aircraft Configuration Schema) [23] is an XML-based, standardized data format designed to provide a consistent and continuous exchange of aircraft data and requirements. These include detailed definitions of the geometry of individual aircraft components, aerodynamic polars, and engine performance data.
Each tool integrated into a RCE workflow reads the required inputs from an input XML file, in which the data is stored in the CPACS format. After completing the calculations, the tool writes the results into an output XML file, again utilizing the CPACS format. The consistent employment of the CPACS format by all tools permits the linking and chaining of individual tools to form complex workflows, thereby facilitating iterative design processes, sensitivity studies, and other complex aircraft design and analysis tasks.
A flowchart that represents the workflow utilized in this study is provided in Figure 1. This flowchart shows the main tools used and their integration into a conceptual aircraft sizing process.

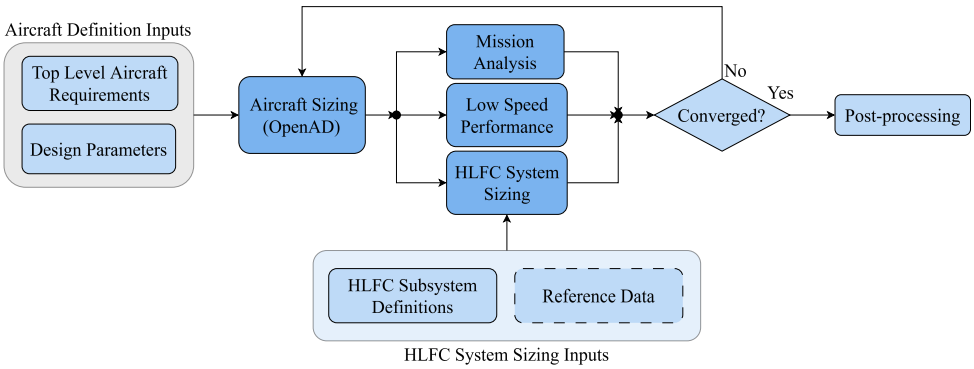

Fig. 1 Flowchart of the conceptual aircraft design process integrated in the RCE workflow

As illustrated in Figure 1, the workflow incorporated four major software tools. The sizing process began with providing an input XML file to the aircraft sizing tool, containing the essential TLARs, along with geometry definitions, performance requirements, and calibration factors stored in the CPACS format. Following the overall aircraft sizing performed by a low-fidelity tool, the results were transferred to three higher-fidelity design and analysis tools, namely two aircraft performance analysis tools and a HLFC system sizing tool, which all operated in parallel. The results of their calculations were then merged and fed back as input for the aircraft sizing tool in the subsequent iteration, thereby completing the design process. This process was repeated until all convergence criteria were met, at which point the results were transferred to the post-processing. The convergence criteria was set to 20kg and 0.1% of absolute and relative convergence error respectively, for both maximum take-off mass (MTOM) and operational empty mass (OEM), compared to the previous two iterations.
The following chapters provide an overview of the function and general working principle of each of the tools utilized in the workflow.

2.2 Overall aircraft design

The central component of the workflow was the semi-empirical conceptual aircraft sizing tool OpenAD [24], which integrates a multitude of conventional aircraft sizing methods into a robust, iterative sizing process. This low-fidelity tool utilizes mostly calculations described in the standard aircraft design literature such as Torenbeek [25], Raymer [26], Anderson [27] or Roskam [28]. OpenAD has been validated for a wide range of aircraft sizes and offers an extensive capability to design aircraft concepts utilizing various configurations and layouts as well as different types of propulsion architectures, including turboprop and turbofan engines. [24]
In the presented workflow, OpenAD performed the preliminary aircraft sizing and outputted the resulting aircraft definition, including aerodynamic polars and engine performance data.

2.3 Aircraft performance analysis

Mission calculations were performed by an analytical tool that enables a gradual, two-dimensional simulation and assessment of an aircraft's mission, with the objective of determining the fuel consumption for each flight phase, including those of a reserve mission. Additionally, the tool optimizes the fuel consumption by selecting the optimal initial cruise altitude and by performing optimal stepwise increase in cruise altitude. The calculations are based on fuel fractions for taxi, take-off, approach, and landing, while the climb, cruise, and descent phases are analyzed by solving two-dimensional equations of motion for a clean configuration. The optimization of altitude steps is based on maximizing specific range, which encompasses both aerodynamic and engine performance.
The tool's main output employed in this workflow is the estimation of the fuel required for the various flight phases and the values of the major flight performance parameters, including the cruise lift coefficient, lift-over-drag ratio, thrust-specific fuel consumption, and thrust. These parameters were utilized in subsequent analyses to compare different aircraft concepts and to explain the differences in their performance.
A second aircraft performance analysis tool was implemented for the purpose of evaluating the aircraft's low-speed performance. The data for this evaluation was provided by means of aerodynamic polars and engine performance data generated by OpenAD. This low-speed performance tool performed a stepwise evaluation of two-dimensional equations of motion to assess the aircraft's take-off, approach and landing performance under all engine operational (AEO), one

engine inoperative (OEI), and rejected take-off (RTO) scenarios. This enabled the estimation of crucial performance parameters, including take-off and landing field lengths under the different conditions. A particularly important output of the tool was then the value for balanced field length (BFL), which was used to determine the maximum thrust requirement for engine sizing.

2.4 HLFC system sizing

In order to perform the design and analysis of HLFC subsystems for different components, a tool developed by the author for this purpose was incorporated into the conceptual aircraft sizing workflow.
This tool, further referred to as the HLFC system sizing tool, estimates the mass and power offtakes of a HLFC subsystem by utilizing the methodology developed by Pe and Thielecke [14].
In order to perform HLFC system sizing, three sets of inputs are required. The first set of inputs is the geometric definition of the component to which the HLFC system should be applied.
The second set of inputs defines the HLFC system itself, including the extent of applied suction as well as the number and dimensions of its individual components.
Lastly, the value of parameters that describe the suction performance of the system are needed. Of these so-called suction parameters, the two most significant are the mass of the air to be sucked-in by each suction segment and the pressure difference across the suction sheet necessary to achieve this mass flow.
The suction parameters can be provided in two forms. The first option is to provide the suction data directly if the value is known, for example, from prior aerodynamic calculations or experiments. The second option is to provide a reference suction data set, including the definition of the HLFC system for which the data was obtained and the definition of the geometry of the component to which the system was applied. In this case, an interpolation or extrapolation of the reference data for the specified flight conditions is performed first. The resulting values are then scaled based on a selected scaling parameter, typically the suction area. The suction area is the area of the perforated suction panels through which the air is sucked into the component.
Once the suction parameters have been established, the next step is calculation of the pressure losses occurring in the suction plenum, across the structural ribs, and through the transfer duct, contraction to the compressor inlet, and the exhaust duct. This further requires an iterative calculation of the pressure ratio that must be delivered by the compressor. Using the pressure ratio and the mass flow, the required isentropic suction power is obtained as:

$$P_{isentropic} = \dot{m} \left(\frac{\gamma}{\gamma - 1} \right) R T_{duct} \left(PR^{\frac{\gamma-1}{\gamma}} - 1 \right) = \dot{m} Y \tag{1}$$

Dividing the isentropic power by the efficiency of the various electronic components them provides the total power that must be delivered by the aircraft's engines.
Next, the tool implements the methodology described by Teichel et al. [29] to determine the dimensions and masses of the individual components of the compressor and electric motor drive. It should be noted that at the time of this study, the tool could only be used for systems featuring axial compressors, as no analogous low-fidelity method for sizing diagonal and radial compressors was identified. Consequently, axial compressors are employed exclusively for all HLFC systems presented in this work.
Empirical relations, also provided by Teichel et al. [29], are used to calculate the masses of the electrical wiring (accounting for its length), inverters, and rectifiers. The mass of the ducts and the exhaust is determined on the assumption of a flow speed of Mach 0.2, with the result being dependent on the mass flow through them and their required length, material, and wall thickness. The structural mass of the system is calculated by considering the mass of the suction sheets, ribs, and the internal support structure. The mass of the original wing skin and leading-edge material, which is substituted by the suction panel, is accounted for as well.

2.5 Laminarity calculations

This chapter first introduces a parameter that describes the extent of laminar flow over a given component. It then discusses the importance of this parameter and how its value was obtained in the separate cases of HLFC and NLF.

2.5.1 nLam Parameter

In order to calculate the zero-lift drag, the preliminary aircraft sizing tool OpenAD, introduced in Chapter 2.2, implements a component buildup method as described by Raymer [26]. This method involves calculating the component's friction drag using a weighted sum of the turbulent and laminar values of the equivalent flat-plate friction coefficients. The

weights correspond to the fraction of the component's wetted area exposed to the turbulent or laminar flow, relative to its total wetted area:

$$C_f = \frac{S_{lam}}{S_{wet}} \cdot C_{f,lam} + \frac{S_{turb}}{S_{wet}} \cdot C_{f,turb} = nLam \cdot C_{f,lam} + (1 - nLam) \cdot C_{f,turb} \tag{2}$$

Equation 2 also introduces a new parameter called nLam, defined as:

$$nLam = \frac{S_{laminar}}{S_{wet}} \tag{3}$$

This parameter, which represents the percentage of the component's wetted area exposed to laminar flow, is accepted as an input by OpenAD. This input is then used in the calculation of the friction drag, as part of the process of generating the aerodynamic polars. These polars are further used in OpenAD for subsequent steps in the aircraft sizing process, and are exported as one of its primary outputs.

The nLam parameter is therefore used extensively in the following discussion, as a way to express what extent of laminar flow the laminar technologies are capable of providing for different configurations, assumptions and flight conditions. It is therefore essential to obtain an accurate estimation of the value of nLam on the given component for the assumed location of the transition point in order to obtain accurate aerodynamic polars and consequently, an accurate estimation of the fuel saving potential.

In order to achieve this, the functionality of the HLFC sizing tool, as detailed in Chapter 2.4, was expanded to accommodate the calculation of the nLam parameter for both NLF and HLFC configurations of all three components under consideration.

The calculation of nLam performed by the tool is purely geometrical, based on the geometry of the component and the location of the prescribed laminar-to-turbulent transition point. The details of the calculations for both NLF and HLFC will be described in the following chapters. It should be noted, that in either case, the tool does not perform any aerodynamic calculations to obtain or verify the location of the transition point.

However, the tool accounts for the fact that the two surfaces (upper and lower for the wing and HTP, left and right for the VTP) can contribute to the frictional drag produced by the component by a different amount, depending on the component's shape and the resulting flow characteristics. In the case of the empennage, it was assumed that both surfaces contributed equally to the total friction drag, as the empennage is assumed to feature symmetrical airfoils without lift production during the cruise phase.

However, in contrast to the empennage, the wing generates substantial lift during cruising flight and features asymmetric airfoils. As a result, the flow over the upper surface is considerably different from that over the lower surface. Consequently, the contribution of both surfaces to the wing's friction drag is not equivalent. Prior research has demonstrated that the upper surface is responsible for approximately two-thirds of the wing's friction drag, while the lower surface accounts for only one-third [30]. Accordingly, the value of nLam for the entire wing was calculated as:

$$nLam_{wing} = 2/3 \cdot nLam_{wing,top} + 1/3 \cdot nLam_{wing,bottom} \tag{4}$$

A separate value of nLam was introduced in Equation 4 for individual surfaces in order to account for the varying extents of laminar flow over them. This is due to the fact that, as a result of the presence of extensive unfavorable pressure gradients, it is generally considered unfeasible to achieve a significant extent of laminar flow over the bottom surface of the wing. Given its comparatively smaller contribution to the overall friction drag and less favorable conditions for laminar flow, the lower surface is typically accepted as turbulent and utilized for storing leading-edge high-lift devices. This allows the upper surface to remain clean of any panel gaps, which would inevitably result in an early transition.

It is important to note that the nLam parameter is relevant for both laminar and turbulent aircraft. In this study, the default turbulent values of nLam were set at 10% for the empennage and 5% for both surfaces of the wing. The value for the empennage was obtained from [26], while the value for the wing was acquired from the aircraft that served as the starting point for all aircraft concepts developed in this work. This so-called baseline aircraft, will be introduced in Chapter 3.1. A detailed wing design, including high-fidelity CFD simulations, was carried out for this baseline aircraft, resulting in a more accurate estimate of nLam of 5%, used in this study instead of the 10% suggested by Raymer [26].

As a final consideration regarding the nLam parameter, it was assumed that both the NLF and HLFC provide laminar flow exclusively during the cruise phase, while the default turbulent nLam values were maintained for other phases of the mission. This conservative approach was based on the recognition that, in other mission phases, additional factors may become relevant, which could significantly reduce the achievable extent of laminar flow, but require a more detailed analysis for their accurate assessment. Such effects include, for example, the deflection of high-lift devices, ice formation, or early transition due to flight through clouds.

2.5.2 Laminarity calculations for NLF

In order to estimate the transition location in the context of NLF, the methodology proposed by Wilson [9] was incorporated into the HLFC system sizing tool. The method assumes that the transition at any given location results from one of two possible causes. The first potential cause is the reaching of the transition Reynolds number. The transition Reynolds number is defined as:

$$Re_t = \frac{\rho v x_t}{\mu} \tag{5}$$

Thus, for a given value of the transition Reynolds number, the distance x_t to the transition point, measured from the leading edge, can be calculated as:

$$x_t = \frac{Re_t \mu}{\rho v} \tag{6}$$

Equation 6 demonstrates that, for a given transition Reynolds number and flight conditions, the distance of the transition point from the leading edge remains constant along the entire span. Consequently, the transition line defined by this parameter is a straight line at a constant distance from the leading edge.

The second factor limiting the extent of laminar flow over a given component in the case of NLF, is the location of pressure recovery. To prevent transition due to an unfavorable pressure gradient, NLF airfoils aim to maintain a favorable pressure gradient over most of their chord. However, at some point the pressure must increase (recover) to achieve a continuous pressure field over the trailing edge. For NLF airfoils, this recovery is relatively abrupt and requires careful consideration to prevent separation or formation of strong shock waves with the associated increase in drag. However, such a strong adverse pressure gradient is detrimental to laminar flow, and so the transition usually occurs at the point of pressure recovery at the latest, if not triggered earlier by other factors. Assuming that the airfoil design does not vary significantly along the span, the pressure recovery point can be assumed to be located at constant chord fraction, forming a second potential transition line.

In summary, the flow at any given spanwise location is assumed to transition either by reaching the transition Reynolds number or by reaching the point pressure recovery, whichever occurs first. This is graphically illustrated in Figure 2.

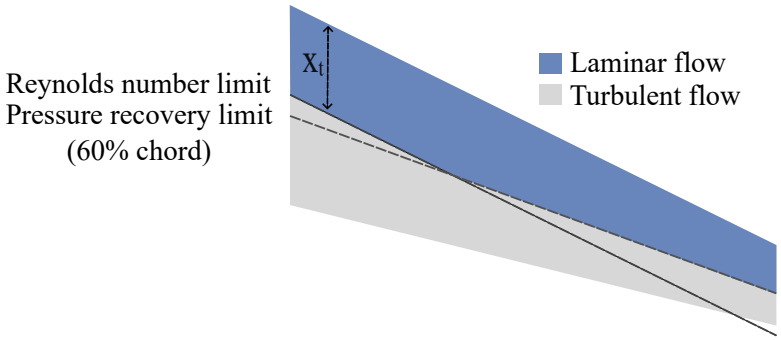

Fig. 2 Transition model utilized for natural laminar flow

The described model was implemented into the HLFC sizing tool. The tool determines the transition locations across the entire span by assessing which of the two factors is constraining at each spanwise section. Both the transition Reynolds number and the chordwise location of the pressure recovery are inputs provided by the user.

In the presented study, it was assumed that the pressure recovery point was at 60% of the chord for all components, for both HLFC and NLF. The transition Reynolds number for each component was obtained from empirical data as a function of Reynolds number and leading-edge sweep. The component's Reynolds number was calculated for the cruise Mach number and the altitude at which the aircraft remained for the majority of the cruise phase, specifically 35,000 ft. The impact of altitude changes during the cruise on the transition location was not considered. This simplification was justified by the fact, that during a design mission, the short-to-medium range aircraft was not expected to perform more than a single altitude change during the cruise phase. For the even shorter evaluation mission, no altitude change was anticipated at all. For other flight phases, the system was considered inactive.

2.5.3 Laminarity calculations for HLFC

In the case of components equipped with HLFC systems, it was always assumed that the flow transition would be postponed up to the location of pressure recovery. This location was considered to be at 60% of chord for all components of all configurations across all flight conditions.

An additional consideration for all HLFC suction segments is the presence of so-called turbulent wedges. These are regions of turbulent flow that originate at the leading edge due to the presence of a physical surface gap at the spanwise edges of each suction panel. Such a gap introduces disturbances into the flow, causing its transition at the given point at the leading edge. As the flow propagates in the chordwise direction, the turbulence spreads at a constant angle, forming a triangular turbulent region, which is referred to as a turbulent wedge. The presence of such wedges results in a reduction of the laminar area over the component, which in turn leads to a decrease in the value of nLam and an increase in the friction drag, ultimately resulting in a reduction in fuel savings. The turbulent wedges between the individual suction segments can be clearly seen in Figure 3, which shows the result of a CFD simulation for a wing equipped with an HLFC system developed in the Clean Sky 2 project HLFCWin. The HLFCWin project was an EU-funded initiative focused on developing HLFC technology for aircraft wings. The project successfully developed a working demonstrator and generated extensive publicly available data [31, 32].

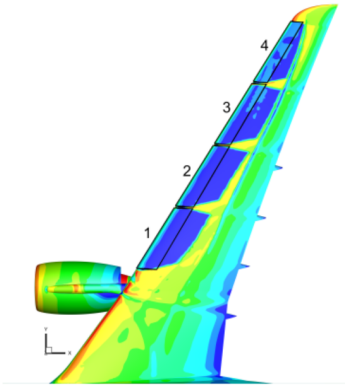

Fig. 3 Laminar regions and turbulent wedges simulated in the project HLFCWin [31]

The HLFC system sizing tool has the capacity to model the turbulent wedges based on a user-specified value of their spreading angle. In this study, the angle was assumed to be 15 degrees, which is consistent with the value observed in the HLFCWin project, as can be seen in Figure 3. The tool positions a turbulent wedge at both spanwise ends of each suction panel and calculates the resulting reduction in nLam. Furthermore, half of a turbulent wedge is also positioned at the point where the component's leading edge intersects with the fuselage, to model the turbulent area that is typically observed in this region.

A turbulent region was also assumed to exist downstream of the engine and its pylon. This region was identified in CFD simulations conducted as part of the HLFCWin project, which further determined that integrating a suction system into this part of the wing would be challenging due to the engine pylon attachment structure. These findings led to the conclusion that maintaining laminar flow in this area is not feasible, even with HLFC. The CFD simulations, however, also showed that this turbulent region was not of the same width as the engine, but narrower. Based on this observation, the region was always assumed to cover the full chord of the components and to be centred around the spanwise position of the engine, with a width equal to the nacelle diameter multiplied by the so-called engine factor. A value of 0.7 was assumed for all calculations presented, indicating that the turbulent region was assumed to have a width of 70% of the engine diameter. This value was derived from the CFD results from the HLFCWin project. The turbulent wedge at the fuselage intersection and the turbulent region behind the engine were also considered for all NLF calculations.

Finally, it should be noted that in the HLFCWin project, HLFC was not applied to the region of the wing inboard of the engine, as shown in Figure 3. This was because the HLFC system was retrofitted onto an existing wing planform that had not been optimized to promote laminar flow. The complex flow topology in this region then prevented achieving any significant extent of laminar flow, even with applied suction. However, the authors concluded that this issue could be resolved through appropriate adjustments to the wing planform and airfoil redesign [31]. This work therefore assumes that achieving extensive regions of laminar flow in this area is feasible.

3 Aircraft and System Configurations

This chapter introduces the concepts of reference and baseline aircraft and provides fundamental information on the aircraft utilized for the purpose of this study. The second part of this chapter describes in detail the HLFC subsystems applied to the different components of the baseline aircraft as part of the process of developing the final laminar aircraft.

3.1 Reference and baseline aircraft

The term "reference aircraft" refers to the aircraft that is currently in operation and which the laminar concept developed in this study is intended to replace in the corresponding market sector by 2035. In this study, the Airbus A321neo was identified as an exemplary representative of the short-to-medium range aircraft category. As discussed in the introduction, this category was deemed critical with respect to the ability of the aviation industry to meet its sustainability goals. For these reasons, the Airbus A321neo was selected as the reference aircraft.

In the case of a baseline aircraft, the concept is predicated on the recognition that it would be inaccurate to compare the characteristics of a futuristic aircraft concept with those of an aircraft currently in service. This is because, by the time the new concept enters service, in this case 2035, the conventional aircraft would be expected to also undergo additional evolutionary improvements through its new production versions. These new versions would benefit from technological advancements in various fields, including but not limited to aerodynamics, engine technology, new lightweight materials, and more efficient structural design. Therefore, upon entering into service, the new aircraft concept will have to compete with a new generation of conventional aircraft featuring these new technologies.

Additionally, the sensitivity of aircraft performance to certain design choices can also be influenced by its technology level. For instance, utilizing a new ultra-high bypass ratio engine could affect the extent to which fuel consumption increases due to additional power off-takes, a highly relevant factor when evaluating HLFC systems. Accurately capturing the impact of a new technology on aircraft performance, therefore, requires the aircraft to reflect an overall technology level representative of the timeframe in which the technology is expected to be implemented.

To address this, DLR conducted a design process, detailed in [33] and illustrated in Figure 4, to develop a baseline aircraft with a technology level corresponding to its assumed entry into service in 2035.

Fig. 4 Aircraft design process from the A321neo reference aircraft to the D239 and the DLR-F25 configurations [33]

The initial stage of the process was the design of a representative model of the Airbus A321neo, referred to as D239, within the DLR's aircraft design software environment. This model was developed based on the TLARs from A321neo, presented in Table 1, and additional inputs obtained from publicly available geometry and performance data [34]. The software design tools and their inputs were thereby calibrated in such that the geometry, design masses, and performance of D239 would correspond to those of the Airbus A321neo.

Table 1 TLARs for Airbus A321neo [33]

Parameter	Value	Unit
Design Range	2500	nm
Evaluation Range	800	nm
Design PAX (single class)	239	-
Mass per PAX	95	kg
Design Payload	25000	kg
Max. Payload	25000	kg
Cruise Mach number	0.78	-
Max. operating Mach number	0.82	-
Design dive speed	380	kts
Maximum operating speed	350	kts
Max. operating altitude	40000	ft
TOFL (ISA +0K SL)	2200	m
Rate of Climb @ TOC	>300	ft/min
Approach Speed (CAS)	136	kt
Wing span gate limit	<36	m
Alternate Distance	200	nm
Holding Time	30	min
Contingency	3%	-

Note that as mentioned in the introduction, the laminar aircraft concept developed in this work was also designed based on the TLARs of the reference aircraft presented in Table 1, with these requirements remaining fixed throughout the conceptual design process. Furthermore, while the aircraft was sized for a design mission of 2,500 nm, its performance was evaluated on a shorter range of 800 nm, representative of the most common mission performed by the reference aircraft in real-world operations.
Once calibrated, the same tools and procedures were employed to generate the baseline aircraft, called DLR-F25, thus ensuring a comparable and consistent design. The DLR-F25 was derived from the D239 by applying a series of technology factors based on the technological advancements believed to be available for future aircraft with an assumed entry to service in 2035 [33]. These assumptions are summarized and justified in Table 2.

Table 2 Technology assumptions applied during the conceptual design phase of the DLR-F25 baseline aircraft [33]

Component	Technology Factor	Rationale (Compared to D239)
Engine Performance	+4%	Compared to a 2015 state-of-the-art geared turbo fan, Bypass-ratio: 15, improved thermal efficiency
Fuselage Mass	-5%	Advanced Al-alloys, improved manufacturing and assembly methods, revised production and certification requirements
Empennage Mass	-3%	Improved manufacturing and assembly methods
Wing Mass	-30%	Application of CFRP, advanced load alleviation, active flutter suppression, adaptive dropped hinge flaps, foldable wing tips
System Mass	-5%	Improved on-board system architecture

The technology factors in question are based on the utilization of a number of novel technologies. The most important are the ultra-high bypass ratio engine, the high aspect ratio wing with foldable wingtips, the active flutter suspensions, and the lighter onboard systems. The effect of these technologies on the aircraft performance and the associated assumptions are discussed in detail in [33], which also compares the key performance and geometry characteristics of the DLR-F25 to those of D239.
In this study, the DLR-F25 served as the starting point from which all new laminar aircraft concepts were derived. This was achieved by applying different laminar technologies to the wing, HTP, and VTP of the DLR-F25. The performance of the new aircraft concepts was then evaluated by comparison to that of the DLR-F25.

3.2 HLFC Subsystem Configurations

This chapter presents the aspects of this work related to the design of HLFC systems. It begins with an introduction to the general HLFC system architecture, followed by an overview of the assumptions made in the design of all HLFC systems. Finally, the chapter describes the individual HLFC subsystems applied to the wing, VTP, and HTP. Note that the term "subsystem" refers to an HLFC system applied to a specific component.

3.2.1 General HLFC system architecture

An example of a modern HLFC system is shown in Figure 5, which illustrates an HLFC system concept developed by DLR as part of the HLFCWin project [32].

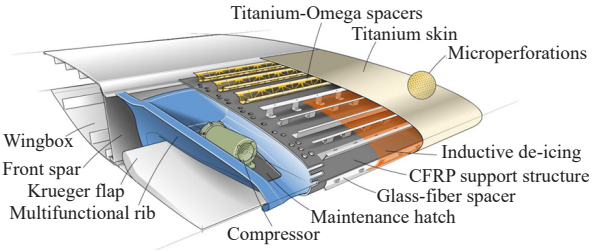

Fig. 5 HLFC system for a wing developed in CleanSky 2 HLFCWin project [32]

The first fundamental element of any modern HLFC system is the perforated suction sheet (also referred to as a suction panel or suction skin), which enables the required amount of air to be drawn from the boundary layer on the component's surface into its interior. After passing through the suction sheet, the drawn air enters a suction chamber (also referred to as a suction plenum). The pressure in the plenum is maintained lower than the pressure at the component's surface, creating the necessary pressure difference to draw air from the boundary layer through the perforations in the suction sheet.
In this work, the suction chamber is assumed to be formed by the space between the suction sheet and a secondary support structure positioned behind it. The suction sheet is further assumed to be connected to the support structure by a series of stringers or ribs, the number of which depends on the specific subsystem under consideration. The distance between the suction sheet and the support structure is then referred to as the plenum gap.
In the suction chamber, the air flows in the spanwise direction until it reaches the end of the chamber, where it passes through a contraction into a transfer duct that directs it to the compressor inlet. Alternatively, the transfer duct may be omitted. In such cases, the contraction would either channel the air directly to the compressor inlet, or the compressor inlet would be positioned directly at the end of the suction chamber. In this work, the first option is assumed for such cases. The function of the compressor is to generate a sufficient pressure ratio to maintain the required low pressure within the suction chamber. After compression, the air passes through an exhaust duct, which directs it outside the aircraft. Alternatively, the exhaust duct may be omitted, with the air being expelled directly into the space housing the compressor. From there, the air can escape to the atmosphere through gaps in the component's surface. This approach is feasible due to the relatively low mass flow requirements of a single compressor in an HLFC system, typically ranging from tens to hundreds of grams per second.
In addition to the described pneumatic assembly, an HLFC system requires supplementary components to drive the compressors. Modern designs exclusively utilize electric induction motors, powered by electricity generated by the aircraft's engines and transmitted to the motors via an electrical cable network. If the design incorporates a DC cable network, rectifiers are necessary to convert the current from AC to DC between the engine generators and the cables.

Similarly, inverters are required to convert the current from DC back to AC between the cables and the motors.
As previously mentioned, integrating an HLFC system into a component furthermore requires the implementation of additional structural elements to ensure the structural integrity of the assembly. These elements include the mentioned support structure as well as additional ribs or stringers. The design of any structural elements placed within the suction chamber must allow for the passage of sucked air through or around them with minimal pressure losses. Reducing pressure losses is critical for minimizing the pressure ratio required from the compressors, thereby reducing the system's overall power requirements.
Finally, Figure 5 shows that the system developed in the HLFCWin project featured a Krueger flap instead of conventional slats. The Krueger flap is the leading-edge high-lift device of choice for most HLFC system concepts due to its dual benefits. First, unlike slats, it keeps the top surface free of surface gaps and steps that would otherwise cause transition. Second, a Krueger flap can be designed to shield the leading-edge surface when deployed, significantly reducing its contamination from insects and dirt at low altitudes. For these reasons, also this work assumes the use of Krueger flaps on wing sections equipped with HLFC systems. It is further assumed that this device does not introduce any additional mass penalties and provides high-lift performance equivalent to that of slats [31].

3.2.2 Global Assumptions

Certain assumptions were applied uniformly across all HLFC subsystems, regardless of the component to which the subsystem was applied. The most critical assumptions included calibration factors for the masses of different parts of the system and the efficiencies used to calculate engine power offtakes based on the isentropic suction power required to achieve the necessary pressure ratio. Other global assumptions included the material and thickness of various system components, the mass density of cables, and the roughness of the transfer ducts and exhausts, which affects the pressure losses within them. Table 3 gives an overview of the most important assumptions.

Table 3 Assumptions made in the design and evaluation of all HLFC subsystems

Parameter	**Unit**	**Value**
Compressor efficiency	%	85 [29]
Motor drive efficiency	%	95 [29]
Inverter efficiency	%	98.6 [29]
Generator efficiency	%	98.6 [29]
Wiring efficiency	%	98.8 [29]
Plenum gap	mm	20
Number of compressor stages	–	1
Compressor type	–	Axial
Suction panel material	kg/m^2	Titanium (4500) [35]
Suction panel thickness	mm	0.8
Original skin material	kg/m^2	Aluminum (2700)
Inner support structure material	kg/m^2	CFRP (1750) [36]
Inner support structure thickness	mm	3.65
Duct and exhaust material	kg/m^2	Aluminum (2700)
Duct and exhaust wall thickness	mm	3 [17]
Compressor casing, hub, and blades material	kg/m^2	Aluminum (2700) [29]
Compressor shaft material	kg/m^2	Steel (7900) [29]
Cable unit mass	kg/(kW·m)	0.0027 [29]
Compressor and motor drive mass factor	–	0.724
Invertor and rectifier mass factor	–	2.224
Duct and exhaust mass factor	–	1.143

The calibration factors were obtained through a calibration process by first modeling an HLFC system for a VTP of an

Airbus A320, as described by Krishnan et al. [15]. The system mass and power consumption were calculated using the provided suction data and a set of assumptions for parameters that were not specified in [15]. The calibration factors were then calculated by taking a ratio between the reported and calculated masses of different parts or categories of parts. A detailed description of the calibration process and additional results are provided in Chapter 1.2 of the supporting material.
The thickness of the inner support structure was obtained by modelling the prototype developed by DLR, described in detail in [36], and varying the thickness of the support structure until the same structural mass was obtained.
Finally, the size of the plenum gap was obtained from data for a prototype of a VTP suction segment, provided in [36]. The same plenum gap size was then assumed for all components. This assumption was deemed justified based on an inspection of another prototype constructed in the past, a wing suction segment produced as part of the HLFCWin project [31]. This prototype is shown in Figure 6.

Fig. 6 HLFC suction segment prototype developed in the project HLFCWin [31]

Finally, the number of compressor stages was kept to one, since calculations showed that all compressor designs in this study remained under or within the maximum pressure ratio range of 2.3-2.5, given by Teichel et al. [29] for single stage axial compressors. A second rationale for increasing the number of compressor stages would be to restrict the compressor diameter. In this study, which did not investigate the details of the system integration, all calculations were performed with a diameter limit of 30 cm. This limit was satisfied with single-stage compressor design for all subsystems.

3.2.3 HLFC Subsystem for the wing

The default configuration of the wing HLFC subsystem, consisting of three suction panels, one inboard and two outboard of the engine, is illustrated in Figure 7. Furthermore, Table 4 provides an overview of the subsystem's key design parameters.

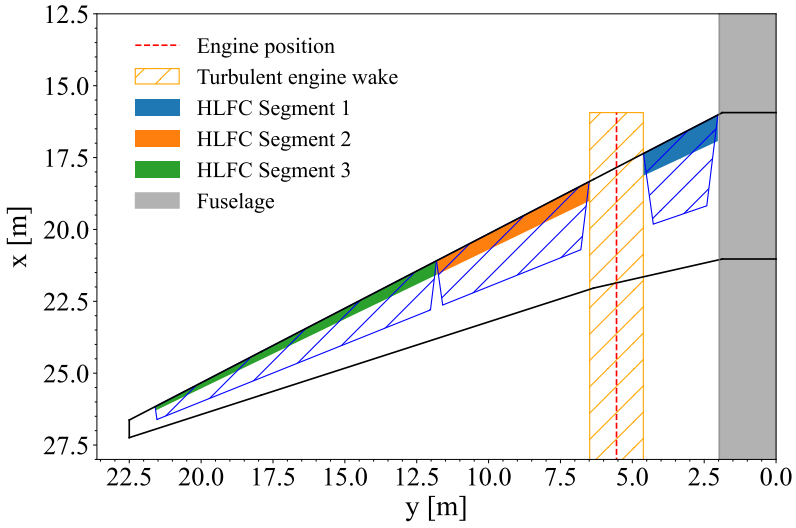

Fig. 7 Default HLFC subsystem configuration for the wing

Table 4 Parameters of the HLFC subsystem for the wing

Parameter	Segment 1	Segment 2	Segment 3
Spanwise start position	9%	28.9%	52.5%
Spanwise end position	20.5%	52.5%	96%
Suction area	2.3 m^2	3.3 m^2	3.3 m^2
Transfer duct length	0 m	0 m	0 m
Exhaust duct length	3.8 m	2.8 m	2 m
Cable length	18 m	23 m	28 m

The decision to utilize three suction segments was made with the intention of achieving suction areas comparable to those of the segments applied to a wing in the HLFCWin project. This was done in order to minimize the magnitude of scaling performed to obtain the mass flow and pressure difference required for each segment.
The chordwise extent of all segments was set to 18%, which is the same value used in HLFCWin and is consistent with the typical location of the front spar beyond which, by the definition of HLFC systems, suction should not be applied. This is to avoid associated problems with the structural integrity of the wingbox, fuel tank volume reduction, or fuel leakage into the system.
The wing subsystem employed a decentralized architecture with one compressor per suction segment. No duct was utilized between the plenum and the compressor, as the air was assumed to flow directly from the plenum to the compressor inlet, as was the case for HLFCWin, as shown in Figure 5 in Chapter 3.2.1. The compressor for each suction segment was therefore assumed to be positioned at the inboard end of that segment. The length of the exhaust duct from each compressor was calculated as 75% of the chord length at the compressor's spanwise location, based on the assumption that the exhausts are located at the wing's trailing edge. The cable length for each segment was calculated as the sum of the spanwise distance from the compressor to the fuselage centerline and the distance from the wing root to the nose of the aircraft, where the EE bay is traditionally located.
Furthermore, as indicated in Table 4, the spanwise extent of the two outboard segments was selected such that the suction area for both would be the same. The motivation behind this decision stems from the fact that the suction parameters (mass flow and pressure difference) for the wing system were obtained by scaling a reference suction data by the suction area of the individual suction segments (see Chapter 2.4). As a result, utilizing the same suction area would lead to identical suction requirements for both segments.
Ensuring the same suction requirements for both segments is advantageous in the context of compressor design, as the HLFC system sizing tool identifies the most critical compressor across all suction segments of the given component and applies its design to all remaining compressors. This is done as it is likely that the same approach would be used in a real production as well, in order to eliminate the additional design, manufacturing and maintenance costs associated with the use of multiple compressor designs. The equal mass flow and pressure difference requirements for multiple suction segments allow for all compressors to operate at or near the optimal design conditions, maximizing their efficiency.
However, it was not possible to achieve the same suction area for the most inboard segment. This limitation resulted from its spanwise extent being constrained by the presence of the fuselage on the inboard end, and by the turbulent wake behind the engine (see Chapter 2.5.3) on the outboard end. Consequently, the suction area of the inboard segment was 30% smaller compared to the suction areas of the outboard segments, leading to proportionally lower suction requirements as well.

3.2.4 HLFC Subsystems for the VTP

The HLFC subsystem for the VTP represented a unique case, as numerous prior investigations, both theoretical and experimental, had focused on the application of HLFC on the VTP of an Airbus A320 [15, 36–41]. Taking advantage of the fact that the Airbus A321neo and consequently the DLR-F25 utilize the same VTP geometry as the A320, the data reported by Krishnan et al. [15] for flight level FL350 were used in this study. The data were provided directly as input to the HLFC system sizing tool without any additional scaling or correction. While this meant that the tool would not automatically vary the suction parameters with flight conditions. This limitation was accepted since it was observed that the cruise flight conditions did not vary significantly during any of the missions considered, nor between different aircraft concepts. Therefore, the assumption of constant suction parameters was justified.
The subsystem design for the VTP was driven by the intention to approximate as closely as possible the system layout

for which the data by Krishnan et al. [15] was obtained, in order to maintain consistency with the suction data. The main parameters of the resulting configuration are summarized in Table 5. Figure 8 then shows the resulting VTP with the implemented suction system and the laminar region produced, as modelled by the HLFC sizing tool.

Table 5 Parameters of the HLFC subsystem for the VTP

Parameter	Value
Spanwise suction extent	9.5% - 95%
Chordwise suction extent	0% - 18%
Suction area	7.2 m^2
Number of suction panels	1
Number of compressors	1
Duct length	0 m
Exhaust length	8 m
Number of ribs	0
Cable length	40 m
Mass flow	385 g/s
Plenum pressure	18,097 Pa

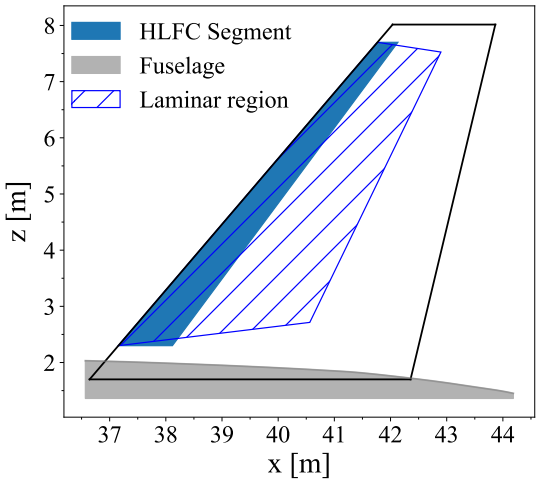

Fig. 8 HLFC subsystem applied to the VTP

The dimensions of the suction plate in both spanwise and chordwise directions were adopted from [40]. The size of the plenum gap and the absence of ribs were taken from the study in [36], which found this configuration to be optimal in terms of weight and structural performance. The compressor was assumed to be located at the inboard edge of the suction segment, as for the suction segments on the wing, thus eliminating the need for a transfer duct. The exhaust length was determined by measuring the distance between the assumed compressor location and the end of the fuselage where the air could be expelled through the exhaust opening for the auxiliary power unit. Similarly, the length of the wiring was set to the distance between the compressor and the assumed location of the avionics bay in the front of the fuselage.

3.2.5 HLFC Subsystem for the HTP

In contrast to the VTP, no reference suction data from previous investigations were found for the HTP. It was therefore decided to utilize the data available for the VTP, and to scale it with respect to the suction area of both components. This approach was supported by the observation that, once the suction system had been defined, it became apparent that both the VTP and HTP featured similar total suction areas. In addition, as with the VTP, it was assumed that the HTP would not generate lift during the cruise phase when the HLFC system is active.

However, a significant difference between the HTP and the VTP is the leading-edge sweep, which plays a dominant role in the flow transition (particularly through its effect on the magnitude and intensity of cross-flow instabilities) and the overall extent of laminar flow. However, as no low-fidelity method was available that would adequately capture the relationship between the leading-edge sweep, the suction parameters, and the transition location, it was decided that this factor would not be considered in this study.

This decision was partially justified by the fact that the HTP has a lower leading-edge sweep angle (32.3°) than the VTP (40.5°). Since a lower leading-edge sweep results in weaker boundary layer instabilities and a later transition, the less swept HTP should require less suction than the VTP for the same extent of laminar flow. The resulting power requirements obtained without accounting for the difference in sweep angle, should therefore be considered a conservative estimate.

The observation that the combined suction area over both the left and right planes of the HTP was similar to the total suction area of the VTP resulted in the decision to implement a centralized architecture for the HTP. A centralized architecture employs a single compressor to provide suction for the both planes of the HTP, where the resulting mass flow and pressure difference requirements approximate those for the VTP. This configuration allows for the use of the same compressor design for the complete empennage, thereby reducing the production and maintenance costs, as previously discussed in the context of the wing subsystem. Figure 9 illustrates the centralized architecture for the HTP.

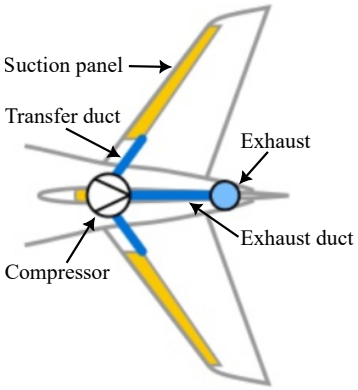

Fig. 9 Centralized HLFC System Architecture for the HTP [14]

Furthermore, a study conducted by Pe et al. [14] demonstrated that a centralized architecture is advantageous in terms of both system mass and power offtakes. However, one disadvantage of this solution is that a failure of the central compressor would result in a complete loss of suction, leading to a considerable reduction in laminarity across the entire component. Nevertheless, this risk was accepted, and the implications of such a failure in terms of additional block fuel are discussed in Chapter 4.5. The results presented by Pe et al. [14] further indicate that the minimum system mass and power offtakes would be achieved by utilizing a single compressor for both VTP and HTP. However, this configuration was not selected, since the consequence of a compressor failure would be even more severe, resulting in a loss of laminarity over the complete empennage.
Table 6 now presents the key design parameters of the HLFC subsystem for the HTP, while Figure 10 illustrates the HTP equipped with the subsystem and the laminar region produced.

Table 6 Parameters of the HLFC subsystem for the HTP

Parameter	**Value**
Spanwise suction extent	25% - 95%
Chordwise suction extent	0% - 18%
Suction area	5.6 m^2
Number of suction panels	1
Number of compressors	1
Duct length	2 m
Exhaust length	6 m
Number of ribs	0
Cable length	40 m
Mass flow	300 g/s
Plenum pressure	18,097 Pa

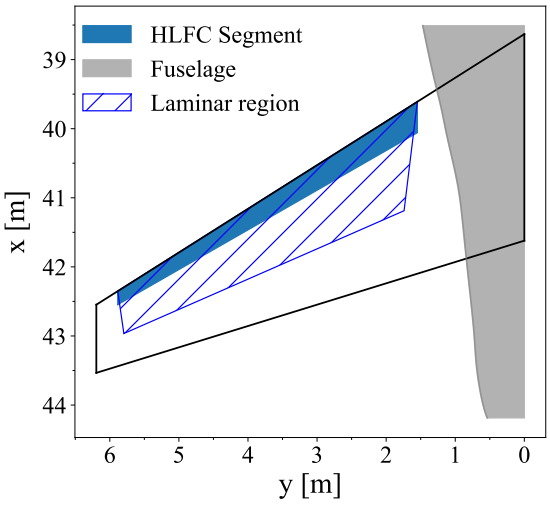

Fig. 10 HLFC subsystem applied to the HTP

Note that, in contrast to the wing and the VTP subsystems, the implementation of a central architecture with a single compressor located at the root of the HTP required the use of transport ducts to transfer the air from both suction chambers to the compressor.
Furthermore, while the suction panel ends at same fraction of span as for the VTP (95%), it begins approximately 10% of the span further outboard (at 25% compared to 9.5%) than the segment on the VTP. This is because a considerably larger area of the HTP is covered by the fuselage in comparison to the VTP, especially near the leading edge. The start position of the suction segment was therefore selected such that the same distance to the fuselage, in terms of span percentage, would be maintained instead.

The lengths of the ducts, exhaust, and cables were then calculated based on the geometry and placement of the HTP, assuming that the compressor is located at the centerline at 25% of the root chord.

4 Results and discussion

This chapter presents the results obtained in the process of developing the laminar aircraft concept. The results are presented in a sequence that corresponds to the process through which the final configuration was derived, beginning with the turbulent baseline aircraft and gradually introducing the laminar flow technologies. It additionally presents two sensitivity studies conducted as part of this process, one for each laminar flow technology. A comparison is then provided between the obtained laminar aircraft and the original baseline aircraft. The chapter concludes with a failure analysis in which the laminar aircraft was no longer resized, and the impact of various failure scenarios on its performance were assessed.

4.1 Combined application of laminar flow technologies on aircraft level

As mentioned in the Introduction, previous studies have primarily focused on evaluating the effects of a single laminar flow technology applied across multiple components. This study, therefore, adopted a more holistic approach, aiming to evaluate the benefits of applying the most suitable laminar flow technology to each of the considered components, namely the wing, VTP, and HTP.

To achieve this, both technologies were individually applied to each component of the baseline aircraft, followed by a full resizing process to estimate the resulting block fuel savings, including the compounding of masses (referred to as the "snowball effect"). The technology yielding the highest block fuel savings was then selected for each component. Finally, the baseline aircraft was resized with the selected laminar flow technologies applied simultaneously across all components. The resulting block fuel savings were compared with those obtained for an aircraft utilizing either NLF or HLFC exclusively across all components.

4.1.1 Effects of NLF

As an initial step in the development of a laminar aircraft, NLF was applied to all three components. Table 7 presents a summary of the reference nLam values for the turbulent baseline aircraft, the assumed transition Reynolds numbers, and the nLam values obtained after applying NLF. The values of the transition Reynolds number were obtained as a function of the leading-edge sweep of each component, based on experimental data retrieved from the work of Grasmeyer et al. [42]. These data were gathered during experiments with an NLF glove applied to the wing of a Boeing 757.

Table 7 Performance of NLF on different components
(BF = Block fuel, DM = Design mission, EM = Evaluation mission)

Component	Reference nLam	Transition Re	Laminar nLam	ΔBF DM	ΔBF EM
Wing	5%	$6.6 \cdot 10^6$	24.3%	3.0%	1.8%
VTP	10%	$5 \cdot 10^6$	21.4%	0.4%	0.2%
HTP	10%	$5.6 \cdot 10^6$	44.8%	1.3%	0.9%

As shown in Table 7, the implementation of NLF resulted in an additional 19% of the wing's total wetted surface being laminarized. It is important to note, however, that laminar flow technologies were applied only to the wing's top surface (see Chapter 2.5.1). On the top surface alone, the NLF achieved a 29% increase in laminarity.

Furthermore, it was observed that up to 73% of the wing span, the transition was initiated by the flow reaching the transition Reynolds number. Beyond this span, the transition was driven by the pressure recovery limit, which was assumed to occur at 60% of the chord for all three components. As discussed in Chapter 2.5.2, the transition Reynolds number limit results in a transition line positioned at a constant distance from the leading edge. For the wing, these results indicate that the transition occurred at a distance of 1.1 m from the leading edge for sections up to 73% of the span.

Note that in this spanwise region, where the transition was governed by the transition Reynolds number limit up to 73% of the span, the wing's high aspect ratio of 15.6 enhanced the effectiveness of the NLF. This is because, for a given wing area, a higher aspect ratio results in shorter chord lengths across the span. Consequently, when the flow over a given section transitions at a specific distance from the leading edge, this distance represents a larger fraction of the chord as

the chord becomes shorter. As a result, if the transition of a component is determined by the transition Reynolds number limit, relatively high values of nLam can be achieved, provided the component's aspect ratio is sufficiently large.
Despite the wing's high aspect ratio, NLF achieved laminarization of only 21% of the root chord. This highlights the limited effectiveness of NLF in regions with high leading-edge sweep angles and large chord lengths, such as the inboard region of the wing.
Considering the VTP, Table 7 shows that implementing NLF on both sides of the component led to a laminarity increase of 11%. This relatively small improvement was primarily due to the VTP's high leading-edge sweep angle of 40.5 degrees, which resulted in the lowest transition Reynolds number among the three components. Combined with its low aspect ratio of 1.7, this caused the Reynolds number limit to determine the chordwise transition location across the entire span of the VTP, without the advantage of a high aspect ratio as observed in the case of the wing.
The high leading-edge sweep angle and low aspect ratio present a significant challenge in implementing NLF on the VTP, as both are employed to maximize its stall angle. Maintaining a sufficiently high stall angle is crucial to ensure that the VTP provides sufficient yaw stability and control, even in demanding flight scenarios. Consequently, these parameters cannot be significantly modified to enhance the amount of laminar flow achievable with NLF. This leads to the conclusion that NLF technology is generally incompatible with the design requirements of the VTP.
Finally, Table 7 indicates that the implementation of NLF on the HTP resulted in the largest laminarity enhancement among the three components, with an increase in nLam of 35%. This improvement can be attributed to the HTP's combination of a lower leading-edge sweep angle of 32.3° and a considerably higher aspect ratio of 6.2 compared to the VTP. As a result, the transition on the HTP was governed by the Reynolds number limit up to 73% of the span. Beyond this point, the transition was driven by the pressure recovery limit at 60% of the chord.

4.1.2 Effects and system penalties of HLFC

In the case of HLFC, the aerodynamic effects are more straightforward to interpret than those of NLF, as it was assumed that for all components, HLFC postpones the transition up to the pressure recovery point at 60% of the chord. However, HLFC influences the aircraft's performance not only through its aerodynamic effects but also through additional penalties in the form of power offtakes and increased masses of the individual subsystems. Table 8 presents these penalties, calculated for the separate HLFC subsystems described in detail in Chapter 3.2, and compares the nLam values before and after the application of the considered subsystem. Table 8 also highlights the overall changes in block fuel for both the design and evaluation missions, achieved by applying HLFC to the given component, relative to the baseline aircraft.

Table 8 Performance and penalties of HLFC subsystems on different components
(BF = Block fuel, DM = Design mission, EM = Evaluation mission)

Component	Reference nLam	HLFC nLam	Power Offtakes	System Mass	ΔBF DM	ΔBF EM
Wing	5%	32.9%	39.65 kW	268 kg	3.8%	2.2%
VTP	10%	49.7%	10.7 kW	72 kg	1.0%	0.6%
HTP	10%	48.7%	8.6 kW	59 kg	1.2%	0.7%

Table 8 indicates that, due to the same assumed chordwise location of the transition point, the nLam value achieved through the application of HLFC was similar across all components, including the wing's top surface, which attained an nLam of 47.5%. For HLFC, the extent of laminar flow over all components was reduced by the presence of turbulent wedges at the spanwise edges of each suction segment, as discussed in Chapter 2.5.3. This reduction was most pronounced for the wing, which featured three suction segments, in contrast to the HTP and VTP, both of which utilized only one suction segment (see Chapter 3.2.3). Similar to NLF, the total nLam of the wing was further reduced by the turbulent lower surface and the turbulent engine wake.
Regarding the masses and power offtakes of the individual HLFC subsystems, Table 8 shows the expected result that both values scale with the size of the component and the associated area over which suction is applied.

4.1.3 Selection of laminar flow technologies for individual components

Figures 11 and 12 summarize the reduction in block fuel achieved when the baseline aircraft was resized with the two laminar flow technologies applied individually to each component.

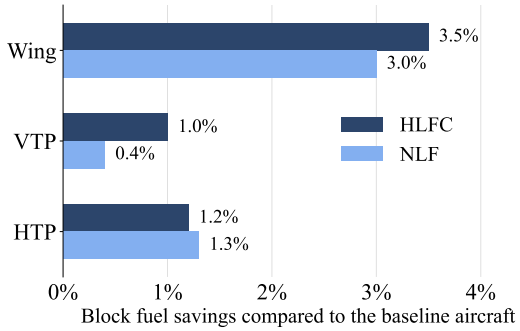

Fig. 11 Block fuel savings on design mission

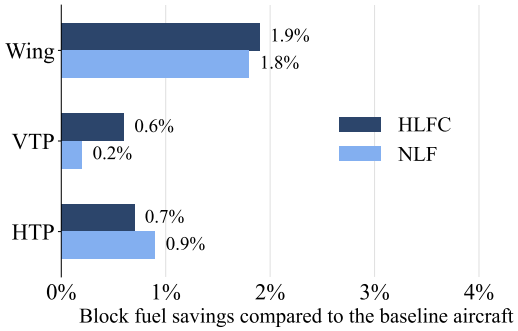

Fig. 12 Block fuel savings on evaluation mission

The first conclusion of this analysis is that if the NLF technology were to be applied to all components, the resulting block fuel savings would be 4.6% on the design mission and 2.9% on the evaluation mission. Similarly, the application of only HLFC would yield block fuel savings of 5.9% on the design mission and 3.4% on the evaluation mission.
At the component level, the results presented in Figure 11 and Figure 12 are consistent with the discussion in previous chapters regarding the different impact of the two technologies on the extent of laminar flow over the individual components. It is evident that both the wing and the VTP benefit from HLFC on both missions, with notable additional fuel savings compared to NLF. However, the situation differs for the HTP, where the NLF outperforms the HLFC on both missions. As discussed in Chapter 4.1.1, this resulted from the relatively low sweep and high aspect ratio of the HTP, which enabled NLF to achieve a value of nLam close to that delivered by HLFC, without the additional penalties of system mass and power off-takes.
It is further evident that the advantage of HLFC over NLF diminishes with a shorter range. This is due to the fact that the mass and power offtakes of the HLFC suction system remain the same regardless of the length of the cruise phase, while the fuel savings gained from the reduction in drag are proportional to the length of the cruise segments. Since NLF does not suffer from these additional penalties, its benefits do not decrease as fast with the shorter range as it is the case for the HLFC.

4.1.4 Estimation of block fuel benefits from combined application of laminar flow technologies

Based on the findings presented in Chapter 4.1.3, it was determined that HLFC should be utilized on the wing and the VTP, while NLF should be used on the HTP. The baseline aircraft DLR-F25 has been therefore resized with these technologies applied simultaneously. The resulting aircraft configuration is referred to as the "mixed configuration". Figures 13 and 14 compare the resulting block fuel savings with those obtained when the technologies were considered separately, on both the design and evaluation missions respectively.

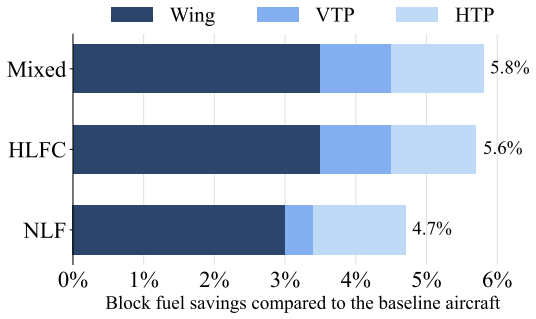

Fig. 13 Block fuel savings on design mission

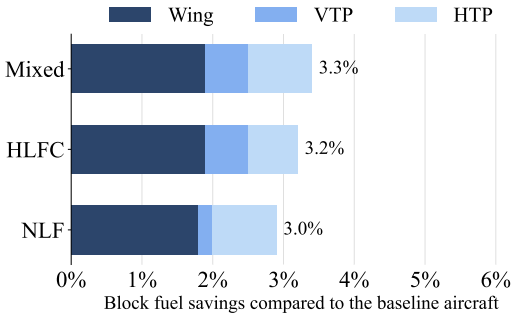

Fig. 14 Block fuel savings on evaluation mission

It can be observed that the combination of technologies in this case leads to an additional block fuel saving of 0.3% on both the design and evaluation mission compared to a pure HLFC configuration. Compared to pure NLF, the mixed configuration provides additional block fuel savings of 0.6% and 0.7% for the design and evaluation mission,

respectively.
While the magnitude of the additional fuel savings is not particularly large when compared to the pure HLFC option, the mixed configuration offers the additional benefit of eliminating an entire HLFC subsystem and the associated design, production and maintenance costs.
As part of this analysis, additional calculations were performed to determine whether a summation of the block fuel savings obtained from laminarizing the individual components would yield the same result as the full resizing calculation performed with all components laminarized simultaneously. The resizing of the DLR-F25 with all components laminarized at the same time demonstrated additional block fuel savings of 0.16% compared to the summation of benefits from the individual components. This difference can be attributed to the snowball effect and is considered sufficiently small to conclude that summing the savings from the individual components would be a safe and conservative practice for the initial estimation of savings at the aircraft level.

4.2 Sensitivity studies

To assess the impact of the most significant uncertainties in the employed methodology, a sensitivity analysis was performed for both laminar flow technologies. For NLF, the analysis evaluated variations in block fuel savings based on different assumed extents of achievable laminar flow. For HLFC, the sensitivity of block fuel savings was analyzed with respect to variations in wing subsystem mass and power offtakes.

4.2.1 Sensitivity of NLF fuel saving benefits to the extent of laminar flow

One of the primary sources of uncertainty in the presented work was the methodology employed for transition prediction in the context of NLF. The method, described in Chapter 2.5.2, was based exclusively on empirical data for the transition Reynolds number. While this data captured the two primary factors influencing transition, namely the leading-edge sweep and the Reynolds number, numerous additional factors, such as the component's relative thickness, nose radius, or surface finish, could not be considered. A sensitivity study was therefore conducted, in which the extent of laminar flow on individual components was varied through the nLam parameter. This was done in order to quantify the sensitivity of the results in terms of block fuel savings to this parameter.
The results of the sensitivity study are provided in Figure 15 and Figure 16 for the design and evaluation missions respectively.

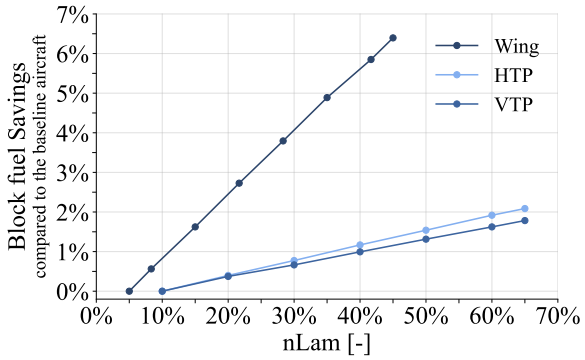

Fig. 15 nLam Sensitivity on the Design Mission

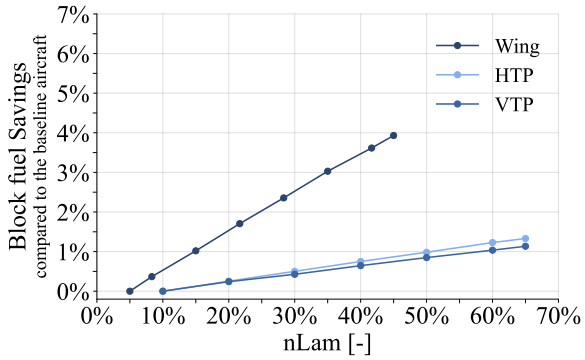

Fig. 16 nLam Sensitivity on the Evaluation Mission

The values of nLam considered in this analysis ranged from the reference value, which depended on the component, to 0.65. It should be noted that the curve for the wing does not reach this value because, unlike the empennage, only the value for the upper surface was varied while the lower surface remained turbulent. Using the Equation 4, a value of 0.65 for the upper surface combined with 0.05 for the lower surface gives a total value of nLam of 0.45, as seen in the figures. The maximum value of 0.65 for all components was chosen based on the reasoning that in the most optimistic case, the transition on each component would be caused by pressure recovery at 60% of the chord over the entire span of the component, resulting in nLam of 0.6. The value of 0.65 accounts for the potential scenario where future developments, such as novel airfoil designs, allow the pressure recovery to be shifted further downstream, up to 65% of chord.
The variation in the slope of the curves for individual components on a given mission results from the difference in the wetted areas of the components. For larger components, a given increase in nLam represents a larger increase in the

wetted area covered by laminar flow, a larger drag reduction, and therefore larger block fuel savings. The difference in the starting points of the curves for the wing and the empennage follows from the fact that a different reference (turbulent) value of nLam has been assumed for the wing (0.05 in contrast to 0.1 for the empennage), as discussed in Chapter 2.5.2. For a detailed explanation of the reasons behind the lower benefits observed during the evaluation mission, please refer to Chapter 4.1.3.
As demonstrated in Figure 15 and Figure 16, the block fuel savings increase linearly over the full range of nLam values investigated. Furthermore, while it is expected that greater fuel savings would result from laminarizing the component with the larger wetted area, the presented results offer insight into the actual magnitude of the difference, taking into account additional snowball effects.
Furthermore, the results of this sensitivity study are particularly valuable when considered in combination with the conclusion drawn in Chapter 4.1.3, which states that the overall fuel savings on the aircraft level can be reliably estimated by summing the benefits from laminarization of the individual components. As a result, the data presented in 15 and 16 can be used to effortlessly update any results obtained for the NLF technology in this study. If a more accurate information on the nLam values for any of the three components become available, the different potential block fuel reduction can be read of these figures. This is particularly relevant for the discussion in Chapter 4.1.3, where aircraft configuration utilizing only NLF was considered, as well as for the selection of laminar technologies for the different components.
The presented results also make it possible to calculate the extent of laminar flow that NLF would need to provide on individual components to match the fuel-saving benefits achieved through the use of HLFC. This is shown in 9 and 10, where the columns labeled "nLam req." present the values of nLam required for NLF to match the block fuel savings achieved by HLFC on the design and evaluation missions, respectively. The columns labeled "ΔnLam req." show the difference in nLam that these required values represent compared to the values actually observed for NLF on the given component.

Table 9 Performance comparison of NLF and HLFC on the design mission

Component	**ΔBF NLF**	**ΔBF HLFC**	**nLam NLF**	**nLam Req.**	**ΔnLam**
Wing	-3.0%	-3.8%	23.3%	28.4%	5.1%
HTP	-1.3%	-1.2%	44.8%	40.8%	-4.0%
VTP	-0.4%	-1.0%	21.4%	40.2%	18.8%

Table 10 Performance comparison of NLF and HLFC on the evaluation mission

Component	**ΔBF NLF**	**ΔBF HLFC**	**nLam NLF**	**nLam Req.**	**ΔnLam Req.**
Wing	-1.8%	-2.2%	23.3%	26.7%	3.4%
HTP	-0.9%	-0.7%	44.8%	38.0%	-6.8%
VTP	-0.2%	-0.6%	21.4%	37.9%	16.5%

The results show that this required increase in nLam is nearly identical across all three components and varies only between the two missions. This may be attributed to the consistent assumption of transition at 60% of chord for all HLFC subsystems or the global assumptions discussed in Chapter 3.2.2. Nevertheless, it can be concluded that for the aircraft under consideration, utilizing NLF on any of the three components provides the same benefit as HLFC, provided that 40% of the component's wetted area can be laminarized on the design mission and 38% on the evaluation mission. While for the wing, the required increase in laminarity of approximately 8% on the upper surface for the design mission could be considered as potentially achievable, the NLF on the VTP would require laminarization of an additional 19% of its wetted area. Taking into consideration the previously discussed design constraints for the VTP, this reinforces the conclusion that NLF is not a suitable option for application to this component. Lastly, the HTP has already been shown to satisfy the threshold nLam value to support the use of NLF. Therefore, Tables Figure 15 and Figure 16 in this case show that this choice of laminar flow technology would be justified even if NLF provided a 4% smaller extent of laminar flow on the design mission and up to a 7% on the evaluation mission.

However, it is important to note, that the ultimate selection of a laminar flow technology for a given component should not be based solely on the potential fuel savings. Additional factors, such as production and maintenance costs, risk and effects of contamination, and the potential impact of system failure, must also be considered.

4.2.2 Sensitivity of HLFC fuel saving benefits to the technology level

A sensitivity analysis was conducted in which the HLFC system sizing tool was removed from the aircraft sizing workflow and the power offtakes and mass of the wing subsystem were provided directly as independent inputs. The extent of laminar flow over the HTP and VTP was assumed to be the same as for the baseline aircraft.
The considered values for power offtakes and mass of the wing subsystem were obtained from Figure 17, which provides the values of both parameters as a function of the suction area, based on the results of previous studies.

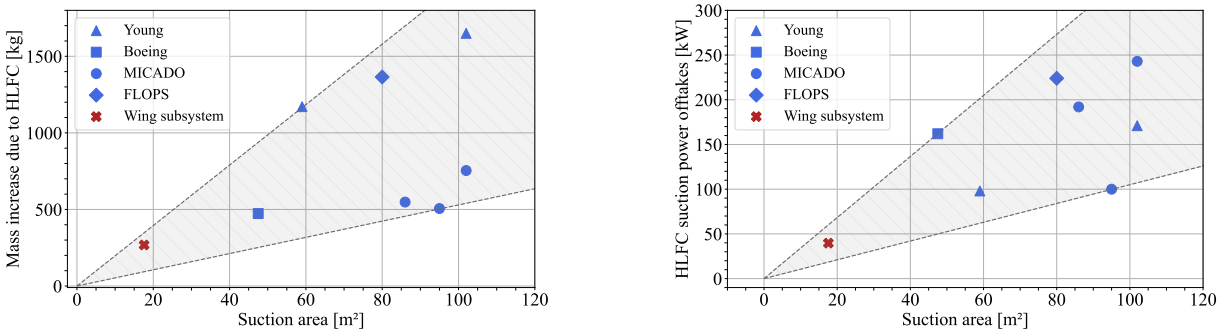

Fig. 17 Comparison of wing subsystem penalties compared to systems developed in previous works [43]

The highlighted points represent the results obtained for the wing subsystem, as described in Chapter 4.1.2. Figure 17 shows that the calculated results for both the mass and power of the wing subsystem, are situated well within in the region predicted, by Teichel et al. [29] for the considered suction area, based on previous works. This observation serves to validate the methodology employed in this study.
Furthermore, Figure 17 illustrates the observation made in the introduction that previous studies did not consider the application of the HLFC technology to smaller aircraft. This is evident from the absence of any reference points for the suction area sizes comparable to those considered in this work.
The sensitivity study was conducted with the system mass and power offtakes set at three values representing the upper boundary, lower boundary, and midpoint of the region defined by Figure 17 for the wing's suction area of 17.2m^2. Although a correlation between the two parameters might be anticipated, this study considered them as independent variables, resulting in nine combinations of mass and power offtakes for which the baseline aircraft was resized.
Tables 11 and 12 now show the calculated block fuel savings for the design and evaluation mission respectively.

Table 11 Block fuel savings - Design mission

Mass \ Power	20kW	40kW	60kW
90kg	-4.0%	-3.8%	-3.5%
220kg	-3.9%	-3.6%	-3.3%
350kg	-3.6%	-3.2%	-3.0%

Table 12 Block fuel savings - Evaluation mission

Mass \ Power	20kW	40kW	60kW
90kg	-2.4%	-2.2%	-2.0%
220kg	-2.2%	-2.0%	-1.8%
350kg	-2.0%	-1.7%	-1.6%

The results indicate that the maximum uncertainty in block fuel savings for the design mission is approximately ±0.5%. In the case of the evaluation mission, this value is reduced to ±0.4%.
Furthermore, recalling that applying NLF to the wing resulted in block fuel savings of 3.0% on the design mission and 1.8% on the evaluation mission (see Table 7 in 4.1.1), it can be observed that, for certain combinations of system masses and power off-takes, the block fuel savings achieved by the HLFC system are comparable to or even lower than those achieved by NLF. For the design mission, this occurs only for the combination of the highest mass and highest power offtakes, where the block fuel savings from NLF match the benefits of HLFC. For the evaluation mission, the NLF

system also matches the benefits of an HLFC system with a mass of 200 kg and power offtakes of 60 kW. However, it outperforms the HLFC systems with a mass of 350 kg and power offtakes of both 40 kW and 60 kW.

4.3 Combined application of HLFC and NLF on the wing

As the final step in the development of the laminar aircraft concept, the potential for combining the HLFC and NLF technologies on the wing was explored. The logic behind this investigation becomes evident when one considers the laminar regions that are present on the wing equipped solely with NLF. As it was observed in Chapter 4.1.3, beyond a certain spanwise location, the extent of laminar flow is constrained by the pressure recovery limit at the 60% of chord. Given that the pressure recovery was assumed to occur at the same chord percentage for both NLF and HLFC, it can be concluded that beyond this spanwise location, HLFC does not offer any additional laminarity benefits compared to the NLF. It can thus be concluded that additional fuel savings could be achieved if this region were laminarized via NLF instead of HLFC, which requires additional system power and mass. Furthermore, it is possible that the benefit could be further increased by extending the NLF region even more inboard. This is because the associated reduction in the mass and power penalties from the HLFC might outweigh the corresponding sacrifice in the extent of laminar flow.
The objective of this analysis was, therefore, to identify the optimal spanwise location where laminarization via HLFC should end and NLF should start, and to quantify the resulting benefit in block fuel savings when compared to configurations equipped with a wing featuring only one of the technologies at a time. Note that in this analysis, the extent of laminar flow over the HTP and VTP was assumed to be the same as on the turbulent baseline aircraft.
Furthermore, two HLFC system configurations were evaluated, with the objective of investigating the potential for further increasing the fuel savings and reducing the complexity of the suction system. Both configurations employed a single suction segment inboard of the engine, but while the first configuration featured two suction segments to laminarize the outboard wing, the second configuration used only one suction segment for this purpose. The two HLFC system configurations and their combination with NLF on the wing are visualized in Figures 18 and 19.

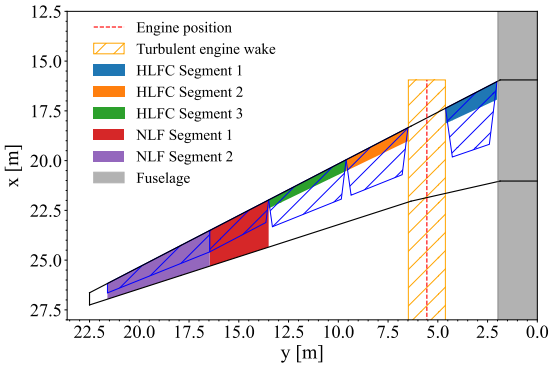

Fig. 18 Wing configuration with NLF and 3 HLFC suction segments

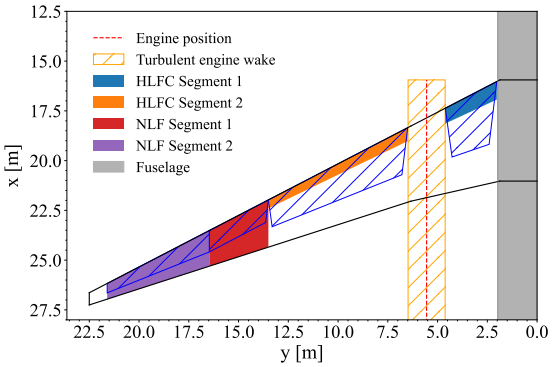

Fig. 19 Wing configuration with NLF and 2 HLFC suction segments

For the three-segment configuration, the spanwise location where the second suction segment ended and the third started was for in all scenarios selected, such as to achieve an equal suction area for both outboard segments. This is the same approach that was utilized when developing the pure HLFC wing subsystem, as described in Chapter 3.2.3. The NLF region was then assumed to extend from the spanwise location where the most outboard HLFC segment ended, up to the wing tip.
The base aircraft DLR-F25 was resized for a series of hybrid wing configurations, where "hybrid wing" refers to a wing laminarized by a combination of NLF and HLFC. These configurations differed in the spanwise location where the HLFC ended, beyond which the wing was laminarized by NLF up to the wing tip. This series of calculations was then performed twice: once utilizing the two-segment HLFC system and once utilizing the three-segment variant. Figure 20 presents the block fuel savings obtained for different proportions of HLFC and NLF on both the design and evaluation missions.

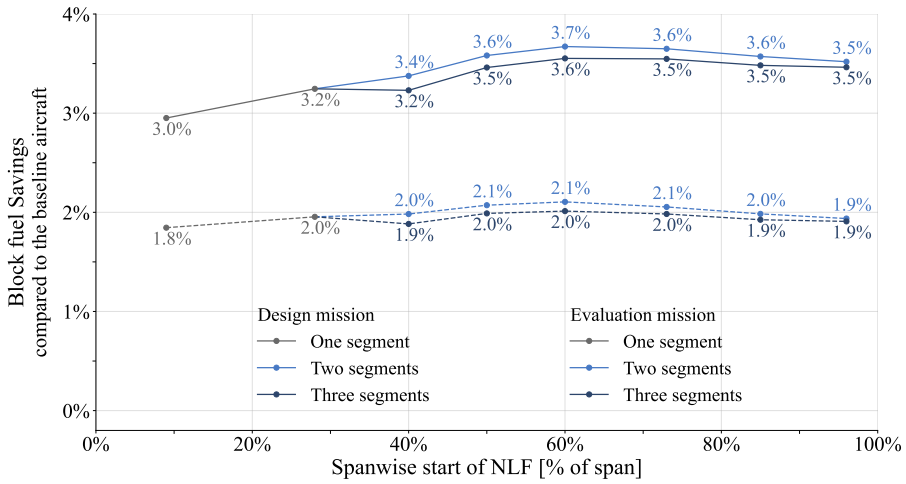

Fig. 20 Block fuel savings obtained for different hybrid wing configurations

The most left point of each curve in Figure 20 represents the scenario in which the wing is laminarized purely by NLF, while the point at the right end of each curve represents the pure HLFC scenario. The figure also presents two sets of curves for each mission, representing the two- and three-segment configurations previously described. The subsequent discussion applies equally to both missions.

Starting from the left end of the curves, additional block fuel savings are observed when the start of the NLF segment is shifted to 28% of span, the location of the inboard edge of the turbulent region behind the engine. These additional fuel savings are due to the first HLFC segment being introduced into the inboard wing. As a result, the transition in this region shifts from a fixed distance to the leading edge, determined by the Reynolds number limit, to the pressure recovery limit at 60% of the chord. As this is the segment of the wing with the largest chord lengths, this shift in the transition point results in a significant increase in laminarised area and therefore a significant reduction in drag. It is also apparent that the curves for the two HLFC system configurations are identical up to 28% point. This outcome is to be expected, given that the two HLFC system configurations differed only in the segments located outboard of the engine. Therefore, until the start of the NLF is shifted to the 40% of the span, the outboard wing is laminarized entirely by the NLF, while the inboard region is laminarized by a single HLFC segment, which was identical for both system configurations.

A notable drop in block fuel saving potential is observed for all curves when the start of the NLF segment is shifted to the 40% of the span. While the two-segment configuration continues to yield additional block fuel savings, this is not the case for the three-segment configuration. This is an effect of introducing the HLFC technology to the wing outboard of the engine-induced turbulent region. The reduction in block fuel savings potential results from the mass and power offtakes of the additional segments applied to the outer wing, combined with the relatively minor increase in laminarity provided by these segments. In the case of the three-segment configuration, the offtakes even negate the benefits completely, resulting in a performance that is inferior to that of the version with a single HLFC segment inboard of the engine.

As the start of the NLF is shifted further outboard, both configurations exhibit an increase in block fuel savings. This is due to the HLFC system providing sufficient additional laminar flow to offset the penalties and outperform NLF.

However, a local maximum in the block fuel savings is reached when the start of NLF is placed at 60% of span. Beyond this point, extending the HLFC segments leads to an increase in block fuel for both configurations. This indicates that when the HLFC is extended beyond 60% of the span, the increase in laminarity is insufficient to justify the additional mass and power penalties.

The observed optimal spanwise start location of the NLF region lies inboard of the point where transition on the NLF segments stops being driven by the transition Reynolds number limit and is instead caused by the pressure recovery. This point, identified to lie at 73% of the span in Chapter 4.1.1, is also visible in Figures 18 and 19. This confirms the previously stated hypothesis that sacrificing a small amount of laminar flow to reduce the extent of the HLFC system is beneficial, as the resulting reduction in additional mass and power off-takes outweighs the associated increase in drag.

Additionally, it can be observed that the 3-segment configuration consistently demonstrated lower benefits than the 2-segment configuration. However, the difference between the two configurations diminishes as the HLFC segments

are extended further outboard. In addition to the greater fuel savings, the two-segment configuration offers a notable reduction in the complexity of the system. This is achieved by the elimination of two suction panels, compressors, and motor drives, which would likely result in a considerable reduction in the system's production and maintenance costs. The resulting reduction in system mass was approximately 70 kg, representing a 26% decrease compared to the original wing subsystem, while the power off-takes were reduced by 11 kW, or 28%. Meanwhile the value of nLam decreased by mere 1.5%.
However, one potential disadvantage of the two-segment configuration is that a failure of the outboard suction segment would result in a more significant loss of laminar flow. Nevertheless, when all the factors were considered collectively, the two-segment option was still regarded as the more advantageous.

4.4 Final laminar aircraft concept

The final laminar aircraft concept was developed by applying the most suitable laminar flow technologies to the three components of the baseline aircraft, DLR-F25, based on the results presented in the previous chapters. Specifically, NLF was applied to the HTP, HLFC to the VTP, and a combination of both technologies to the wing. The hybrid wing, as developed in the previous chapter, incorporated an HLFC system with two suction segments extending to 60% of the span, while the remaining span was laminarized using NLF.
Table 13 now provides a comparison of key parameters for the baseline aircraft DLR-F25, which served as the starting point in this process, to those of the final laminar aircraft.

Table 13 Updated comparison of the key characteristics of the laminar aircraft concept to the DLR-F25. Parameters marked by (*) were fixed and not altered in the sizing process.

Key Sizing Parameters	**Unit**	**DLR-F25**	**Laminar Aircraft**	**Delta %**
W/S=MTOM/Sref	kg/m^2	658.18	653.77	-0.7%
T/W=SLST/MTOM	-	0.286	0.286	+0.0%
Masses				
Max. Take-Off Mass	t	85.2	84.7	-0.6%
Max. Landing Mass	t	73.8	73.8	+0.1%
Max. Zero Fuel Mass	t	70.9	71.1	+0.3%
Operating Empty Mass	t	45.9	46.1	+0.4%
Max. Fuel Mass	t	16.5	16.6	+0.1%
Block Fuel (Design Range)	t	12.0	11.3	-5.9%
Block Fuel (Evaluation Range)	t	4.1	4.0	-3.4%
Systems mass	t	4.9	5.2	+5.8%
Geometry				
Wing Span*	m	45	45	0.0%
Wing Aspect Ratio	-	15.6	15.6	-0.1%
Wing Ref. Area	m^2	129.4	129.5	+0.1%
Propulsion				
Eq. static thrust (Sea-level/ISA)	kN	119.5	118.8	-0.6%
TSFC cruise average (800nm)	g/s/kN	14.2	14.4	+1.6%
Power offtakes at cruise	kW	50.0	89.4	+78.8%
Aerodynamics				
cL cruise (800nm)	-	0.592	0.593	+0.1%
cD cruise (800nm)	-	0.0300	0.0275	-8.4%
L/D cruise average (800nm)	-	19.7	21.6	+9.3%

Table 13 shows that the total block fuel savings were 3.7% on the design mission and 2.1% on the evaluation mission. These savings result from the observed 9.3% increase in lift-over-drag ratio, driven by a reduction in drag of 8.4%, due to the decrease in friction drag achieved through the application of laminar flow technologies.
Furthermore, the operating empty mass increased by 0.4%, primarily due to the additional mass of the HLFC subsystems, which is also reflected in the increased systems mass. Additionally, the thrust-specific fuel consumption increased by 1.6% as a result of the additional power offtakes. The wing geometry remained essentially unchanged, while all masses that do not consider the mass of the fuel increased due to the mentioned increase in the operational empty mass. Finally, a slight reduction in thrust is observed, by 0.2%. This is due to the fact that the engine was sized by the takeoff-field length requirement of 2200m. A reduction in the maximum takeoff mass, resulting from the decrease in fuel mass, therefore led to a slight reduction in the required takeoff thrust. The smaller thrust requirement then also resulted in a slight decrease in the engine mass, which lowered the final increase in the operational empty mass.
Considering the overall performance, the payload-range diagram (PRD) in Figure 21 illustrates the improved efficiency of the laminar aircraft compared to the baseline aircraft.

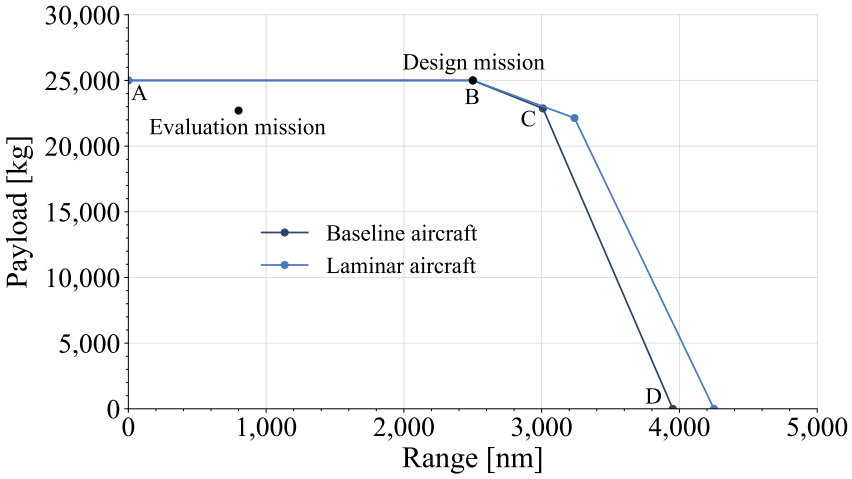

Fig. 21 Payload-range diagram comparison

In Figure 21, the increased efficiency of the laminar aircraft is evident in segment B-C, where the aircraft operates at the MTOM. The higher efficiency allows the laminar aircraft to cover longer distances for the same additional fuel mass obtained by reducing the payload mass. This is reflected in the lower slope of segment B-C for the laminar aircraft.
Additionally, due to its higher efficiency, the laminar aircraft requires less fuel to perform the design mission, allowing its fuel tanks to be filled to a lower percentage of their total volume. However, the total fuel tank volume is virtually identical between the two aircraft. The extra free space in the fuel tanks enables a trade-off between payload and additional fuel at point C, resulting in a lower payload mass (approximately 730 kg less) and a higher range (around 230 nm more) for the laminar aircraft.
The higher fuel efficiency of the laminar aircraft is also evident in the reduced slope of segment C-D, resulting in an increase in ferry range (point D) by approximately 300 nm.
Finally, Figure 22 provides a comparison of various flight performance parameters between the laminar and baseline aircraft during the evaluation mission.

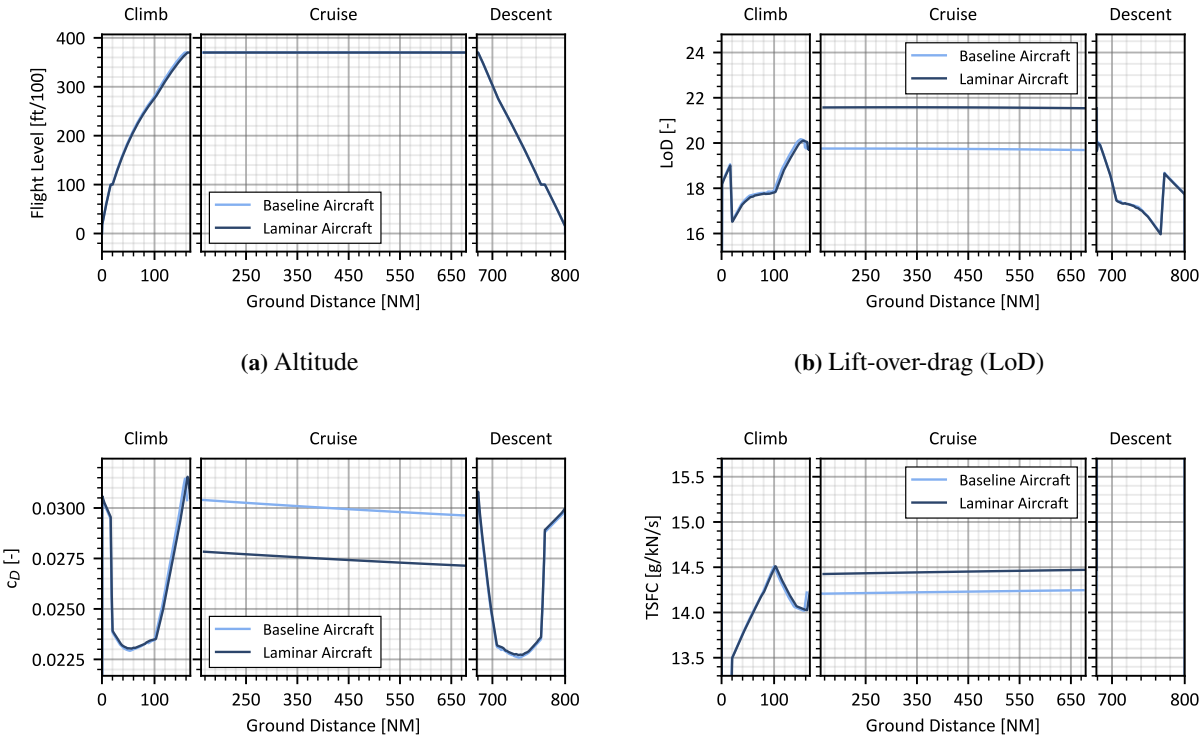

(a) Altitude

(b) Lift-over-drag (LoD)

(c) Drag coefficient (C_D)

(d) Thrust-specific fuel consumption (TSFC)

Fig. 22 Flight performance comparison between the baseline and the laminar aircraft on the evaluation mission

Figure 22a illustrates that no altitude change occurred during the cruise phase of the evaluation mission. Figure 22c depicts the reduction in drag coefficient during cruise, where both NLF and HLFC systems were considered operational, while also confirming that the aircraft was assumed to operate in a fully turbulent regime during the other flight phases. The reduction in cruise drag is further reflected in the increase in cruise lift-over-drag ratio shown in Figure 22b. Note that the cruise lift coefficient did not differ significantly between the two aircraft, as shown in Table 13. Lastly, Figure 22d highlights the higher TSFC of the laminar aircraft, attributed to the power offtakes from the HLFC subsystems applied to the wing and VTP.
A three view of the final laminar aircraft concept, along with its most important dimensions, is shown in Figure 23.

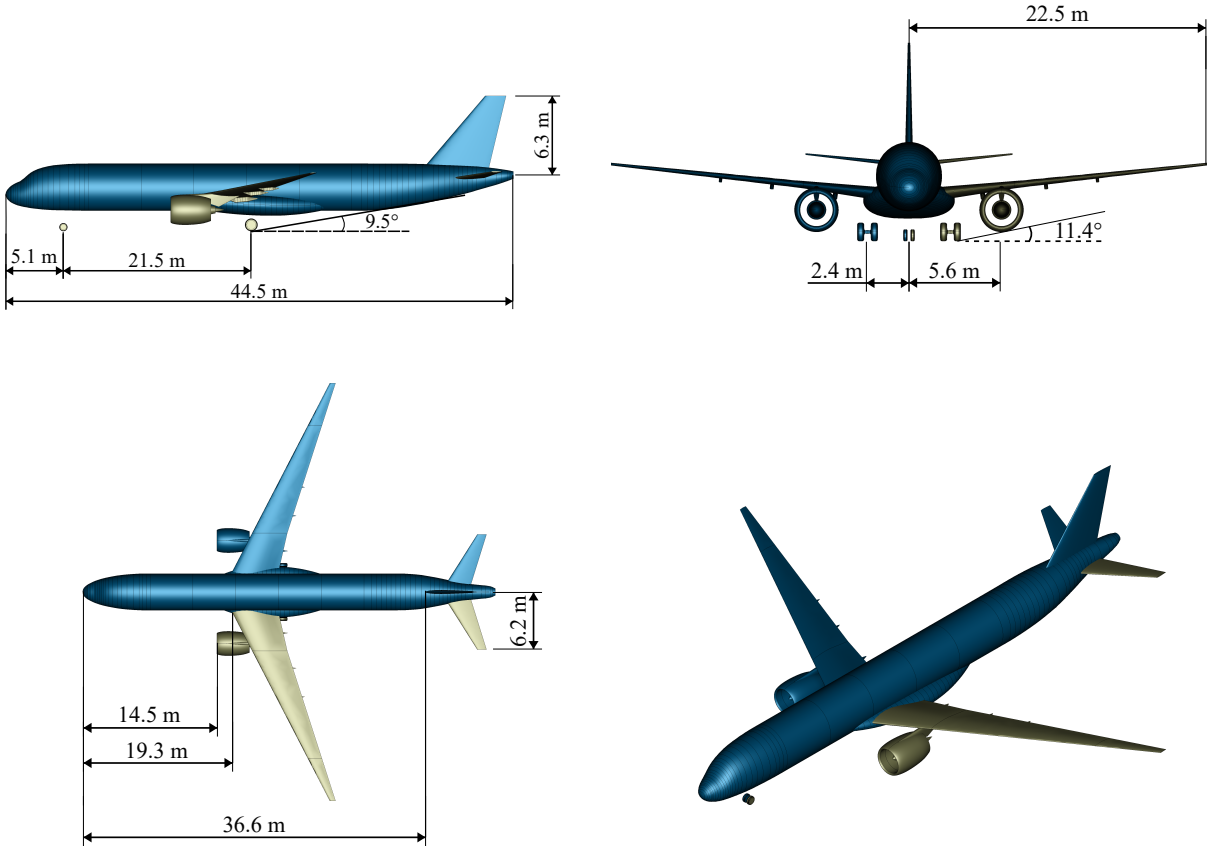

Fig. 23 Three view of the developed laminar aircraft concept

4.5 Failure Analysis

After obtaining the final laminar configuration by selecting the most suitable laminar technology for each component and performing the aircraft sizing process, the obtained converged aircraft design was subjected to failure analysis. The goal of this analysis was to determine the increase in block fuel resulting from different failure scenarios of the two laminar flow technologies on the different components. Knowledge of the potential impact of these failure scenarios is a critical starting point for developing appropriate mitigation strategies, defining the most suitable fueling policies, and evaluating the overall economic feasibility of the aircraft. Note that in this analysis, the aircraft design was considered fixed and was no longer resized, nor were the laminar technologies altered in any way. Rather than its design, the performance of the laminar aircraft was the focus point in this stage of the research.

The calculations were performed using a custom RCE workflow, which took the CPACS definition file of the converged laminar aircraft, and substituted its cruise aerodynamic polars and cruise engine performance data for versions that represented a specific failure scenario. The new aircraft file with the new aerodynamic polars and engine performance data was then forwarded to an instance of the mission analysis tool, which calculated the new fuel mass required for the evaluation mission. The evaluation mission was selected for this analysis as it represents the mission on which the aircraft is expected to operate most frequently, thereby ensuring that the outcomes of this analysis address scenarios most likely to be observed in real-world operations. The result of the calculation for each failure scenario was then the takeoff fuel required to perform the full mission with the given failure. As such, the results presented here represent scenarios where the failure is known prior to take-off and the amount of fuel onboard is adjusted accordingly. Therefore, the resulting increase in block fuel also includes the effect of the extra fuel mass. Since this approach produces a conservative estimation of the additional fuel required, the results still considered as a valuable first indication of the magnitude of the effects of different failures on the aircraft's fuel consumption that can provide a useful insight for the

top-level contingency planning.
Note that it would not be possible to directly apply the described methodology for failure analysis to the design mission, as the aircraft was sized by OpenAD under the assumption that the design mission is flown at the MTOM. Consequently, accounting for the additional take-off fuel required for the failure would result in a take-off mass exceeding the MTOM. Finally, for all considered scenarios, it was assumed that the failure would affect the entire cruise phase, the only mission phase where laminar technologies were considered to impact the aircraft's performance. This approach was taken to assess the most critical scenarios and maintain consistency with the assumption that the failure would be known prior to take-off.
The Table 14 now presents the calculated difference in block fuel for all failure scenarios considered, ordered by their magnitude, and with respect to both the fully functional laminar aircraft and the turbulent baseline.

Table 14 Calculated block fuel increase for different failure scenarios

Index	**Scenario**	**ΔBF Laminar**	**ΔBF Baseline**
1	Fully turbulent aircraft with offtakes	+4.1%	+0.7%
2	Fully turbulent aircraft without offtakes	+3.8%	+0.4%
3	Complete HLFC failure with offtakes	+2.6%	-0.8%
4	Complete HLFC failure without offtakes	+2.3%	-1.1%
5	Wing HLFC failure with offtakes	+1.9%	-1.5%
6	Wing HLFC failure without offtakes	+1.7%	-1.8%
7	Contamination of all NLF surfaces	+1.5%	-2.0%
8	Wing NLF surface contamination	+0.7%	-2.7%
9	HTP NLF surface contamination	+0.7%	-2.7%
10	VTP HLFC failure with offtakes	+0.7%	-2.7%
11	VTP HLFC failure without offtakes	+0.6%	-2.8%

These scenarios represent combinations of three potential types of failures. The first possible failure is one in which the HLFC on a given component is no longer capable of postponing transition, yet the compressors remain operational, consuming electrical power. The second possibility is that the failure is identified and the compressors are deactivated, either manually by the pilots or automatically by a control system. This type of failure would also result in drag increase, but its effect on the fuel consumption should be partially offset by the decrease in power offtakes from the engines. Finally, a contamination of an NLF surface is the third failure type, causing a turbulent flow over the component but not affecting the engine offtakes.
It should be noted that a full loss of laminarity over the failed component was assumed for all three types of failure. In future studies, it would be beneficial to consider partial reductions in laminarity, such as those resulting from the failure of only one suction panel or only partial contamination of the surface.
Considering now the results in Table 14, as anticipated, the two scenarios leading to the largest increase in block fuel are those where all surfaces equipped with laminar technologies are assumed to operate in a turbulent regime. This results in an additional 4.1% and 3.8% of fuel required compared to the fully functional laminar aircraft, with and without HLFC offtakes respectively. This case represents the most severe case of surface contamination, which would affect all components. Such contamination could result from flying through an insect swarm or a volcano cloud.
Here it is crucial to note that the quantity of additional fuel exceeds the reserve fuel, defined by regulation as 3% of the total block fuel. This implies that if the aircraft were designed to complete the evaluation mission under the most severe failure scenario, it would require approximately 1.1% of additional fuel, not accounting for the potential snowball effect.
The next two scenarios represent situations in which all HLFC systems fail, while all NLF surfaces remain laminar. This is deemed an improbable occurrence, as the HLFC subsystems at individual components are largely independent of one another. Therefore, their collective failure would require a complete loss of power by the aircraft.
The same line of reasoning may then be extended to the scenario with a complete failure of the wing's HLFC system. This is due to the fact that individual suction segments are equipped with independent compressors, thereby minimizing the likelihood of a collective failure.
The contamination of all NLF surfaces represents the next most critical failure case. This type of failure could occur

if, for example, maintenance in the form of cleaning of the surfaces was neglected for an extended period, leading to the accumulation of contamination particles on the NLF surfaces. This scenario also assumes that the HLFC surfaces are equipped with an anti-contamination system or are inherently less susceptible to contamination. The remaining scenarios then represent failures of the laminar technologies on the individual components.
Based on these findings, the following conclusions can be drawn:

- In the worst-case and extremely unlikely scenario of a combined failure of all HLFC systems with power off-takes still present, along with contamination of all NLF surfaces, the required block fuel would increase by 4.1% (scenario 1).
- The laminar aircraft concept outperforms the baseline aircraft in terms of block fuel required in all considered failure scenarios, except for the highly improbable operation in a fully turbulent regime (Scenarios 1 and 2).
- Turning off a failed HLFC subsystem is not critical. Even in the extremely improbable event of a failure of all HLFC subsystems, the fuel increase is reduced by only 0.3% when all compressors are turned off (Scenarios 3 and 4).
- The largest expected increase in block fuel due to the failure of a single HLFC subsystem is 1.9%, occurring in the case a the highly improbable failure of the full wing subsystem with power off-takes still present (Scenario 5).
- The maximum expected increase in block fuel resulting from the possible contamination of all NLF surfaces is 1.5% (Scenario 7).
- The most probable increase in block fuel resulting from the failure of any laminar technology on a single component is approximately 0.7% (Scenarios 8-11).

5 Conclusion

This study aimed to determine the realistic block fuel savings achievable through the combined application of NLF and HLFC technologies in a short-to-medium range aircraft, assumed to enter service in 2035. The evaluation considered the integration of laminar flow technologies during the aircraft's conceptual design phase, using a fixed set of TLARs identical to those of an existing aircraft in the same market sector. The results revealed an overall potential for block fuel savings of 5.9% on the design mission and 3.4% on the evaluation mission. These findings indicate that, contrary to common belief, laminar flow technologies can provide significant fuel-saving benefits even for short-range aircraft.
Furthermore, this work demonstrated that selecting the most appropriate laminar flow technology for different components allows for a reduction in the extent of HLFC systems, leading to lower complexity and a slight enhancement in fuel efficiency. Similarly, it was shown that additional fuel savings and complexity reductions can be achieved through a strategic combination of NLF and HLFC on the wing. The observed benefits of combining laminar flow technologies at both the aircraft and component levels provide strong motivation for further investigation of this approach.
Finally, a failure analysis concluded that the most probable scenario of a partial loss of laminarity would result in a block fuel increase of 0.7%. The most severe failure of a single HLFC subsystem was evaluated to cause an additional 1.7% increase in block fuel, while contamination of all NLF surfaces would lead to a 1.5% increase. These estimations of the potential block fuel increase due to various failure scenarios provide a foundation for more detailed evaluations of fuel planning strategies for laminar aircraft.
The methodology of this study was primarily limited by the absence of higher-fidelity aerodynamic calculations, which would have allowed for more reliable prediction of transition. For HLFC, an additional limitation resulted from the need to rely on reference data from previous HLFC concepts to determine the required suction levels. The combination of these constraints also meant that the relationship between the amount of suction applied and the resulting transition location on components equipped with HLFC could not be captured. These limitations were, however, addressed by conducting sensitivity studies, the results of which could be utilized in the future to readily update the findings of this work if more accurate transition or suction performance data become available.
Regarding the potential for extending the results of this work, future studies should investigate the influence of cruise flight conditions, specifically altitude and Mach number. This would allow for assessing whether altering these parameters could lead to further block fuel savings, considering the associated variations in the required suction levels. Additionally, future research should explore both the potential and feasibility of passive HLFC systems, which promise to eliminate power off-take penalties entirely and further reduce system complexity. Detailed aerodynamic simulations are also necessary to confirm the feasibility of applying NLF in the wingtip region, with particular attention to the risks of tip stall and boundary layer contamination caused by flow disturbances propagating from the inboard region of the wing. Finally, evaluations comparable to this study could be extended to additional aircraft configurations, such as those featuring forward-swept or truss-braced wings, which are particularly suitable for the application of laminar flow technologies.

References

[1] Xu, J., and Kroo, I., "Aircraft Design with Active Load Alleviation and Natural Laminar Flow," *Journal of Aircraft*, Vol. 51, No. 5, 2014, pp. 1532–1545. https://doi.org/10.2514/1.c032402.

[2] Allison, E., Kroo, I., Sturdza, P., Suzuki, Y., and Martins-Rivas, H., *Aircraft conceptual design with natural laminar flow*, 2010.

[3] Kruse, M., Wunderlich, T., and Heinrich, L., "A conceptual study of a transonic NLF transport aircraft with forward swept wings," , 2012. https://doi.org/10.2514/6.2012-3208, URL https://www.scopus.com/inward/record.uri?eid=2-s2.0-84878559661&doi=10.2514%2f6.2012-3208&partnerID=40&md5=3d1ad05ccb4c4d06c77271700d7fb15d.

[4] Zhao, Y., Chen, H., and Zhang, Y., *An Aircraft Conceptual Design and Optimization Platform and Its Application for Nature Laminar Flow Aircraft Study*, 2015. https://doi.org/10.2514/6.2015-0516.

[5] Fan, Z., Yu, X., Qin, N., and Zhu, M., "Benefit Assessment of Low-Sweep Transonic Natural Laminar Flow Wing for Commercial Aircraft," *Journal of Aircraft*, Vol. 58, No. 6, 2021, pp. 1294–1301. https://doi.org/10.2514/1.C036138, URL https://doi.org/10.2514/1.C036138.

[6] Seitz, A., Hübner, A., and Risse, K., "The DLR TuLam project: design of a short and medium range transport aircraft with forward swept NLF wing," , 2020. https://doi.org/10.1007/s13272-019-00421-1, URL https://www.scopus.com/inward/record.uri?eid=2-s2.0-85073943417&doi=10.1007%2fs13272-019-00421-1&partnerID=40&md5=26a05462c144abc467b5094b34cc40d6.

[7] Karpuk, S., Radespiel, R., and Elham, A., "Assessment of Future Airframe and Propulsion Technologies on Sustainability of Next-Generation Mid-Range Aircraft," *Aerospace*, Vol. 9, No. 5, 2022, p. 279. https://doi.org/10.3390/aerospace9050279.

[8] Chiba, T., and Rinoie, K., "Integrated conceptual design method considering advanced aircraft systems and aircraft trajectory," International Council of the Aeronautical Sciences, University of Tokyo, Tokyo, 113-8656, Japan, 2016. URL https://www.scopus.com/inward/record.uri?eid=2-s2.0-85013670980&partnerID=40&md5=e63252242ec8058bf7e04e9d96a3caf2.

[9] Wilson, R., "The Introduction of Laminar Flow to the Design and Optimisation of Transport Aircraft," Phd thesis, Mar. 1997. URL https://books.google.de/books?id=u66D0AEACAAJ.

[10] Effing, T., Schültke, F., and Stumpf, E., "HLFC-optimized retrofit aircraft design of a medium-range reference configuration within the AVACON project," *CEAS Aeronautical Journal*, Vol. 12, No. 2, 2021, pp. 441–456. https://doi.org/10.1007/s13272-021-00510-0, URL https://doi.org/10.1007/s13272-021-00510-0.

[11] Effing, T., Schmitz, V., Schültke, F., Peter, F., and Stumpf, E., "Combined Application of Hybrid Laminar Flow Control and Variable Camber in Preliminary Aircraft Design," International Council of the Aeronautical Sciences, Bauhaus Luftfahrt e.V., Willy-Messerschmitt-Str. 1, Taufkirchen, 82024, Germany, 2022, pp. 106–126. URL https://www.scopus.com/inward/record.uri?eid=2-s2.0-85159616916&partnerID=40&md5=f0f365d966a99cc1352d97d935d2e0ff.

[12] Young, T. M., "An investigation into potential fuel savings for 110-130 seat passenger transport aircraft due to the incorporation of natural laminar flow or hybrid laminar flow control on the engine nacelles," *Proceedings of the Institution of Mechanical Engineers, Part G: Journal of Aerospace Engineering*, Vol. 227, No. 8, 2013, pp. 1300–1324. https://doi.org/10.1177/0954410012454812, URL https://www.scopus.com/inward/record.uri?eid=2-s2.0-84883711523&doi=10.1177%2f0954410012454812&partnerID=40&md5=4fff713a7d32f59fad6fc74662b2efbd.

[13] Young, T. M., "Fuel sensitivity analyses for active drag reduction systems," *The Aeronautical Journal*, Vol. 108, No. 1082, 2004, pp. 215–221. https://doi.org/10.1017/s0001924000000129.

[14] T.Pe, F. T., "Synthesis and Topology Study of HLFC System Architecturesin Preliminary Aircraft Design," *3rd CEAS Air&Space Conference, 21st AIDAA Congress*, 2011.

[15] Kalarikovilagam Sri, G., and Bertram, O., "Assessment of a Chamberless active HLFC system for the vertical tail plane of a mid-range transport aircraft," *Deutscher Luft- und Raumfahrtkongress 2017*, 2017. URL https://elib.dlr.de/113848/.

[16] Kalarikovilagam Sri, G., and Bertram, O., "Preliminary Design and System Considerations for an Active Hybrid Laminar Flow Control System," *Aerospace*, Vol. 6, No. 10, 2019. URL https://elib.dlr.de/129642/.

[17] Risse, K., "Preliminary overall aircraft design with hybrid laminar flow control," Phd thesis, Technischen Hochschule Aachen, Aug. 2016. https://doi.org/10.18154/RWTH-2017-00974.

[18] Risse, K., and Stumpf, E., "Conceptual aircraft design with hybrid laminar flow control," *CEAS Aeronautical Journal*, Vol. 5, No. 3, 2014, pp. 333–343. https://doi.org/10.1007/s13272-014-0111-6, URL https://www.scopus.com/inward/record.uri?eid=2-s2.0-84921403820&doi=10.1007%2fs13272-014-0111-6&partnerID=40&md5=bf9d38e834b0f8ade1cd8d9907bafc87.

[19] Streit, T. S., Seitz, A., Hein, S., and Kunze, P., "NLF Potential of Laminar Transonic Long Range Aircraft," *AIAA Aviation 2020 Forum*, American Institute of Aeronautics and Astronautics, 2020. https://doi.org/10.2514/6.2020-2748.

[20] Arcara, P. C., Bartlett, D. W., and McCullers, L. A., "Analysis for the Application of Hybrid Laminar Flow Control to a Long-Range Subsonic Transport Aircraft," *SAE Technical Paper Series*, SAE International, 1991. https://doi.org/10.4271/912113.

[21] Graver, B., Rutherford, D., and Zheng, S., "CO2 Emissions from Commercial Aviation - 2013, 2018, and 2019," Tech. rep., The International Council on Clean Aviation, 2020.

[22] Boden, B., Flink, J., Först, N., Mischke, R., Schaffert, K., Weinert, A., Wohlan, A., and Schreiber, A., "RCE: An Integration Environment for Engineering and Science," *SoftwareX*, Vol. 15, 2021, p. 100759. https://doi.org/10.1016/j.softx.2021.100759, URL https://www.sciencedirect.com/science/article/pii/S2352711021000820.

[23] Alder, M., Moerland, E., Jepsen, J., and Nagel, B., "Recent Advances in Establishing a Common Language for Aircraft Design with CPACS," *Aerospace Europe Conference 2020*, 2020.

[24] Wöhler, S., Atanasov, G., Silberhorn, D., Fröhler, B., and Zill, T., "Preliminary Aircaft Design within a Multidisciplinary Andmultifidelity Design Environment," *Aerospace Europe Conference 2020*, 2020.

[25] Torenbeek, E., *Advanced aircraft design*, Aerospace series, John Wiley Sons Inc, Chichester, West Sussex, United Kingdom, 2013. Includes bibliographical references and index.

[26] Raymer, D. P., *Aircraft design: a conceptual approach*, sixth edition ed., AIAA education series, American Institute of Aeronautics and Astronautics, Inc., Reston, VA, 2018. Includes bibliographical references and index.

[27] Anderson, J. D., *Aircraft Performance Design*, The McGraw-Hill Companies, 2012.

[28] Roskam, J., *Roskam*, 4^{th} ed., Vol. 1, DARcorporation, Lawrence, Kansas, 2005.

[29] Teichel, S. H., Dörbaum, M., Misir, O., Merkert, A., Mertens, A., Seume, J. R., and Ponick, B., "Design considerations for the components of electrically powered active high-lift systems in civil aircraft," *CEAS Aeronautical Journal*, Vol. 6, No. 1, 2014, pp. 49–67. https://doi.org/10.1007/s13272-014-0124-1.

[30] Seitz, A., and Horstmann, K.-H., "Design Studies on NLF and HLFC Applications at DLR," *ICAS 2010*, Conference Proceedings, Vol. 27, edited by I. Grant, International Council of the Aeronautical Sciences, 2010. URL https://elib.dlr.de/78537/.

[31] Fröhler, B., Pohya, A. A., Häßy, J., Kilian, T., Bismark, A. H., Radestock, M., and Cruz, D., "Performance and Economic Assessment of a Wing-Integrated Hybrid Laminar Flow Control System," *34th Congress of the International Council of the Aeronautical Sciences, ICAS 2024.*, 2024.

[32] van de Kamp, B., Kleineberg, M., and Schroder, A., "Hybrid Laminar Flow Control ready for Series Application," *Aerospace Europe Conference 2023 – 10 EUCASS – 9 CEAS*, 2023. https://doi.org/10.13009/EUCASS2023-647.

[33] Sebastian Wöhler, V. K., Jannik Häßy, "Establishing the DLR-F25 as a Research Baseline Aircraft for the Short-Medium Range Market in 2035," *ICAS 2024, Florence*, 2024.

[34] Airbus, "Aircraft Characteristics, Airport and Maintenance Planning, A321," , 2024. URL https://aircraft.airbus.com/sites/g/files/jlcbta126/files/2023-02/Airbus-techdata-AC_A321_0322(2).pdf.

[35] Young, T. M., Humphreys, B., and Fielding, J. P., "Investigation of hybrid laminar flow control (HLFC) surfaces," , 2001. https://doi.org/10.1016/S1369-8869(01)00010-6, URL https://www.scopus.com/inward/record.uri?eid=2-s2.0-0035355482&doi=10.1016%2fS1369-8869%2801%2900010-6&partnerID=40&md5=5fb0334c35f13817d47bcef52b1ce6b6.

[36] Kilian, T., and Horn, M., "Verification of a chamberless HLFC design with an outer skin of variable porosity," *CEAS Aeronautical Journal*, Vol. 12, No. 4, 2021, pp. 835–845. https://doi.org/10.1007/s13272-021-00528-4.

[37] Schrauf, G., and von Geyr, H., "Hybrid Laminar Flow Control on A320 Fin: Retrofit Design and Sample Results," *Journal of Aircraft*, Vol. 58, No. 6, 2021, pp. 1272–1280. URL https://elib.dlr.de/146436/.

[38] Schrauf, G., and von Geyr, H., "Simplified Hybrid Laminar Flow Control for the A320 Fin Aerodynamic and System Design - First Results," *AIAA Scitech 2020 Forum*, 2020. URL https://elib.dlr.de/133922/.

[39] Schrauf, G., and Frhr. von Geyr, H., "Simplified hybrid laminar flow control for transport aircraft," *ECCOMAS 2012 - European Congress on Computational Methods in Applied Sciences and Engineering, e-Book Full Papers*, 2012, pp. 3831–3842.

[40] Horn, M., SEITZ, A., and SCHNEIDER, M., "Novel tailored skin single duct concept for HLFC fin application," 2017. https://doi.org/10.13009/EUCASS2017-44.

[41] Henke, R., ""A 320 HLF Fin" flight tests completed," *Air & Space Europe*, Vol. 1, No. 2, 1999, pp. 76–79. https://doi.org/10.1016/S1290-0958(99)80019-7, URL https://www.sciencedirect.com/science/article/pii/S1290095899800197.

[42] Grasmeyer, J., Naghshineh-Pour, A., Tetrault, P.-A., Grossman, B., Haftka, R., Kapania, R., Mason, W., and Schetz, J., "Multidisciplinary Design Optimization of a Strut-Braced Wing Aircraft with Tip-Mounted Engines," 1998.

[43] Pohya, A. A., Wicke, K., and Kilian, T., "Introducing variance-based global sensitivity analysis for uncertainty enabled operational and economic aircraft technology assessment," *Aerospace Science and Technology*, Vol. 122, 2022, p. 107441. https://doi.org/10.1016/j.ast.2022.107441.

Part II

Literature review

1 Aerodynamics of laminar flow

Certain elementary aerodynamic concepts require a brief explanation to understand the working principles of the investigated technologies and the associated benefits, drawbacks, and limitations. A general discussion of these concepts is the purpose of this chapter, which covers the basics of viscous flow, laminar-turbulent transition, and instability mechanism. Finally, this section presents an overview of the various techniques for achieving and maintaining laminar flow.

1.1. Fundamentals of boundary layer flow

When a viscous fluid flows around a body at a given velocity, for example, a wing of an aircraft, the friction between them causes the relative velocity of the fluid at the surface to be zero. This phenomenon is called a zero-slip condition. The fact that the fluid is viscous means that shear forces develop between the adjacent layers of fluid that have different velocities relative to each other. These shear forces create a thin layer of fluid close to the body. As the distance from the surface decreases, the velocity of the fluid gradually decreases from free-stream velocity to zero at the surface itself. This layer, known as a boundary layer Figure 1.1, shows a typical flow velocity variation with distance from the surface, a so-called velocity profile. Figure 2.1 provides a schematic visualization of both of these phenomena:

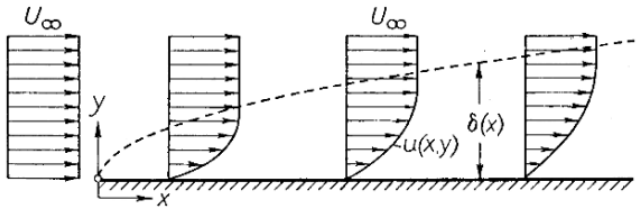

Figure 1.1: Schematic boundary layer and velocity profile at a flat plate at zero incidence [1]

Another crucial characteristic of any viscous flow is the Reynolds number, which represents this ratio between the inertial and viscous forces:

$$Re = \frac{\rho U_\infty l}{\mu} = \frac{U_\infty l}{\nu} \tag{1.1}$$

Where ρ is the fluid density, U_∞ the free-stream velocity, l is the characteristic length (chord in the case of wings), μ is the dynamic viscosity, and ν is the kinematic viscosity. Furthermore, a so-called local Reynolds number is defined using position x instead of the characteristic length. For wings, this value is typically the distance of the considered location to the wing's leading edge.
While any physical fluid will always possess some non-zero level of viscosity, Ludwig Prandtl recognized that at high free-stream Reynolds numbers, the viscous forces are dominant only in the boundary layer and introduced an approach, today called Prandtl's boundary layer theory, in which he divided the flow around a body into two distinct regions. The boundary layer, where viscosity must be considered to meet the no-slip condition, and an inviscid far-field where the effects of viscosity can be neglected [1]. This separation allows to obtain equations that describe the behavior of the boundary layer. The boundary layer equations and their derivation are not presented here but can be found, for example, in [1]. Furthermore, in the context of this thesis, it is crucial that any flow, and therefore, the flow in the boundary layer, can exist in two distinctive states: laminar and turbulent.
Laminar flow is an orderly, predictable flow in which the layers of the fluid move with different velocities but without significant transfer of particles in the direction perpendicular to the flow direction. Turbulent flow is then characterized by highly chaotic, random, and fluctuating movement of the particles, resulting in significant momentum exchange across the different layers of the fluid.

In a turbulent boundary layer, the chaotic transverse motion of the particles results in higher average velocities near the surface and, therefore, in higher velocity gradients at the wall. According to Newton's law, the wall velocity gradient relates to the wall shear stress τ_w as:

$$\tau_w(x) = \mu \left(\frac{du}{dz}\right)_w \tag{1.2}$$

Based on this shear stress, the local skin friction coefficient is:

$$c_f(x) = \frac{\tau_w(x)}{\frac{1}{2}\rho U_\infty^2} \tag{1.3}$$

Integrating the skin friction coefficient over the wetted surface of the body gives the total skin friction drag coefficient $C_{D,f}$, one of the components of the total drag coefficient of the body. These observations lead to the conclusion that the presence of a turbulent boundary layer results in a higher skin friction drag coefficient that contributes to the total drag coefficient of the body. Furthermore, the value of the friction coefficient varies with the Reynolds number, where a higher Reynolds number leads to lower values of the friction coefficient. Larger components exposed to larger flow velocities will, therefore, show a lower value of the average friction coefficient. Note, however, that a lower value of friction coefficient does not mean a lower value of absolute drag [2]. Figure 1.2 shows the variation of the friction coefficient with the type of flow and the Reynolds number.

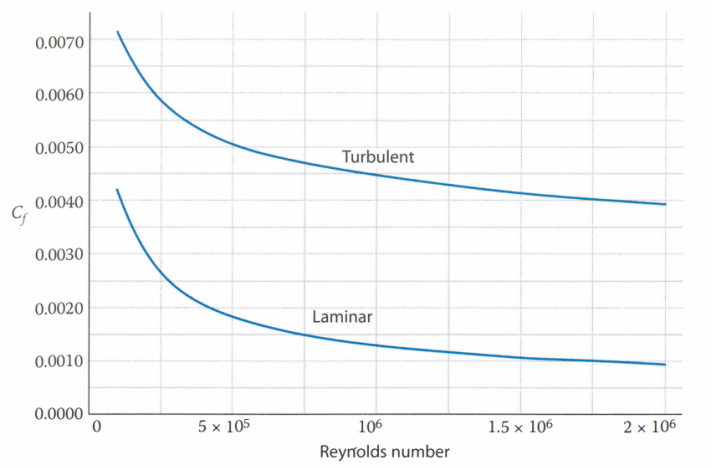

Figure 1.2: Flat plate skin friction coefficient vs. Reynolds number [3]

This lower value of skin friction coefficient for laminar flow is then the essential motivation behind all laminar flow control technologies, which aim to prevent the transition of the boundary layer from laminar to turbulent to minimize the skin friction drag of a given aircraft, with the ultimate goal of reducing fuel consumption.

1.2. Laminar-turbulent transition

In the late 19th century, Osbourne Reynolds demonstrated that flow through a pipe transitions from laminar to turbulent after reaching a certain critical Reynolds number [2]. This observation applies to all boundary layers, and the critical Reynolds number is the lowest local Reynolds number at which any disturbance causes the boundary layer to become unstable and to transition from laminar to turbulent. While the transition occurs gradually over a certain distance, for practical analysis, it is customary to identify the distance at which the transition starts x_{tr} and treat all the flow downstream of this point as turbulent. The critical Reynolds number is then [4]:

$$Re_{cr} = \frac{\rho U_\infty x_{tr}}{\mu} = \frac{U_\infty x_{tr}}{\nu} \tag{1.4}$$

If this value of the critical Reynolds number is known for a given type of flow and given body, the definition in equation Equation 1.4 directly gives the location of the transition point. The value of the critical Reynolds number can be obtained from multiple sources such as experiments, simulations, or semi-empirical methods but can be very difficult and/or expensive to obtain [4].
Furthermore, in practice, the transition is influenced by many other factors, for example, pressure gradients, surface roughness, freestream disturbances, vibrations, or acoustic waves. Placing objects into the boundary layer also leads to an immediate amplification of the instabilities and promotes transition. The last category of instabilities results from three-dimensional flows. These will be covered separately in the subsequent chapter. All these aspects can cause the critical Reynolds number to vary randomly over time, making transition predictions even more difficult [2].
The Mach number also has a significant influence on the onset of transition. While it does not affect the stability of the boundary layer itself, a higher Mach number causes the disturbances to propagate at higher velocities. That means that, for example, on a wing, disturbance located at a certain distance from the wing's leading edge will not be as amplified at higher values of Mach number because it had less time to grow under the same amplification rate. Therefore, it can be concluded that higher Mach numbers are favorable for postponing transition [2].
The transition process itself is also very complex and consists of stages that are very chaotic and interdependent. In a two-dimensional flow, the transition starts with so-called receptivity, in which disturbances enter the developing boundary layer. These instabilities result in nearly two-dimensional Tollmien-Schlichting (TS) waves [1]. The unstable TS waves grow and become three-dimensional. These vortices then longitudinally stretch and break down into smaller structures. The breakdowns take place most intensely in discrete spots that appear at random locations and times near the wall. These spots then serve as sources of turbulences that propagate downstream, forming typical turbulent wedges and gradually developing in a fully turbulent flow [2]. Figure 1.3 schematically shows this process on a flat plate at zero incidence:

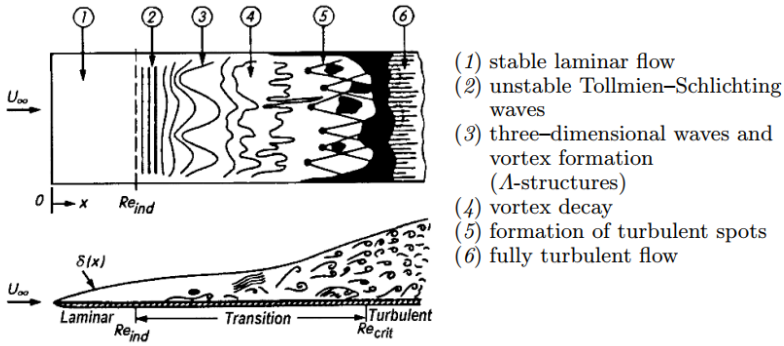

Figure 1.3: Sketch of laminar– turbulent transition in the boundary layer on a flat plate at zero incidence [1]

1.3. Instability mechanisms

As mentioned in Chapter 1.2, additional transition mechanisms occur in the case of three-dimensional flows, like swept wings on modern aircraft, making it even more challenging to maintain laminar flow. The description of these mechanisms is the topic of this subsection.

Tollmien–Schlichting instabilities (TSI)

Tollmien–Schlichting waves are disturbances already mentioned in the case of two-dimensional flow in which they initiate the transition process. The TS waves are also present in three-dimensional flows over wings, where they dictate the transition process if the sweep is moderately low, below approximately 25 degrees [5].
Tollmien–Schlichting waves are damped by favorable pressure gradients and amplified by adverse pressure gradients. They are also sensitive to the free stream Reynolds number and to surface quality. The roughness of the surface leads to destabilization of the waves and the development of typical turbulent wedges [5].
While boundary layer suction dampens the TS waves, ensuring a sufficiently smooth surface finish and

favorable pressure gradients is generally the most effective way to prevent their growth [5].
Transition due to TSI occurs mainly in the mid-chord region and can be successfully delayed close behind the minimum pressure point [2].

Cross-flow instabilities (CFI)

Cross-flow instability (CFI) is a transition mechanism that occurs only in three-dimensional flows, characteristic of its stationary vortex structure. This structure, sometimes called cat-eye structure, is an assembly of corotating vortices with their rotational axis aligned with the streamwise direction. The breakdown of these vortices leads to a transition along the wing span [2].
CFI typically dominates at wings with high values of sweep (approximately above 25 degrees) in the regions of favorable pressure gradients, typically near the leading edge. Furthermore, the effect of CFI strongly depends on the surface roughness. Higher roughness promotes the formation of the vortex structure and its breakdown, resulting in an earlier transition. Boundary layer suction, however, successfully damps the CFI and can be used to delay the transition [5].

Attachment-line transition (ALT)

Attachment line transition (ALT), is caused by an instability along the attachment line, a virtual line connecting all maximum pressure points along the leading edge. This instability can then cause an early transition near the wing's leading edge and, therefore, lead to a significant loss of laminarity. [2].
The flow at the attachment line can become unstable due to external disturbances, which can furthermore propagate along it. That is typically the case for swept wings in modern transonic aircraft, where significant disturbances originating at the junction of the fuselage and the wing can propagate along the attachment line. This phenomenon is called leading-edge contamination and is highly undesirable as the propagation of disturbances can cause transition along the whole wing span. Stopping the disturbance propagation can be done by using the so-called Gaster bump at the leading edge that diverts the turbulent boundary layer and allows the development of a new, laminar one. Other effective methods to prevent transition due to the attachment line instability are reducing the leading edge sweep, the airfoil nose radius, or the unit Reynolds number. Suction along the leading edge also damps the ALT and prevents leading edge contamination [5].

Görtler vortices

Görtler vortices are the last type of instability that can occur in three-dimensional flows over wings. These stationary vortices result from centrifugal forces that arise in a flow along concave surfaces. However, concave surfaces are found only at the aft pressure sides of airfoils, where the cross-flow instability is much more prominent [2]. Görtler vortices are of little concern on swept wings due to their insignificance compared to the cross-flow instabilities, even on wings with minimum sweep angles. On unswept wings, use of proper airfoil shaping completely prevents their formation. [2]. Furthermore, achieving laminar flow at the aft wing regions is often already impossible due to the presence of high lift devices and control surfaces with the associated gaps and other surface imperfections. Görtler vortices are, therefore, of little practical relevance and do not need the same care as the instability mechanisms considered earlier.
As a summary, Figure 1.4 schematically shows what instability mechanisms dominate in different regions on a three-dimensional swept wing:

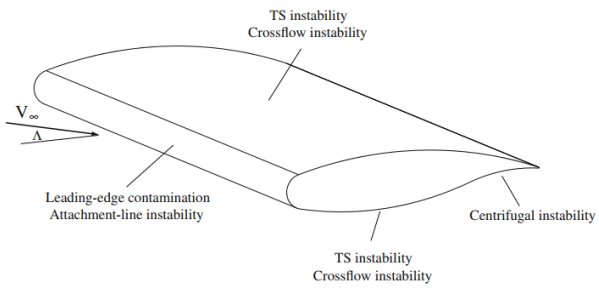

Figure 1.4: Visualization of the dominant instability mechanisms in different regions on a swept wing [2]

2 Laminar flow technologies

This chapter provides an extensive overview of laminar flow technologies, covering their fundamental working principles, historical background, limitations, and challenges associated with their modeling and evaluation.
First, three fundamental laminar flow technologies are introduced in section 2.1. These techniques include Natural Laminar Flow (NLF), Laminar Flow Control (LFC), and Hybrid Laminar Flow Control (HLFC). Next, section 2.2 offers a historical overview of research on laminar flow technologies. This is followed by section 2.3, which discusses the practical challenges of deploying laminar flow technologies in real-world operations.
Finally, section 2.4 examines the difficulties involved in accurately modeling the effects and performance of laminar flow technologies during the conceptual aircraft design process.

2.1. Overview of laminar flow technologies

Laminarization of a component means to maintain laminar flow at local Reynolds numbers for which transitional or even turbulent flow would occur under normal circumstances. It is important to emphasize that laminarization does not consider turning a turbulent flow into a laminar one but merely postponing the transition. Techniques that aim to turn turbulent flow into laminar are called re-laminarization technologies. Although it is possible to use the same active flow control systems for both laminarization and re-laminarization, the energy requirements for the latter one can be an order of magnitude larger than for laminarization. This thesis does not further consider re-laminarization, but the distinction is crucial. [6]
With that, Vos et al.[2] then presents a boundary layer equation that provides fundamental strategies for postponing transition:

$$\mu \frac{\partial^2 u}{\partial y^2} = \rho v_0 \frac{\partial u}{\partial y} + \frac{\mathrm{d}p}{\mathrm{d}x} - \frac{\mathrm{d}\mu}{\mathrm{d}T} \frac{\partial T}{\partial y} \frac{\partial u}{\partial y} - f_x \tag{2.1}$$

The interpretation of this equation follows from an empirical observation that fuller boundary layer profiles result in lower disturbance growth and are, therefore, more stable. A fuller boundary layer in this context means a more convex velocity profile, meaning a more negative value of the second derivative of velocity with respect to the distance from the wall y. This term multiplied by viscosity is then the left-hand side of Equation 2.1, and so to stabilize the boundary layer, the right-hand side should be as negative as possible.
The first option is to maintain a negative (favorable) pressure gradient, which results in lower disturbance growth, whereas a positive (adverse) pressure gradient promotes growth. The next option for stabilizing the boundary layer is to increase the temperature gradient by cooling the wall. Heating the wall would have the opposite effect. The last option is applying suction of air through the wall.
All three approaches have resulted in the development of laminar flow technologies that aim to postpone the transition on aircraft components to reduce fuel consumption by reducing friction drag. This section will present the ones utilizing the favorable pressure gradients and the wall suction. The wall-cooling approach is not considered in this work. Figure 2.1 visualizes the three laminar flow technologies that will be discussed in further detail, which are natural laminar flow (NLF), laminar flow control (LFC), and hybrid laminar flow control (HLFC).

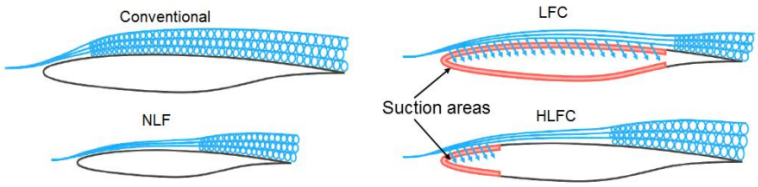

Figure 2.1: Schematic visualization of different laminar flow technologies [7]

2.1.1. Natural laminar flow (NLF)

The first method to maintain laminar flow is natural laminar flow (NLF), or NLF for short. NLF is a passive technique that avoids boundary layer transition by profile shaping to achieve velocity and pressure profiles that damp the flow instabilities. That generally means to avoid adverse pressure gradients for as long as possible since these amplify the two-dimensional TS wave instabilities.
Being a passive technique makes NLF a highly desirable laminarization method, as it not only maximizes the benefits of achieving laminar flow but also avoids additional complexities that are unavoidable in the case of more complex laminarization methods. This simplicity then results in lower manufacturing and maintenance costs. The lack of need for additional components also means that NLF does not necessarily increase the operational empty mass of the aircraft.
However, NLF also presents several disadvantages and limitations that make its use for modern transport aircraft difficult. First, while NLF can be very effective in preventing transition due to two-dimensional instabilities, it cannot prevent the transition due to the growth of instabilities present in a three-dimensional flow over swept wings, e.g. CFI, and ALT.
Reducing the airfoil nose radius prevents ALT for wings with moderate sweep, but this strategy is no longer sufficient for sweep angles above approximately 25 degrees. Furthermore, a smaller nose radius leads to an earlier stall onset and, therefore, a lower value of the maximum lift coefficient achievable at the given wing section. A sharper nose at a wing tip can also lead to the tip stalling before the root of the wing, resulting in an unstable stall characteristic of the whole aircraft [2, 3]. Regarding the cross-flow instabilities, NLF is not capable of its mitigation. Even worse, since favorable pressure gradients destabilize CFI, the intentional shaping of an NLF to create favorable pressure gradients to avoid TSI directly contradicts the strategies for mitigating CFI.
The inability of NLF to mitigate ALT and CFI then effectively prevents applying this laminarization method on wings with high sweep angles. Unfortunately, modern passenger transport aircraft fly at high transonic speeds and, therefore, require high sweep angles to limit the wave drag due to compressibility effects.
The challange with mitigating three-dimensional instabilities is not the only limitation of NLF. Another drawback is the fact that NLF is extremely sensitive to surface irregularities. Even the slightest surface imperfection can cause an immediate loss of laminarity and performance. This sensitive behavior demands high manufacturing precision which increases the cost of the technology. Even then, imperfections can still occur in real-world operations due to surface contamination from dust, dirt, insects, or ice crystals. This results in the need for additional efforts to prevent or remove such contamination throughout the aircraft's operations.

2.1.2. Laminar flow control (LFC)

An alternative to the passive natural laminar flow approach is laminar flow control or LFC. LFC is a technique of applying boundary layer suction over the full component length, typically over the whole wing chord. The suction stabilizes the boundary layer and partially avoids disturbances and instabilities. That allows maintaining laminar flow over large extents of the component even at high values of local Reynolds number, much beyond the capabilities of NLF. Furthermore, since suction dampers CFI and ALT, this technique is not limited to wings with moderate sweep.
However, this technique suffers from many limitations as well. First of all, active suction requires pumps that provide the necessary pressure difference to suck the desired amount of air through a perforated suction skin sheet. These pumps are driven either by engine bleed air, an old approach not considered in modern designs, or by electric motors that use electrical power generated by the engines, increasing the engine's electrical power consumption. In either case, the required energy to drive the pumps

ultimately affects the specific fuel consumption (SFC) of the engine, offsetting the fuel savings achieved by the laminar flow technology.
Furthermore, LFC introduces a great degree of complexity, not only because of the use of pumps but also because the sucked air must be transferred by ducts from the suction sheet to the pumps and from the pumps to the outside of the aircraft. Older LFC designs also worked with assemblies of suction chambers under the suction sheet and control systems, including control units and valves. This complexity leads to significant manufacturing and maintenance costs and increases the risk of system failure. Furthermore, all the additional components add to the operational empty mass of the aircraft and cause space allocation problems. The second issue is particularly problematic when LFC is applied to wings. The system spans over the complete chord of the wing including the wing box, which reduces the volume available for fuel storage. The system also makes storing high-lift devices or anti-ice system components at the leading or trailing edges difficult.
Another challenge is ensuring that the wing box has adequate strength and low weight, particularly given the perforations in the suction sheet over a significant area of the skin. Moreover, if suction is applied to both the upper and lower surfaces of the wing, it becomes necessary to integrate inspection panels into the suction surfaces, thereby raising the challenge of ensuring that the resulting gaps or steps are sufficiently small not to cause a transition. The same challenge is also present for high-lift devices in stored positions. Finally, the system's installation in the wing box, typically utilized for fuel storage, poses a significant risk of fuel leakage into the suction system.
Overall, while LFC provides undisputable aerodynamic benefits that can lead to significant fuel savings, from a practical point of view, its integration into real aircraft is very challenging due to its high complexity and the associated problems. However, if the flight conditions or the geometry of the laminated component become too demanding, the LFC might be the only option for achieving large extents of laminar flow. A typical example is the inboard sections of the wings on modern airliners, where the chord lengths (and consequently the Reynolds number) are so large that LFC is the only way to maintain laminarity up to the desired 50 or 60% of the chord.

2.1.3. Hybrid laminar flow control (HLFC)

Hybrid laminar flow control (HLFC) is a technique that combines NLF and LFC strategies for laminarization. In HLFC, suction is applied only over a limited portion of the chord, typically in front of the front spar, while a favorable pressure gradient, achieved through the airfoil shape, maintains the laminar flow over the mid-chord section of the airfoil.
The suction applied over the leading edge suppresses the instabilities due to the presence of the suction peak and their amplification by the associated adverse pressure gradient. Suction in this region also prevents transition due to contaminations that can be carried along the attachment line, while suction over the first 15 to 20% of the chord damps cross-flow instabilities that dominate the transition process here. While suction eliminates the amplification of TS waves, this amplification is the dominant transition mechanism aft of the suction. The amplification rate is, therefore, reduced by a favorable pressure gradient achieved by appropriate airfoil shaping in this region, the same as in the case of NLF. An alternative approach is then the application of a mildly adverse pressure gradient that reduces the extent of laminar flow but also reduces the acceleration of the flow and, therefore, the local Mach number, which leads to improved high-speed performance.
This combination of limited suction and airfoil shaping addresses the main limitations of both NLF and HLFC approaches. The advantage of HLFC compared to NLF is its ability to suppress much stronger instabilities through suction in the critical regions. HLFC can therefore achieve large extents of laminar flow even at components with higher values of local Reynolds number or with higher sweep, such as swept wings on large transport aircraft. The high effectiveness of HLFC to damp instabilities also lowers the requirements for surface quality and makes the surface less sensitive to contamination during operation.
The HLFC approach also significantly reduces complexity compared to LFC, as the suction is applied over only a fraction of the chord, requiring a fewer components and less modifications to the wing itself. The leading edge alone can store all the necessary ducting and be made removable for easier inspection and maintenance. Storing the system in the leading edge also eliminates the risk of fuel leakage into the ducting and does not reduce the volume in the wing for fuel storage. Furthermore, the limitation of the suction to the leading edge means that the structure of the wingbox is not compromised and does not require significant structural redesign to facilitate the system. All these factors result in lower required

design, manufacturing, and maintenance efforts.
However, the use of HLFC necessitates the implementation of a complex suction system comprising numerous elements. Understanding of the system and its constituent parts is then crucial for effectively addressing all aspects of its integration and evaluating the potential effects of its implementation on the aircraft's design and performance. The following discussion therefore introduces the general architecture of modern HLFC systems in detail.

General architecture of HLFC systems
An example of a modern HLFC system is shown in Figure 2.2, which illustrates an HLFC system concept developed by DLR as part of the CleanSky2 HLFCWin project [8]. It should be noted that, for the sake of simplicity, this chapter describes the HLFC system architectures in the context of an HLFC systems applied to the wing. However, the same design principles and elements would be utilized in the case of an HLFC system applied to any aircraft component.

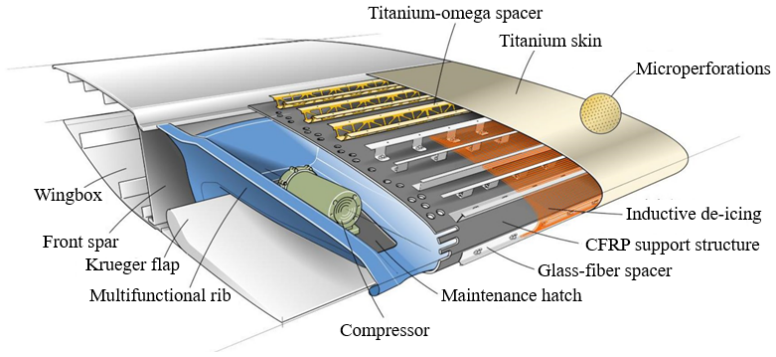

Figure 2.2: HLFC system utilized in HLFCWin project [8]

As depicted in Figure 2.2, a fundamental component of any HLFC system is the suction sheet (alternatively referred to as a suction panel or suction skin), through which the required amount of air is sucked from the boundary layer inside the component. Early experiments frequently considered two types of suction sheets: slotted and perforated. However, modern concepts universally utilize only the perforated option, as slots rapidly lose their effectiveness with increasing sweep angle, particularly in the leading edge region, potentially even causing a transition [9, 10].
After flowing through the suction sheet, the drawn air enters a suction chamber (also referred to as plenum) or series of chambers. The pressure in these chambers is lower than the pressure on the component's surface, thereby generating a sufficient pressure difference to draw the air from the boundary layer through the perforations in the suction sheet.
Subsequently, the air moves in the spanwise direction through the chambers. At the end of the chamber, the air passes through a contraction into a transfer duct that leads it to a compressor inlet. Optionally, the transfer duct might be absent. In that case, the contraction would lead the air directly to the compressor inlet, or the compressor inlet would be placed directly at the end of the suction chamber. The function of the compressor is then to generate a pressure differential, thereby reducing the pressure within the suction chamber. From the compressor, the air passes through an exhaust duct, which directs it to the outside the aircraft. An alternative approach omits the exhaust duct, with the air instead being expelled directly into the cavity housing the compressor. Thereafter, the air can leak through surface gaps to the atmosphere. This approach is feasible due to the relatively modest mass flow requirements of a single compressor in an HLFC system, typically ranging from tens to hundreds of grams per second.
In addition to pneumatic components, an HLFC system necessitates additional components to drive the compressors. Modern designs employ exclusively electric induction motors, powered by electricity generated by the aircraft's engines and delivered to the motors via a network of electric cables. If the design incorporates a DC cable network, rectifiers must be used to convert the current from AC to DC between the engine generators and the cables. Similarly, inverters are required to convert the current from DC back to AC between the cables and the motors.

The integration of an HLFC system into a component may also necessitate the implementation of additional structural elements to ensure sufficient structural integrity of the assembly, even under challenging conditions. In this regard, the possibility of bird strike constitutes a particularly concerning scenario, since collisions with birds affect precisely the leading edges of components where an HLFC system would typically be located. Additionally, the design of structural elements within the suction chamber, such as ribs of stringers, must allow for the passage of sucked air with minimal pressure losses. This is essential to minimize the pressure ratio required to be delivered by the compressors, thereby reducing the system's power requirements.
Finally, a particular type of HLFC system architecture exists that deviates from the general description provided in this chapter so far. This concept is referred to as passive HLFC system.
Passive HLFC systems, in contrast to regular (or active) systems, do not feature compressors. Rather, the required pressure difference across the suction sheet is achieved by utilizing a flap or a hinged door placed at a low pressure region, typically at the suction side of the laminarized component. This flap can lead directly to the suction chamber or be connected to it via a transfer duct, thereby enabling the sucked air to flow from the high-pressure region on the suction surface to a low-pressure area at the exhaust behind the flap. The regulation of suction rates is then achieved by changing the amount by which the flap is opened.
The passive system's simplicity and reduced mass, resulting from the elimination of compressors and their drives, are notable advantages. This system functions without additional energy requirements, thereby eliminating the need for extra engine power offtakes and the associated increase in fuel burn. Consequently, greater fuel savings are achieved compared to active systems for the same extent of laminar flow.The elimination of compressors, motor drives, and electrical components also leads to a substantial reduction in system production and maintenance costs. However, a passive system exhibits a notable disadvantage in its inability to generate the same magnitude of pressure difference (and therefore suction rates) as an active system. Furthermore, the amount of air sucked is smaller than that which can be achieved with active systems. These limitations mean that passive systems are incapable of delivering the same extent of laminar flow over a range of flight conditions as active systems. In addition, active systems may be required for components experiencing significant flow disturbances or requiring a substantial suction extent, such as the inboard region of the wing near the fuselage.

2.2. History of laminar flow technologies

This section provides a historical overview of research on laminar flow technologies, focusing on the histories of NLF and HLFC.
The history of the older technology, NLF, is presented first, followed by the history of HLFC research. Consistent with the convention in many sources, the discussion of HLFC's history is divided into two parts, describing research conducted in the United States and research carried out in Europe. The final part of this section summarizes the historical development of HLFC system architectures, from initial proof-of-concept demonstrators to the latest prototypes and concepts.

2.2.1. History of natural laminar flow research

The first attempts for investigation of NLF track back to 1930's when the National Advisory Committee for Aeronautics (NACA, predecessor of today's NASA) launched a program to develop NLF airfoils, the now famous 6 and 7 NACA airfoil series. The availability of these airfoils ignited interest in NLF in the United States and led to numerous wind tunnel experiments and flight tests. Great Britain also gained invaluable flight experience with NLF airfoils fitted to military fighter aircraft. [6].
However, the overall consensus from all the early experiments was that NLF was not achievable in practical deployment due to manufacturing limitations. While the experiments achieved extensive laminar flow, that was only after considerable effort to achieve smooth and wave-free surfaces. That was possible only in the case of prepared surfaces or airfoil gloves, while the experiments on the production quality surfaces resulted in very little or no laminar flow. The main observed problems were the excessive waviness between ribs and stringers, significant steps or gaps due to skin joints, and protuberances due to rivets [11].
Despite the inability to attain large regions of laminar flow in daily operations, the NLF airfoils nevertheless found applications in aircraft intended for high-subsonic-speed flight for their superior high-speed performance compared to the other airfoil options available at that time. An example of

such an application is the legendary North American Mustang P-51, shown with its NLF airfoil in Figure 2.3 [6, 12].
These applications, however, also contributed to significant conservatism and skepticism regarding NLF due to the relatively high values of unit Reynolds numbers (Re>2 million) encountered in the operation of these fighters, since at such conditions, the boundary layer is susceptible to surface imperfections and insect contamination. This observation resulted in a belief that, to a certain extent, prevails to the present day, that large extents of NLF are unachievable even with modern manufacturing techniques [11].

Figure 2.3: Mustang P-51 and its natural laminar flow airfoil [13]

The interest in NLF significantly decreased after these initial investigations between the 1930s and 1950s, mainly due to the dissatisfying results. The focus and resources shifted to developing the new concept of jet propulsion since the low fuel prices did not provide sufficient initiative for the research of fuel-saving technologies [14].
This status remained until the 1980s when a sharp increase in fuel prices restored the attractiveness of laminar flow and led to a new series of experiments and flight tests. In the United States, these were, for example, tests of NLF gloves on F111 TACT aircraft, Boeing 757, or F14 VSTFE, while in Europe, DLR carried out similar glove experiments with VFW614 ATTAS, shown in Figure 2.4, or Fokker 100 [14–17]. The motivation for these tests was to gather flight data to get insight into the different transition mechanisms, evaluate environmental effects on laminar flow, improve numerical transition prediction techniques, or validate new manufacturing techniques. The tests, however, considered only limited span sections and aimed to answer individual questions regarding laminar flow, not to develop components for operation use on production aircraft.

Figure 2.4: DLR VFW614 ATTAS Aircraft in flight test with NLF glove [18]

This era, however, also saw the first applications of NLF methods to executive jet-sized aircraft, such as Piaggio P.180 Avanti, shown in Figure 2.5a, with laminar wings and fuselage [19]. Recent examples of business jets with laminar flow include the Honda HA-420 with a laminar nose and wing [20] or the

Otto Celera 500L (Figures 2.5b and 2.5c). The latter is planned for unveiling in 2024-2025 and promises to achieve extensive laminar flow over its wings, fuselage, and empennage. Experts in the field, however, question the feasibility of these promises [21, 22].

(a) Piaggio P.180 Avanti [23]

(b) Honda HA-420 [24]

(c) Celera 500L [25]

Figure 2.5: Examples of business jets employing natural laminar flow

General aviation also offers examples of production aircraft using NLF. These include Cessna 210, Mooney M20, or Lancair Legacy, all using laminar wing designs with NLF airfoils [26–28].

(a) Lancair Legacy [29]

(b) Mooney M20 [30]

(c) Cessna 210 [25]

Figure 2.6: Examples of general aviation aircraft employing NLF airfoils

However, the aircraft categories that have utilized NLF with the most success are gliders and sailplanes. Their very high aspect ratios, low weight, and the associated small wing area result in very short chord lengths that, combined with very low air speeds, result in low values of Reynolds number and, therefore, make the sailplane wings ideal for the application of NLF. By further applying advanced NLF airfoils, modern sailplanes can sustain laminar flow up to 75% chord on the upper surface and 95% chord on the lower surface. The flow is often intentionally tripped by so-called turbulators at the trailing edge region of the upper surface to enhance stall performance since a turbulent boundary layer generally separates later than a laminar one [31].
Vertical and horizontal tails of modern sailplanes also use NLF airfoils for further drag reduction. Maintaining laminar flow on the horizontal tail is also easier since sailplanes often employ a T-tail configuration. That is mainly to avoid shielding the rudder in case of spin, allowing an easier recovery, but a T-Tail has the additional benefit of being free of any turbulence propagating from the fuselage that could otherwise cause transition if the horizontal tail was below the vertical one.
Furthermore, modern sailplanes don't achieve laminar flow only over the wing-like surfaces but also employ so-called tadpole fuselages with their forward section shaped to maintain laminar flow. Using single-piece canopies that eliminate the seals and gaps associated with more traditional two-piece ones is another trend that, aside from other benefits, allows a longer extent of laminar flow over the fuselage [32]. Example of such a modern sailplane, Schleicher AS 33, is shown in Figure 2.7.

Figure 2.7: Example of a modern sailplane - Schleicher AS 33 [33]

Unfortunately, smaller aircraft, such as business jets, general aviation aircraft, or sailplanes, are still the only ones utilizing NLF technology in production models. There is not yet a single example of a large passenger transport aircraft that would utilize NLF technology in regular operations.
The more unique is a project called BLADE (Breakthrough Laminar Demonstrator in Europe), which took place under the Clean Sky consortium. In this project, a specially developed NLF with a reduced sweep and span of nine meters replaced the outer wings of an Airbus A340-400 test aircraft for a series of flight tests. These test wing sections are shown in Figure 2.8 at the wing tips. A thermal camera positioned at the top of the vertical tail and other measurement devices allowed precise observation of the laminar flow over these sections across various flight conditions. The goals of the project were:

- Demonstrating the viability of NLF at operational conditions to increase its technology readiness level.
- Lowering the risk associated with the technology via full-scale manufacturing and flight testing.
- Estimating the benefits of the NFL on the aircraft level.
- Gathering of calibration data for improvement of computational transition prediction methods.
- Evaluating the sensibility to different types and sizes of surface imperfections.

The project successfully evaluated two different manufacturing and structural design options, each applied on one side of the wing. The flight tests also included systematic testing of different imperfections applied to the laminar surface to gain insight into the effect of contamination on the performance of the laminar sections. The BLADE project performed 61 test flights and gathered 184 hours of data. The tests included opening the flight envelope, reference flights with clean sections, investigating off-design characteristics, Krueger shielding, receptivity, and operational topics such as cloud encounters.

Figure 2.8: Airbus A340 Flight Lab with laminar wing sections during a flight test as part of the BLADE program [34]

2.2.2. History of HLFC research in the United States

While the United States carried out the first experiments with transition postponement via suction already in 1930s, the idea of applying the suction only over the nose region of an airfoil did not emerge until the 1980s. Until then, researchers considered only a laminar flow control (LFC) approach with suction applied over the complete chord. That was mainly due to a poor understanding of the transition mechanisms, especially the attachment line and cross-flow instabilities associated with three-dimensional flow over swept wings. Furthermore, low oil prices between the 1950s and 70s did not help the efforts to close this knowledge gap as they did not provide sufficient motivation to invest in wind tunnel experiments or flight tests necessary for developing fuel-saving technologies. That changed after the 1970s when OPEC issued an oil embargo that quickly led to a sharp increase in oil prices. Suddenly, fuel-saving concepts such as laminar flow control regained appeal, and the number of programs and experiments investigating these technologies increased significantly. As the tests progressed and delivered more aerodynamic data, it became apparent that suction applied only in the leading edge area was sufficient to increase significantly the transition Reynolds number [6, 10].

The first step towards HLFC technology was made in the LEFT project (1983-1986) on NASA JetStar (Lockheed C-40) aircraft, where the wings featured two test suction systems designed by Lockheed-Georgia Company (slotted section on the left wing) and Douglas Aircraft Company (perforated section on the right wing), as visualized in Figure 2.9. Crucially, these systems applied suction only to the leading edge region of the wings. This decision was motivated by the fact that this region contains the biggest aerodynamic and operational challenges, including insect contamination, de-icing requirements, storage of high-lift devices, and limited space for systems storage. It was, therefore, reasonable to first address the leading edge issues before moving to more extensive suction over the complete chord.

The flight tests then intended to demonstrate that the systems could provide the required extent of laminar flow even under routine operational conditions, so the aircraft operated on regular commercial missions. The results were very satisfactory as the test sections didn't show measurable signs of degradation and provided the required laminarity even after exposure to challenging conditions without causing a dispatch delay or needing extra cleaning or maintenance. However, even more importantly, the project showed that packaging the suction system into the leading edge region was possible, which opened doors for further research of HLFC systems [6].

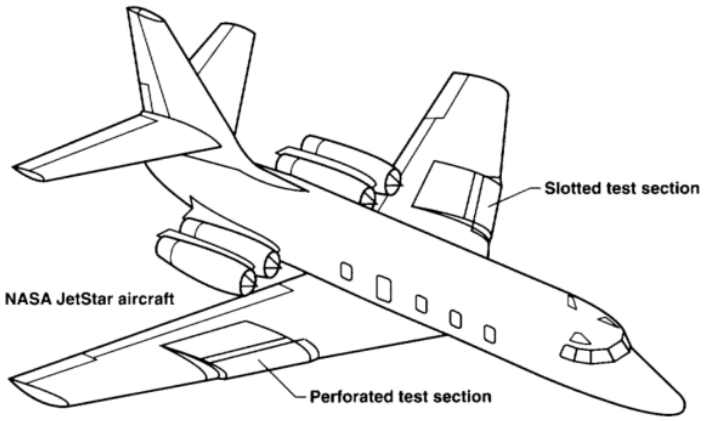

Figure 2.9: Test setup of the NASA JetStar aircraft in the LEFT program [6]

As a direct result of this success, Boeing performed a series of flight tests in 1991, with 757 transport aircraft fitted with an HLFC system highly similar to the one used in the JetStart project, except using hot air instead of liquid ejection for anti-ice protection [6]. The goal was to test the HLFC concept, to evaluate its effectiveness under flight conditions, and to assess the functionality of the high-lift (Krueger flap) and anti-ice systems. The results were encouraging as the system was very effective in postponing the transition, even beyond 65% of the chord, while using less suction power than expected, resulting in a 6% drag reduction on aircraft level [35]. However, the much lower suction rates lead to high uncertainty in the design tools used for the system's development [10] [36]. Furthermore, the system was too complex and extensive to be used in real-world operations, as can be clearly observed from the schematic visualizations of the suction leading edge assembly in Figures 2.19 and 2.10.

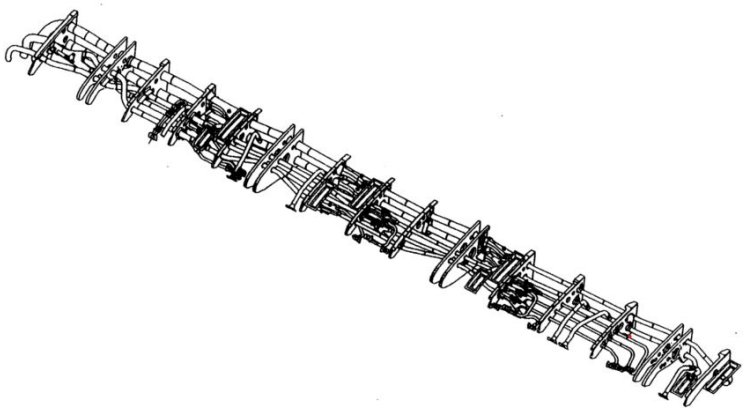

Figure 2.10: Leading edge assembly of the suction system used in the Boeing 757 flight tests [37]

Following this success, a group of partners led by General Electric and NASA carried out a project between 1991 and 1992 that aimed to demonstrate the application of an HLFC system to the nacelles of turbofan engines. The system consisted of two suction panels, one applied to the inboard and one to the outboard side of the nacelle (see Figure 2.11), from which a system of flutes collected the sucked air and transported it to an industrial turbocompressor unit. This system proved extremely efficient in delaying the transition, providing laminar flow over 43% of the nacelle length, independent of altitude. The flight tests also proved the efficiency of the NLF shaping of the nacelle since significant amounts of

laminar flow were present even without any applied suction. This amount, however, did vary with flight altitude. Namely, as the attitude decreased, the unit Reynolds number increased, resulting in the transition closer to the leading edge [35].

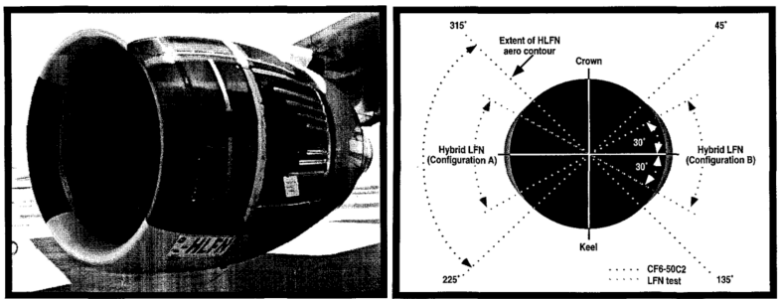

Figure 2.11: System used by General Electric and NASA in the HLFC Nacelle program [35]

The most recent advance in the development of HLFC technologies in the United States came in 2014 when Boeing revealed the application of a passive HLFC system to the horizontal and vertical tails of Boeing 787-9, becoming the first-ever passenger aircraft equipped with this technology. The system utilizes hinged exhaust doors in low-pressure regions that provide the required pressure difference across the suction skin, eliminating the need for active compressors. Boeing patented this technology between 2011 and 2013 and has declared its intentions to make it a standard equipment on all Boeing 787-10 and 777X family aircraft. While the patents are publicly accessible, Boeing has understandably never published any data regarding the system's performance [36, 38]. Figure 2.12 shows the exhaust hinge doors of the passive HLFC system on Boeing 787-9 while Figure 2.13 compares the tails of this aircraft to an older Boeing 787-8 that does not yet feature it.

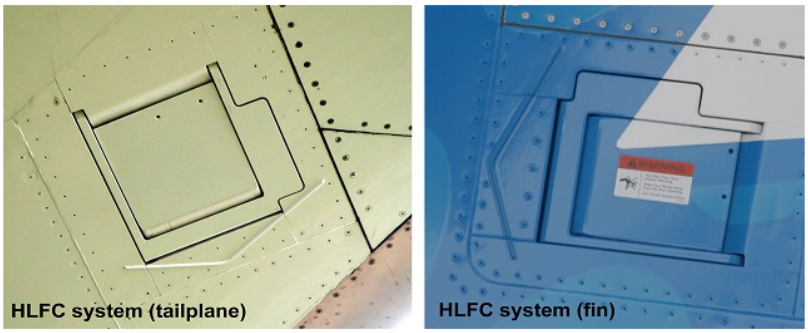

Figure 2.12: HLFC system exhaust hinged doors on the HTP and VTP of Boeing 787-9 [38]

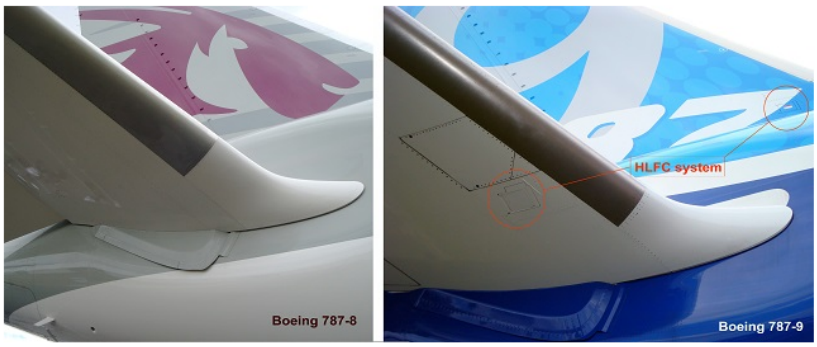

Figure 2.13: Comparison of HTP and VTP on Boeing 787-8 and 787-9 [38]

2.2.3. History of HLFC research in Europe

Investigation of laminar flow technologies in Europe started at the end of the 1980s, motivated by the successful test in the United States. The new projects first investigated the questions related to NLF concepts before shifting the focus to HLFC technologies [36, 39].
In collaboration with ONERA, Dassault Aviation performed the first flight tests between 1985 and 1989 with an NLF section of the vertical tail on Falcon 50. The next series of flight tests followed in 1987 until 1990, using the same aircraft but this time with HLFC glove on the inner leading edge of the wing. The purpose of these flights was to demonstrate the functionality of the suction system and asses transition criteria in real flight conditions. The final set of flight tests took place from 1993 until 1997. For these tests, Falcon 900 was used instead, with HLFC gloves on the leading edges of both sides of the wing. Here, the goal was to demonstrate the validity of the suction technology and the effectiveness of the Gaster bump to prevent leading-edge contamination, validate results from computational tools, and prove the functionality of the leading-edge anti-contamination pump [40]. The experimental setups of the test aircraft used in these experiments are shown in Figure 2.14.

(a) Falcon 50 with NLF vertical tail section [40]

(b) Falcon 900 with HLFC glove [40]

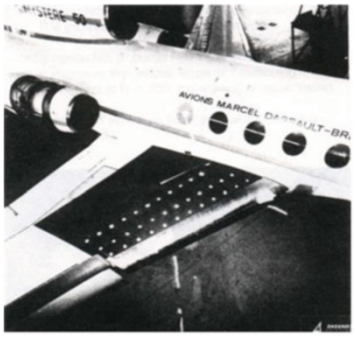

(c) Falcon 50 fitted with an HLFC glove [40]

Figure 2.14: Aircraft used by Dessault aviation in laminarity control flight tests

A second large initiative started in the 1980s was the common strategy LaTec, introduced by European Airbus partners. This extensive effort included analytical studies, wind tunnel tests, and flight tests, which led to the final set of experimental flights in 1998 with an HLFC system integrated into the vertical tail of the Airbus A320. While the flight tests confirmed the potential of the HLFC technology to reduce drag, the system itself was remarkably complex, required extensive volume to be stored, and was in no way feasible for use in real-world operations. The ducting of the system filled the leading edge of the VTP, and the suction system, consisting of three axial compressors, had to be stored in the tail cone of the fuselage, reducing the cabin space, as can be seen in a schematic drawing of the system in Figure 2.15. An additional practical drawback was a complex control system with nine individually controlled valves and flow meters and a lack of anti-contamination or ant-ice systems. However, while this system was not practically feasible, the flight tests provided many significant conclusions: the effect of internal system noise was less crucial than expected, the Gaster bump effectively prevented leading edge contamination, and the surface quality, in terms of both surface imperfections and inhomogeneity, was less critical than expected after wind tunnel tests [36, 39].

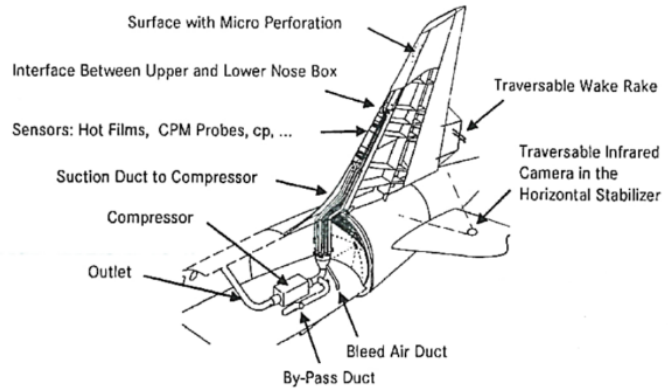

Figure 2.15: Suction system used in A320 HLF Fin project [36]

Another series of analytical investigations of HLFC systems started in 1989 with the ELFIN project that lasted till 1992, followed by the LARA (1993-1994) and ELFIN II (1993-1995) projects. The activities carried out included the development of numerical tools or large-scale wind tunnel tests and addressed operational issues such as anti-ice protection, contamination protection, Krueger flap shielding of the leading edge, investigation of roughness influence, or determination of suction requirements. The research also didn't consider only the laminarization of wings but also the nacelles.
Project HYLDA (1996-1999) was another European project that joined 23 partners in the investigation of the steps needed to increase the technology readiness level of HLFC systems for the wing, engine nacelles, or VTP, for which purpose the project also made use of A320 HLFC Fin from LaTec project for flight tests.
After HYLDA, project HYLTEC (1998-2001) aimed to develop a full-scale HLFC system and to address practical issues such as contamination prevention, de-icing, or improvement of manufacturing methods. One of the significant activities carried out as part of the HYLTEC project was a series of flight tests conducted with a Dornier Do 228 fitted with an HLFC glove. Following the project goals, this glove was equipped with different Krueger flaps and liquid coating to assess its ability to prevent the leading edge from contamination. The tested systems included active fluid coating and bleed air de-icing as well. These tests allowed extensive evaluation of the effectiveness of the different methods, as will be discussed in later sections [36]. The airafts test setup is shown in Figure 2.16.

Figure 2.16: DLR Dornier 228 equipped with an HLFC glove and an infrared camera used for transition detection [41]

Another valuable and extensive experiment in the HYLTEC project was fitting a SAAB 2000 aircraft with two test suction panels without the actual suction system. One panel featured an active system that pumped anti-contamination liquid over the surface, while the other suction panel was left unprotected as a reference. The aircraft was operated for over 1700 flight hours during more than 1900 flights in regular airline service to assess the effects of contamination and the effectiveness of the active system. This experiment concluded that the system was highly effective in preventing insect contamination [36]. Probably the most influential project in the development of modern HLFC systems was the ALTTA project (2000-2003), which successfully developed and tested a significantly simplified HLFC system applied to the vertical tail of an Airbus A320 test aircraft (see Figure Figure 2.17) [42–44]. The impressive results then motivated further investigations into the potential simplifications of the system. One example of such attempts for simplification is a tailored skin concept developed by DLR [45]. These efforts, combined with the availability of novel manufacturing techniques, such as laser drilling, resulted in the most modern concept that arguably achieves the lowest possible suction system complexity by varying the distribution of the holes in the suction sheet. subsection 2.1.3 describes all three concepts in detail.

Figure 2.17: DLR's Airbus A320 equipped with HLFC system on the VTP in ALTTA program [43]

Unfortunately, no further flight tests with a new functional HLFC system followed after the ALTTA program, so any estimation of the in-flight performance of these new concepts is purely theoretical. However, the research on laminar flow technologies in Europe did not end with ALTTA. Many projects have followed since then, and more are planned for the future since the increasing requirements for fuel efficiency do not allow giving up on such promising fuel-saving technology despite the undeniable challenges it might bring.
To conclude, Figure 2.18 presents a timeline with many projects discussed in the section from both Europe and the USA up to 2020.

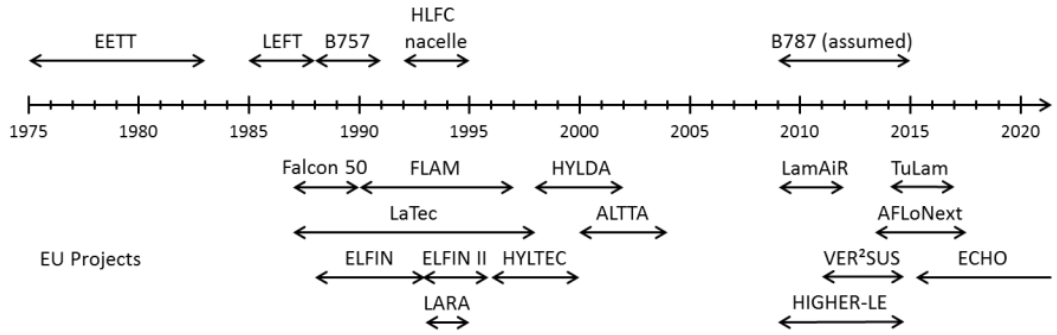

Figure 2.18: Timeline of research programs on laminar flow technologies carried out in Europe and the USA until 2020 [36]

2.2.4. Historical development of HLFC systems

Figure 2.19 presents an illustration of one of the earliest HLFC systems, which was developed by Boeing for a series of flight tests conducted in 1991 with the system applied to the wing of Boeing 757.

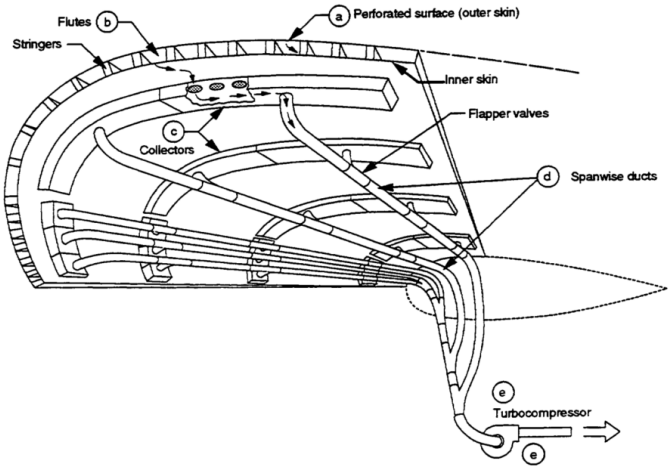

Figure 2.19: Suction system used in flight tests on Boeing 757 in 1991 [37]

As illustrated in Figure 2.19, the earliest HLFC systems featured an inner skin, creating a space between this skin and the suction sheet. This space was further divided by series of stringers that connected the skin to the suction sheet, forming individual suction chambers.The presence of different pressures in the suction chambers ensured varied suction rates in different chordwise regions, depending on the predominant type and intensity of the transition mechanism in that region.
The air exited the chambers through evenly spaced collectors into the ducting system, which transferred it to the turbocompressors.It is noteworthy that the suction rates (and therefore the required suction chamber pressures) vary significantly more in chordwise direction than in the spanwise direction.As a result of this observation, it was possible to connect multiple collectors by a single duct in the spanwise direction, while separate ducting was required for collectors at the same spanwise location. To regulate the different pressures within the various components, a sophisticated control system, comprising numerous valves and flow meters, was then employed.
Despite its success during the flight tests in maintaining extensive regions of laminar flow across various flight conditions, the system's substantial complexity prevented its implementation in production aircraft. [37, 46]
Significant progress towards a simpler, more practical HLFC system was achieved as a result of the European ALTTA project, which was concerned with developing and testing an HLFC system for the VTP of the Airbus A320. The HLFC system developed in this project is illustrated in Figure 2.20.

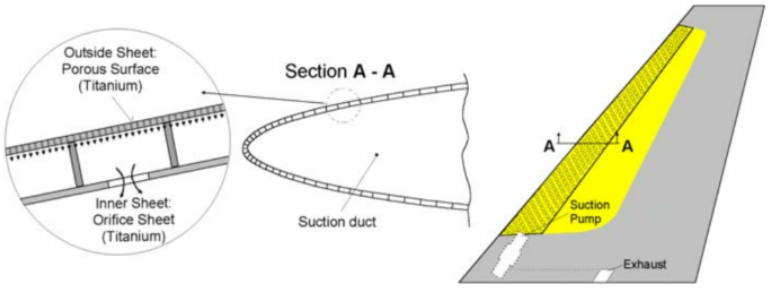

Figure 2.20: Simplified suction system developed in the ALTTA program [18]

Figure 2.20 shows that, similar to the Boeing concept, the ALTTA system also utilized an inner skin sheet and a series of stringers to form the individual suction chambers. However, a crucial distinction

between the two systems is that, in the ALTTA system, the air from the chambers was not collected by a complex ducting assembly. Instead, the air from all chambers was collected into a single large suction duct, with constant pressure throughout its volume. This duct was formed between the inner skin and the front spar, thereby filling the entire volume of the leading edge. The variation in pressure across the individual suction chambers was then accomplished by employing different diameters of the throttling holes present in the inner sheet, through which the air passed into the suction duct.
This approach eliminated the need for additional ducting, collectors, and a complicated control system, thereby reducing the system's complexity and mass, as well as leading to lower manufacturing and maintenance costs. However, the absence of a control system necessitated that the plenum pressure and the dimensions of the holes in both sheets provide acceptable suction performance across the required range of flight conditions, as no active control was possible. The project successfully addressed this challenge, and the self-regulating system demonstrated effective performance in postponing transition across a range of test conditions encountered in a series of flight tests.
Moreover, the system prototype employed in the flight tests was also capable of functioning in passive mode, with the compressor deactivated and the pressure difference being generated by a flap situated in a low-pressure region. This solution was also found to be effective. [42–44]
Figure 2.21 shows the suction flap fitted next to the suction panel.

Figure 2.21: Suction flap on a vertical tail of A320 used for fligt tests in the ALTTA program [43]

This success subsequently led to efforts to further simplify the system by eliminating the inner sheet. The new idea was to develop a so-called tailored or hybrid skin that would cover the perforated outer sheet and would allow to tailor the suction profile, eliminating the need for a second skin sheet. A detailed view of the hybrid skin concept is provided in Figure 2.22.

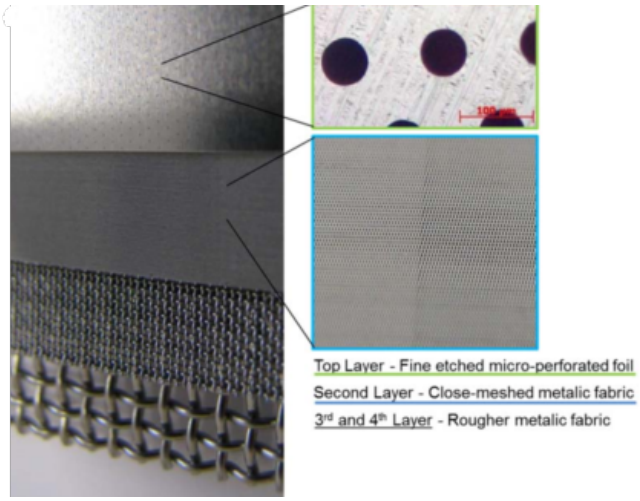

Figure 2.22: Mesh concept for suction velocity regulation [45]

The skin was composed of four distinct layers. The top layer was a thin, micro-perforated foil that ensured a homogenous suction of air from the boundary layer. Below the foil was a metallic mesh that provided variation in suction rates across the surface. This mesh allowed for fine spatial adjustments of the suction rates by varying the number of exceptionally thin wires that composed it to achieve the desired suction profile across the whole suction surface. The final two layers, also metallic meshes, were made of thicker wires, and provided the necessary mechanical stiffness to the laminate. Diffusion welding was then employed to ensure the connection between the layers.
While initial tests have been conducted to assess the design and manufacturing of the hybrid skin, no complete system employing this approach has yet been constructed. One plausible explanation for the absence of a complete system lies in the challenge of preventing chord- and spanwise flow inside the meshed layers [45].
However, an alternative explanation is the emergence of a more straightforward approach that has been contemplated in the past, but was only made feasible by recent developments of new, more precise manufacturing techniques. In the most recent HLFC concepts, the desired suction profile is achieved by means of a precise distribution of millions of microscopic holes in the suction sheet. Regions requiring larger suction rates then feature a greater number of suction holes. The suction chamber of constant pressure is then formed between the suction sheet itself and the front spar (or an additional plastic sleeve that ensures airtightness of the chamber).
This latest strategy considers achieving the desired suction profile by a precise distribution of the holes in the suction sheet, which alone forms a plenum in the leading edge with uniform pressure and carries the sucked air to the pumps. The primary benefit of this design is its simplicity, as it eliminates the necessity for suction chambers, ducting, and vents, as well as the inner sheet or any additional skin, such as the hybrid skin mentioned previously. This reduction in complexity leads to a further decrease in the system's mass, pressure losses (and consequently suction power requirements), and reduction in manufacturing and maintenance costs. However, in addition to the strict manufacturing accuracy requirements for producing the suction sheet, this approach faces a similar challenge to the one encountered in the ALTTA project. Specifically, the suction sheet must demonstrate sufficient performance for transition postponement across a range of flight conditions, with the only way to actively influence the suction rates being to vary the plenum pressure. This necessitates a precise aerodynamic design to determine the optimal distribution of the holes across the suction sheet, accounting for the fact that geometric factors such as sweep or the radius of the leading edge also influence the required suction profile.

2.3. Operational challenges with laminar flow technologies

Several factors can cause a significant loss of laminarity during the daily operation of an aircraft featuring laminar flow technologies, potentially leading to considerable performance degradation. The most critical factors include insect contamination, cloud encounters, ice accumulation, and surface damage. This section evaluates the impact of each factor on laminar flow performance, explores available mitigation strategies, and discusses their implications for the design, operation, and overall performance of the aircraft.

2.3.1. Insect contamination

When an insect strikes a part of an aircraft at a high velocity, its exoskeletal cuticle breaks and releases the hemolymph (fluid equivalent to blood in insects) onto the aircraft's skin. The hemolymph contains high amounts of proteins and amino acids and acts as a glue that attaches the remains of the insect's body to the surface. If the buildup of insect remains becomes large enough, its height may exceed the critical roughness height, triggering boundary layer transition and potentially causing a significant loss of laminarity over the component.
The accumulation of insect residue presents a challenge for both NLF and HLFC surfaces. However, for HLFC, it introduces an additional issue, as the residue can also block the suction holes (see Figure 2.23), thereby reducing the system's effectiveness. [47]

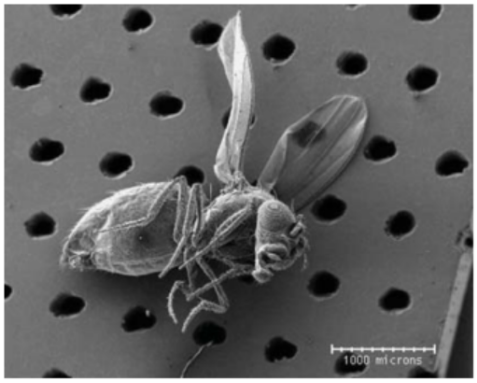

Figure 2.23: Suction hole blockage on an HLFC system by an insect contamination [47]

While surface contamination from a single bug might be negligible and impossible to prevent, accumulation of insect residue, either due to prolonged operation without cleaning or due to encounter of a large swarm, can lead to significant losses of laminarity and consequently to a substantial decrease in the aerodynamic performance of the whole aircraft. Therefore, the design of a laminar aircraft and its systems should consider the effects of insect contamination and its mitigation.
Joslin [10] provides an extensive overview of various strategies previously employed in experiments and flight tests to prevent insect contamination on suction surfaces. However, many of these strategies are impractical for regular use on modern aircraft, such as flammable covers designed to burn insect residue or paper covers pulled into the cockpit by the pilot after takeoff. Young [47] further analyzed the possibilities outlined by Joslin [10], incorporating more recent findings, and concluded that the most practical strategies are liquid discharge and Krueger flap shielding. These methods will now be discussed in greater detail.

Liquid discharge
Liquid discharge involves expelling a liquid over the targeted surface. This strategy is based on observations from several flight experiments, which demonstrated that wet surfaces are significantly less susceptible to insect contamination than dry ones. Such a system should activate during taxiing to coat the surface before takeoff and deactivate once the aircraft climbs to an altitude where insect contamination is unlikely.
This approach is not new and has been featured in numerous flight experiments with LFC and HLFC systems, some of which evaluated its effectiveness under simulated airline operations [6, 10]. The consensus from these experiments is that liquid discharge is highly effective in preventing insect contamination. Additionally, this system could also serve as an anti-ice system if the fluid used is a freezing-point depressant, which prevents ice formation [47].
However, the liquid discharge system also has several disadvantages that complicate its implementation. First, this approach is not feasible for NLF surfaces, which also require protection against contamination but lack suction holes to channel the liquid onto the surface. Employing additional jets for this purpose would introduce further complexities and aerodynamic challenges.
Complexity is the primary drawback of liquid discharge systems. Their implementation requires either an additional system or modifications to the suction system to achieve the necessary negative pressure ratio across the suction sheet for adequate fluid discharge. Furthermore, the system requires a storage tank and a distribution mechanism to ensure uniform fluid coverage over the leading edge. The design must also prevent liquid-induced damage to electrical components and potential damage to metal parts, such as corrosion. These factors substantially increase system complexity, resulting in higher maintenance and production costs.
Another significant challenge is the amount of fluid required to be carried by the aircraft. This is particularly problematic for modern HLFC systems that lack individual suction chambers and instead use the entire leading edge as a suction plenum. In such systems, the fluid would need to fill the entire leading edge volume to reach the surface, which is impractical due to the excessive fluid weight and the resulting stresses on the leading edge. However, this issue can be effectively addressed by using foam instead of liquid [47].

Nonetheless, using foam does not eliminate the need to continuously refill the medium throughout the aircraft's operational life, adding maintenance costs in addition to the cost of the fluid itself."

Krueger flap shielding

The Krueger flap is a leading-edge high-lift device that deploys in front of the leading edge, increasing the wing's effective chord and camber. Crucially, this flap can serve a second purpose of deflecting or blocking insects from striking the sensitive laminar surface, particularly in the leading-edge region where the risk of insect contamination is the highest. Numerous experiments have investigated this idea and concluded that Krueger shielding efficiently avoids insect contamination in the leading edge region. [6, 10, 47].

An additional significant advantage of the Krueger flap is its ability to eliminate gaps on the wing's upper surface, which would otherwise cause immediate transition. This issue is particularly problematic for conventional leading-edge high-lift devices, such as slats, and effectively prevents their application on laminar wings. However, the Krueger flap does not eliminate gaps on the wing's lower surface, making it virtually impossible to achieve larger extents of laminar flow over that area [47].

Some studies have proposed using a morphing leading edge to enhance lift without compromising laminar flow [48, 49]. However, morphing structures are a novel technology with many uncertainties and have yet to be implemented in production aircraft. In contrast, the Krueger flap is a conventional solution already used in existing passenger aircraft. For example, Figure 2.24 illustrates a Krueger flap on the Boeing 747-8. Additionally, replacing a Krueger flap with a morphing leading edge reintroduces the issue of insect contamination.

Figure 2.24: Krueger flap on Boeing 747-8 [50]

For these reasons, the Krueger flap is the preferred device in many aircraft design studies focusing on laminar flow, as it effectively addresses both insect contamination and high-lift requirements for low-speed performance. While liquid discharge appears to be an effective solution for insect contamination, the Krueger flap offers lower complexity, proven operational experience, and fewer design uncertainties, making it a more feasible choice.

2.3.2. Cloud encounter

Cloud encounters represent another possible cause of laminarity loss during the everyday operation of a laminar aircraft. Numerous past flight tests have concluded that entering clouds results in an immediate and complete loss of laminarity over all surfaces. This is caused by the presence of small ice particles within the clouds, which exist in extremely high numbers. These particles act as surface imperfections, introducing strong instabilities into the boundary layer and triggering rapid transition. However, flight tests also revealed that laminarity is fully restored as soon as the aircraft exits the clouds [10].

Therefore, while insect contamination causes a partial loss of laminarity over an extended period, cloud encounters result in a complete but short-term loss of laminarity. Unlike insect contamination, however, no known device or design feature can prevent the loss of laminar flow during the flight through clouds. The only effective solution in this case is careful route planning to avoid areas of extensive cloud cover [36].

Regarding the overall impact of cloud encounters on the feasibility of laminar flow technologies, Pohya [51] determined that the average time spent in clouds for a mid- to long-range aircraft is approximately 10%, corresponding to 10% of cruise time without laminar flow. While this figure appears significant, an extensive NASA study using data from commercial operations of four Boeing 747 airliners on typical North American routes concluded that 'encountering extensive cloud cover on long routes is not large enough, of itself, to make LFC impractical' [52]. This conclusion can similarly be applied to HLFC.
Furthermore, a general failure analysis must consider partial loss of laminarity and other critical scenarios, regardless of their cause, to develop an effective fuel planning strategy for the safe operation of the aircraft. Based on the stated statistics, the effect of cloud encounters does not constitute a unique or critical scenario in this context. Thus, a failure analysis is sufficient to address it without necessitating special consideration.
However, cloud encounters become more significant when estimating operating costs, particularly when factoring in alternative route planning. Previous studies that have incorporated cloud encounters into cost estimations include [49, 51, 53].

2.3.3. Ice accumulation

Ice accumulation, particularly in the leading-edge region, can quickly trigger boundary layer transition if its height exceeds the critical roughness threshold. However, because ice buildup can also cause early flow separation and a subsequent loss of lift, all modern aircraft are already equipped with ice-protection systems, most commonly using engine hot bleed air. Aircraft with HLFC systems could utilize these established bleed air systems, with the added benefit that hot air can flow through the suction holes, enabling faster ice melting and improved system efficiency with reduced engine offtakes. This method, known as transpirational anti-icing, is demonstrated in Figure 2.25, using an example from the Boeing 757 flight experiment. A drawback of this otherwise simple and conventional approach is that the high temperatures of bleed air limit the use of composite materials that would otherwise be suitable for the suction sheet support structures [36].

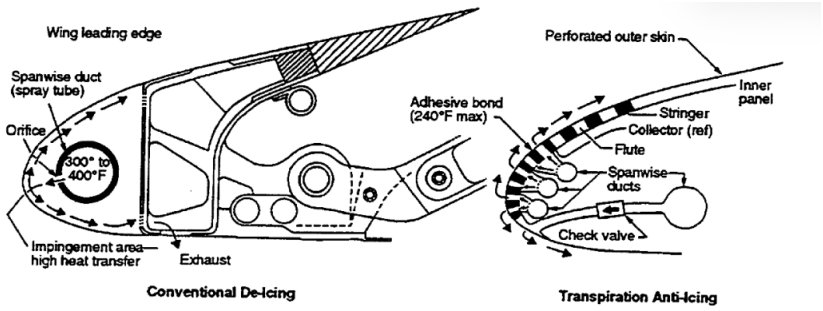

Figure 2.25: Comparison of conventional and transpiration anti-ice protection systems [36]

Apart from the conventional bleed air option, two novel approaches emerge when considering HLFC systems. The first is induction heating of the leading edge, leveraging the fact that modern HLFC designs use metal suction sheets, typically titanium. In this approach, a series of coils inside the leading edge heats the suction sheet to a sufficient temperature to melt accumulated ice. This solution offers several advantages, including the elimination of bulky hot engine bleed air systems, improved efficiency, and lower temperatures, which allow the use of composite materials. [54]
The second option is feasible only if the aircraft already employs a liquid discharge system for insect contamination protection. In this case, the same system could be adapted for icing protection by using freezing-point depressants, such as glycol-based fluids. Integrating the two systems could result in significant weight savings and reduced complexity compared to implementing separate systems. [47]

2.3.4. Surface damage

Potential damage to the laminar surface requires careful consideration for two primary reasons. First, in the event of a heavy impact, such as a bird strike, the structure must maintain its integrity to ensure a safe landing at the nearest airport. Second, even minor surface damage can cause early transition,

either directly from the disturbance created by the surface imperfection or, in the case of HLFC, due to deformation or blockage of the suction holes.
Erosion is an additional concern for HLFC surfaces, as the suction holes allow not only air but also tiny particles and fluids to pass through the suction sheet. For conventional aluminum components, erosion can be effectively mitigated by cladding with pure aluminum or applying a surface coating. However, these solutions are not feasible for HLFC surfaces, as they would block the suction holes. Consequently, HLFC surfaces must be made of materials that are naturally resistant to erosion and do not require additional surface coatings.
This requirement rules out the use of aluminum alloys, which are prone to severe corrosion and erosion when left unprotected. Composites like CFRP also present challenges, as they are difficult to drill with the necessary precision without causing material damage, are vulnerable to fluid damage, exhibit poor erosion resistance, and lose a significant portion of their tensile strength when perforated.
For these reasons, titanium is the material of choice in many HLFC projects. Experiments have demonstrated that titanium maintains its strength even when perforated and exhibits excellent resistance to erosion [9]. However, compared to conventional aluminum alloys, titanium is heavier, more expensive, and its use is associated with higher manufacturing costs.

2.4. Challenges in modeling laminar flow technologies

Accurate modeling and evaluation of laminar flow technologies present significant challenges due to the numerous factors that influence their performance. In the case of NLF, the primary uncertainty arises from the need to predict the transition location with sufficient accuracy, considering the effects of flight conditions and the geometry of the component to which NLF is applied. For the design and evaluation of HLFC systems, the main challenge lies in determining the required amount and intensity of suction applied by the system. Similar to transition prediction, the calculation of these suction parameters must consider the effects of component geometry and flight conditions, as well as the additional influence of the HLFC system's design.
This section examines these challenges in greater detail, reviews the approaches taken in previous studies to address them, and evaluates their applicability within the context of the conceptual aircraft design process.

2.4.1. Transition prediction in the context of conceptual aircraft design

The most challenging aspect of modeling laminar flow technologies in a conceptual aircraft design process is accurately capturing the sensitivity of the transition location to the various factors influencing transition. This difficulty results from the inherent complexity of the transition process, which depends on numerous interrelated factors. Consequently, no low-fidelity aerodynamic method currently exists to enable a quick yet accurate estimation of the transition location for a given component under specific flight conditions as part of the overall aircraft design process.
Accurate transition prediction, therefore, requires the use of high-fidelity aerodynamic tools. However, incorporating these tools into the overall aircraft design process is highly impractical, as even a single run can be extremely time-intensive compared to aircraft sizing tools, which operate within seconds. Preparing these high-fidelity simulations also demands significant additional time and effort. Such long runtimes are incompatible with the philosophy of the conceptual design process, which aims to evaluate numerous design options across the design space with minimal computational effort to identify the most promising directions for more detailed investigations. Consequently, high-fidelity methods are typically reserved for later design stages, once the general aircraft concept has been established.
To address this challenge, previous studies have developed various approaches to capture the sensitivities in transition prediction while minimizing computational effort. The following discussion reviews some of these methods, each representing a trade-off between accuracy and computational cost.

Lower-fidelity aerodynamic tools

The first approach involves using lower-fidelity aerodynamic tools instead of high-fidelity simulations (CFD). However, these tools still offer significantly higher fidelity than those traditionally employed in overall aircraft design. Examples include airfoil design codes, boundary layer solvers, and stability-based transition prediction tools.
While this approach reduces computational time compared to full CFD simulations, the runtimes remain significantly higher than those of low-fidelity methods. Consequently, the design space must still be

substantially narrowed, typically focusing on detailed component geometry design and considering only a limited range of flight conditions. This approach is therefore primarily used in studies focusing on aerodynamic optimization of a specific component, typically the wing, rather than evaluating the performance of the entire aircraft. As such, it is better suited to the later stages of the design process. Examples of studies that utilize such lower-fidelity simulations include those by Catalano et al. [55] and Atkin [56].

Database interpolation

The database approach utilizes high-fidelity CFD simulations or the lower-fidelity aerodynamic tools discussed in the previous approach to generate a database of results for various component geometries or airfoil shapes across a range of flight conditions. This database is then interpolated within the aircraft design process, substantially reducing the computational effort.

This approach is appealing because it captures all the necessary sensitivities with minimal computational requirements during the sizing process itself. However, it still requires high-fidelity simulations to build the database, which can be both expensive and time-consuming. Moreover, the design space is restricted to the geometries and flight conditions covered by the database, with only minor allowable deviations due to the inherent uncertainties of extrapolation. Finally, interpolation errors are inevitable and can become significant if the database is not sufficiently dense.

Nevertheless, once the database is established, it enables efficient analysis with sufficient accuracy and offers the flexibility to extend the database over time or reuse it in future projects. An example of this approach can be found in the work of Risse [5].

(Semi-) empirical models

Using historical experimental data is likely the most widely adopted strategy in aircraft design studies, as it provides a straightforward way to capture the key sensitivities of the transition point location to the most influential factors. This approach establishes relatively simple relationships between various geometrical parameters, flight conditions, and the resulting transition point location, while incorporating simplifying assumptions about less influential factors.

An example of this approach is the method developed by Wilson [57], which utilizes the observation that transition occurs earlier with a larger sweep angle. Based on this observation, the model assumes a linear decrease in the transition Reynolds number with increasing sweep angle, representing a simplified trend derived from empirical data. The model also accounts for the presence of an adverse pressure gradient at the point of pressure recovery, which limits the maximum extent of laminar flow, and assumes that the relative chordwise location of this pressure recovery remains constant across the entire wing span, illustrating a simplifying assumption. The transition point location at any given section is then determined by the more restrictive of these two criteria.

The method proposed by Wilson [57] is an excellent example of an approach that translates empirical observations into a simple model.

Regarding the empirical data itself, the open literature provides numerous plots, here referred to as transition plots, derived from experimental data, which can be used to determine the transition location for both NLF and HLFC (and in some cases for LFC as well). These plots typically show the expected transition Reynolds number for a given leading-edge sweep angle based on previous experiments. Figure 2.26 presents an example of a transition plot derived from historical data.

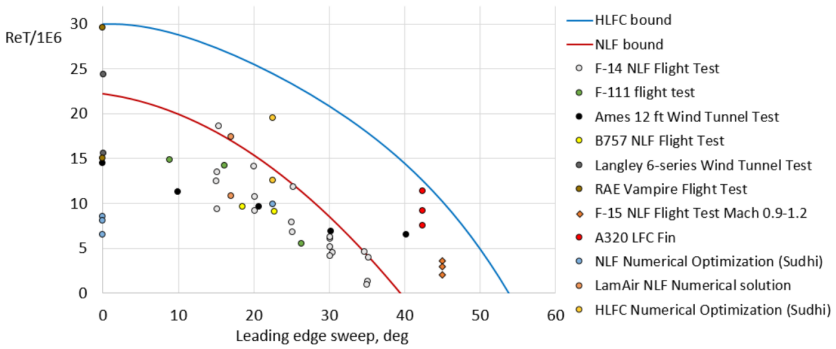

Figure 2.26: Example of transition plot derived from historical data[58]

However, while calculating the transition location using the transition Reynolds number obtained from such plots is undeniably the least computationally expensive approach, it is important to note that the data used to construct these plots may originate from various experimental datasets collected at different times using diverse test setups and methodologies. Additional inaccuracies may also arise from the low quality of experimental data. This is largely because much of the publicly available data on the performance of NLF and HLFC originates from flight experiments conducted in the 1980s and 1990s, often relying on outdated technologies and test aircraft that are not directly comparable to modern airliners.
Finally, the largest limitation of this approach is the fact that majority of the experimental data available in open literature shows the transition Reynolds number only as a function of the leading-edge sweep. This is primarily because laminar flow technologies are most often considered in the context of the wing. On modern airliners with highly swept wings, transition is predominantly driven by cross-flow instabilities (see Chapter 1.3). Consequently, the transition plots can be interpreted as representing the influence of the most restrictive transition mode. However, relying on this assumption could lead to scenarios where the actual transition over a given component occurs earlier than predicted by the transition plots, as the transition process may be driven by a different instability mechanism due to the component's specific geometry. Such an error could result in the aircraft failing to meet the expected fuel efficiency performance due to an overestimation of the achievable extent of laminar flow during the conceptual design phase.
In conclusion, while this approach provides a cost-effective and straightforward method for estimating the achievable extent of laminar flow, its proper application requires careful engineering judgment to assess the background and applicability of the experimental data used.

Fixed transition point
Assuming a fixed position for the transition point is the simplest approach, as it requires no calculations. However, this simplicity shifts the study from design evaluation to potential estimation, as the method does not account for any sensitivities of the transition location to influencing factors. Instead, it treats the transition location as a fixed requirement rather than a calculated result, unlike the previous methods. Consequently, it provides no insights into the extent of laminar flow that is achievable but instead focuses on the benefits that could be expected from achieving a given extent of laminar flow. This approach is, therefore, suitable for setting goals and requirements based on a desired fuel-saving benefit but not for evaluating different aircraft design options.
Examples of studies employing the fixed transition point approach include those by Boeing [59], Fan et al. [60], and Kulfan [61].

2.4.2. Calculation of suction parameters for HLFC systems

To design, size, and evaluate any HLFC system, two fundamental performance parameters must be known. The first is the air mass flow, which represents the amount of air sucked by the system per unit time. The second is the plenum pressure, which ensures the necessary pressure difference across the suction sheet to achieve the required mass flow. Alternatively, the pressure distribution over the component's surface and the suction velocity profile can be used to calculate the mass flow and plenum pressure, provided the properties of the suction sheet, primarily its porosity, are known. [5, 7, 42, 62]. These values, here referred to as suction parameters, largely determine the resulting transition location on the given component and are essential for sizing the HLFC system components, particularly the compressors, as well as for calculating the resulting power offtakes. However, their values vary with both the spanwise and chordwise locations on the component where suction is applied, as they are driven by the type and magnitude of the flow instabilities to be damped at the given location.
The dependence of the suction parameters on numerous factors, including the component's shape, the suction system design, and the flight conditions, makes their calculation a highly complex task. Consequently, obtaining the suction parameters along with the corresponding transition point location has thus far been achieved only through the use of multiple high-fidelity aerodynamic tools integrated into an iterative design and analysis process. This approach combines boundary layer stability analysis, which accounts for the effect of suction, with inverse airfoil design to determine a feasible combination of the component's geometry and the amount of suction applied. However, due to its high computational cost, such a detailed analysis is not suitable for direct integration into the conceptual aircraft sizing process. This makes the database approach, previously discussed for predicting the transition location,

the only viable option for capturing the variation of suction parameters within the conceptual aircraft design process. However, the database must be significantly more extensive than in the case of transition prediction alone, as it must account for at least two additional dimensions corresponding to the two suction parameters. An example of such an iterative process can be found in [5].
Forming a simplified model instead of utilizing a database is currently unfeasible due to the overwhelming complexity of the phenomena involved and the complete absence of publicly available suction data for modern HLFC system concepts. This lack of data also prevents the formation of any reasonable assumptions about the suction parameters, even if their variation is disregarded to simplify the problem.
The final option is to directly assume a certain system mass and power offtakes. However, this approach would significantly reduce the value of the analysis, as it would not allow for an investigation into the influence of varying HLFC system architectures, changing flight conditions, or the relationship between suction strength and transition location.
In conclusion, the determination of suction parameters for the accurate sizing and evaluation of HLFC systems presents a significant challenge, requiring extensive calculations and a high level of detail, with only limited opportunities for simplification when the goal is to accurately capture the relevant sensitivities.

3 Conceptual design of laminar aircraft

This chapter examines how the utilization of laminar flow technologies influences the conceptual aircraft design process, considering secondary consequences beyond the primary effect of reducing friction drag.
The first part of the chapter introduces aircraft configurations that are particularly well-suited for the application of laminar flow technologies, as the choice of configuration significantly affects the extent of achievable laminar flow over various components, primarily the wing. This is followed by a discussion of the additional, more subtle effects of HLFC or NLF on overall aircraft design and performance, including their secondary aerodynamic impacts, off-design performance, and integration challenges.
Lastly, the applicability limits of both NLF and HLFC are discussed. Considering these limits during the conceptual design phase is essential for selecting the most suitable laminar flow technology for a given aircraft or component and ensuring synergy between its effectiveness and the aircraft's operational performance.

3.1. Aircraft configurations

This section provides an overview and evaluation of several aircraft configurations that offer varying benefits for the application of NLF and HLFC. Rather than exhaustively evaluating all possible configurations, it focuses on a top-level discussion of those particularly attractive from the perspective of laminar flow technologies. Configurations so futuristic that they would require the development of entirely new sizing methods are excluded, as this thesis focuses on quantifying the potential of laminar flow technologies rather than exploring novel aircraft configurations.
Furthermore, note that in the following discussion, the term "conventional configuration" refers to an aircraft with a low cantilever wing, wing-mounted engines, and a traditional empennage, where the HTP is positioned below the VTP. This configuration is the most common among modern passenger aircraft and will, therefore, serve as the standard for evaluating the advantages and disadvantages of the alternative configurations.

3.1.1. Fuselage-mounted engines

One of the simplest modifications to the conventional configuration for easier integration of laminar flow technologies is relocating the engines from under the wings to the rear of the fuselage. This relatively traditional configuration can also be found on existing, mostly older passenger aircraft, such as the Embraer ERJ140, Bombardier CRJ series (shown in Figure 3.1), and McDonnell Douglas DC-9.

Figure 3.1: Bombardier CRJ 1000 with fuselage-mounted engines [63]

This configuration offers a clear advantage in enhancing laminar flow over the wing, as it results in a cleaner wing without any aerodynamic disturbances from the engine pylon or the engine itself [57]. Mounting the engines on the fuselage also prevents early transition on the wing caused by structural

vibrations propagating from the engines [64]. This issue is, however, less critical with modern turbofan engines, which are designed to minimize vibrations to reduce cabin noise [6, 57]. This configuration also facilitates easier retrofitting of higher bypass engines with larger diameters, which, in a conventional configuration, would require resizing the landing gear to maintain ground clearance [65].
Unfortunately, despite the benefits of a clean wing for laminar flow, this configuration features several significant drawbacks from an overall aircraft design perspective. The most critical drawback is the associated structural weight penalty, which arises from three main factors. First, in a conventional configuration, the substantial weight of the engines creates a relieving bending moment on the wings, opposing the moment generated by lift and reducing the wing's structural mass. In contrast, fuselage-mounted engines increase the structural mass of the fuselage due to the added engine loads. Finally, placing the engines at the rear of the fuselage requires moving the horizontal tail out of the engine's wake, typically by adopting a cross-tail or T-tail configuration. These designs have a higher structural weight than a conventional empennage, as the vertical tail must now support the additional loads from the horizontal tail [57, 66]. The combination of these factors results in a substantial weight penalty, significantly reducing or even negating the benefits of increased laminar flow from a cleaner wing.
While some studies employed this configuration without addressing the associated mass penalty ([59, 67]), the DLR projects LamAiR and TuLam (which built upon the work of LamAiR) accounted for this effect. The results indicated that placing the engines at the rear of the fuselage would increase the maximum take-off mass by approximately 2% and the design mission fuel by 3%. Although the LamAiR concept retained the fuselage-mounted engine configuration to maintain a clean wing and allow for potential retrofitting of higher bypass ratio engines, the TuLam project reverted to underwing engine placement to avoid this penalty [65, 66]. Figures 3.2a and 3.2b provide a comparison of the LamAiR and TuLam concepts, respectively.

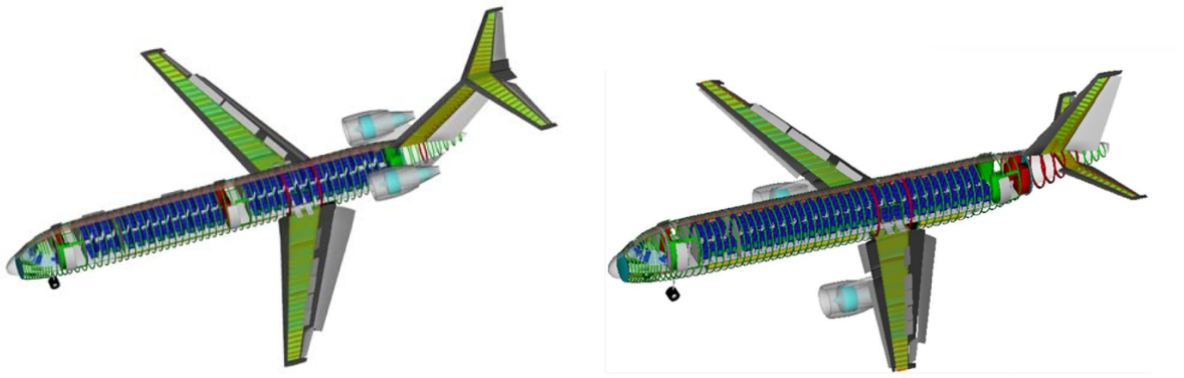

(a) LamAiR concept [65] **(b)** TuLam concept [66]

Figure 3.2: Comparison of the LamAiR and TuLam concepts

3.1.2. Forward-swept wing

A forward-swept wing is the first configuration in this overview that has not yet found its way into a real-world application on large passenger aircraft. The main reason is the problem of aeroelastic divergence. In this phenomenon, an upward bending of the swept-forward wing also induces its torsion, increasing the angle of attack and leading to higher lift and more bending. If this cycle continues, a structural failure is imminent. For long, the only known solution to this problem has been a structural reinforcement of the wing, leading to unacceptably large weight penalties.
However, recent advancements in composite materials research and application suggest a promising new approach. A technology known as aeroelastic tailoring leverages the anisotropic properties of fiber-based composites by strategically layering plies with varying fiber directions [66]. This enables coupling between the wing's bending and torsional deformation, mitigating the divergence phenomenon while minimizing or even eliminating the associated weight penalty. This approach was demonstrated in the aforementioned DLR projects LamAiR and TuLam, which conducted detailed structural and aerodynamic designs of aircraft concepts featuring a forward-swept NLF wing, followed by evaluations of overall performance. The projects concluded that the forward-swept wing concept was feasible and

warranted further investigation, with estimated block fuel reductions of 9% for the LamAiR concept and 12% for the more advanced TuLam concept [65, 66].
The forward-swept wing is an attractive configuration for laminar flow due to simple geometric relationships. On a conventional tapered swept-back wing, the leading-edge sweep angle is always greater than the half-chord sweep angle, which is the opposite of what is desirable for facilitating laminar flow. For such wings, the goal is to minimize the leading-edge sweep angle to prevent transition caused by cross-flow and attachment-line instabilities (see Chapter 1.3) while maximizing the half-chord sweep to limit wave drag at high subsonic speeds. These two requirements conflict on a swept-back wing but can be achieved on a tapered forward-swept wing, where the leading-edge sweep angle is always smaller than the half-chord sweep angle [12]. Figure 3.3 graphically illustrates this principle.

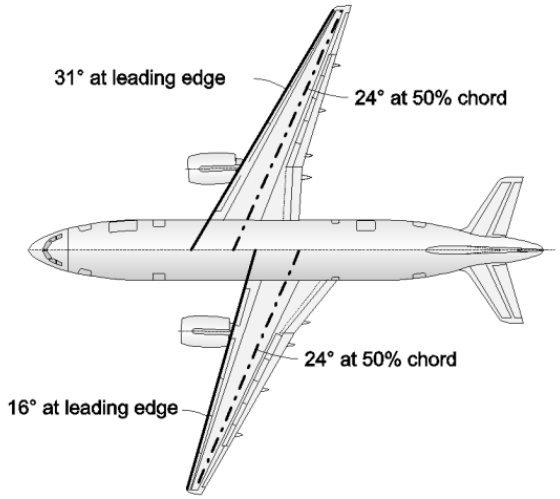

Figure 3.3: Visualization of the different LE sweep for the same 50% chord sweep for forward and backward swept wings [12]

An aircraft with a forward-swept wing could therefore achieve greater extent of laminar flow than a backward-swept wing at the same Mach number, or the same extent at higher Mach number. Flying at higher Mach numbers then benefits flight economy and further delays transition [2]. This advantage is particularly significant for wings with natural laminar flow, where the transition location is highly sensitive to the sweep angle. For HLFC wings, suction mitigates both cross-flow and attachment-line instabilities, enabling the wing to tolerate larger sweep angles without earlier transition. However, this comes at the cost of additional suction system mass and power offtakes. Forward sweep also prevents attachment line contamination, as the boundary layer flows from the wingtip toward the root, avoiding the spread of flow disturbances from the wing-fuselage junction, which is a known issue on swept-back wings [57]
However, despite these undeniable aerodynamic advantages, the uncertainty regarding the structural mass of a composite forward-swept wing remains considerable. A reliable estimation of this mass would likely require a detailed structural design using high fidelity methods, such as finite element method (FEM).

3.1.3. Truss-braced Wing

A truss-braced wing (TBW) is a novel aircraft configuration that incorporates one or more primary struts, with optional jury struts, to relieve part of the root bending moments on the wing. Figure 3.4 presents two examples of truss-braced wing aircraft concepts developed in previous studies.

(a) Truss-braced wing aircraft concept from Lucas Kugler [68]

(b) Truss-braced wing aircraft concept from Boeing [69]

Figure 3.4: Examples of truss-braced wing aircraft concepts

The main strut functions to reduce the bending moment at the wing root. It operates under tension during nominal flight and experiences compression only under specific conditions, such as touchdowns or gusts. Jury struts are incorporated to prevent buckling of the main strut under these compressive loads.
The relief of part of the bending moments from the wing by the strut provides several significant benefits. The most immediate effect is that the wing span, and therefore the aspect ratio, can be significantly increased without adding structural mass or requiring an increase in the wing's thickness.
In a conventional cantilever wing, sections closer to the root require greater absolute thickness to achieve a sufficiently large second moment of area to withstand the high bending moments generated by the wing. Increasing the aspect ratio of such a wing is challenging for two main reasons. First, a larger span increases the moment arm, leading to higher root bending moments. Second, if the relative root thickness remains constant to maintain aerodynamic characteristics, a shorter chord length reduces the absolute root thickness. Consequently, the only way to address the increased root bending stresses is through structural reinforcements, resulting in significant weight penalties.
The TBW configuration addresses this issue by relieving part of the bending moments through the strut. Reducing root bending moments enables the use of thinner root sections, leading to lower wave drag. Consequently, a TBW can feature a lower leading-edge sweep for the same cruise Mach number. Reduced root bending moments also allow for an increased wing aspect ratio without adding structural mass. A higher aspect ratio reduces induced drag and, for a given wing area, shortens chord lengths across the wing span. The combination of lower sweep and shorter chords makes the TBW configuration ideal for applying laminar flow technologies, as local Reynolds number and leading-edge sweep are the two most critical factors influencing transition (see Chapter 1.3). Furthermore, the strut itself can be further designed as a lifting surface and can also support the application of natural laminar flow due to its relatively short chord.
As with any configuration, the benefits of a truss-braced wing must be weighed against its drawbacks. The most significant disadvantages include parasitic, wave, and interference drag from the struts, along with their additional weight. Further drawbacks arise from the configuration requiring the use of a high wing and T-tail, which are traditionally heavier than conventional alternatives. [68]
However, despite these drawbacks, previous studies have shown that this configuration can still deliver significant fuel-saving benefits and that a truss-braced wing might be one of the most promising strategies for future aircraft concepts [68, 70, 71].

3.2. Impact of laminar flow technologies on aircraft design

While the previous sections focused primarily on the function and design of laminar technologies, their applications have significant implications for both the laminarized components and the entire aircraft. These implications extend to the aircraft's geometry, systems, performance, and operations. This section discusses the key factors that must be carefully considered when integrating NLF and HLFC technologies into the aircraft design during the conceptual design phase.

3.2.1. Aircraft design consequences of NLF

In addition to reducing frictional drag by enabling larger extents of laminar flow, NLF introduces secondary effects on aircraft design, many of which are undesirable. These secondary effects primarily result from the specific shape of NLF airfoils, which are designed to maintain a favorable pressure gradient over as much of their chord length as possible. [2].

The first characteristic of NLF airfoils is the presence of a so-called drag bucket. At its design lift coefficient, a typical NLF airfoil exhibits significantly lower drag compared to a turbulent airfoil, owing to the large extent of laminar flow. However, in off-design conditions, NLF airfoils provide lower drag levels only within a relatively narrow range of lift coefficients. Outside this range, the flow transitions to turbulent, causing a sharp increase in drag to levels comparable to or even higher than conventional turbulent airfoils. This behavior is evident on the drag polar as a characteristic bucket shape around the design lift coefficient. Figure 3.5 illustrates this, comparing the drag polars of a typical laminar airfoil and a turbulent one.

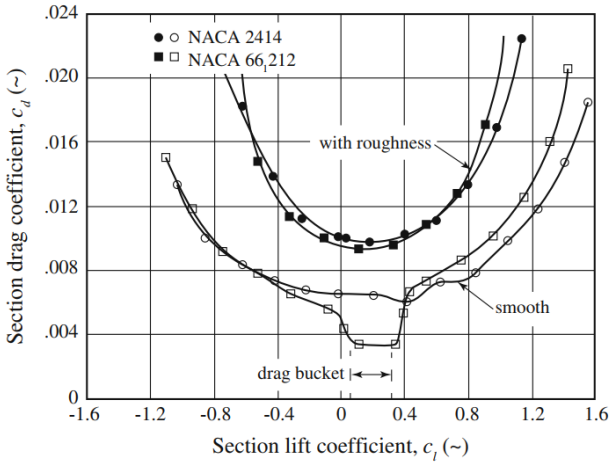

Figure 3.5: Comparison of drag polars of conventional and laminar airfloils with the effect of roughness [2]

Figure 3.5 also illustrates that any disturbance or surface roughness on the airfoil causes the laminar bucket to disappear, resulting in a drag polar similar to that of a conventional airfoil. These observations highlight the importance of operating NLF airfoils close to their design point and maintaining their surface in perfect condition, both of which present challenges in real-world operations. [2] The second performance limitation of NLF airfoils arises from their sharper noses compared to conventional airfoils of the same relative thickness, due to their thickest point being located much further aft. A sharp nose leads to an earlier onset of leading-edge separation and reduces the airfoil's maximum lift coefficient [2]. It can also result in a lower angle of attack at which the maximum lift coefficient occurs, which is particularly concerning for takeoff and flare performance [57].

The more aft location of the thickest point and the associated suction peak also shift the airfoil's center of pressure aft, resulting in a larger nose-down pitching moment [57]. If the aircraft's design does not account for this increased pitching moment, this may lead to a significant trim drag penalty due to the horizontal tail deflection required to compensate for it.

However, the aft location of the thickest point has another, this time positive, effect as it increases the volume available in the middle region of the airfoil, between the spars, which is typically used for fuel storage. This results in a slightly larger fuel capacity for the same wing geometry. However, this benefit is partially offset by a thinner front spar due to the sharper airfoil nose [57].

The final performance consideration for NLF airfoils is their poor high-speed performance. Primarily due to the rapid pressure recovery in their aft region, NLF airfoils generate much stronger shock waves compared to modern transonic airfoils when operated near their critical Mach number, resulting in a significant increase in wave drag [2]. This is a major concern when considering the application of NLF to modern passenger aircraft cruising at high subsonic Mach numbers. However, this issue may be less restrictive for NLF aircraft concepts specifically designed to operate at lower cruise Mach numbers to reduce leading-edge sweep and achieve a larger extent of laminar flow.

3.2.2. Aircraft design consequences of HLFC

Unlike in NLF, the airfoil shape plays only a partial role in maintaining laminar flow with the HLFC approach. Since suction dampens most flow disturbances in the critical nose region, NLF-specific shaping is only required in the mid-chord region to avoid large adverse pressure gradients that could rapidly amplify the Tollmien-Schlichting disturbances [5]. As a result, airfoils used for HLFC are closer to conventional transonic airfoils. While the issues associated with NLF airfoils are still relevant for HLFC sections, the constraints are less severe. This also means that HLFC airfoils perform well in off-design conditions and even in turbulent regimes without applied suction [57]. This capability is particularly important when evaluating the impact of a potential suction system failure.

Nevertheless, implementing HLFC introduces a series of considerations that are crucial for the overall aircraft design, primarily related to system integration, power offtakes, and mass.

Regarding integration, a significant challenge with all HLFC concepts is fitting the system into the limited space available at the leading edge, ahead of the front spar. This is further complicated by the need to accommodate other systems, such as anti-ice systems and high-lift devices, within the same space. Additionally, the system must be designed to allow easy inspection and maintenance of its most critical components, particularly the compressors [5].

Another important consideration for any HLFC system is its mass. While the mass itself is undeniably a critical factor that must be accounted for, its distribution is a less apparent but also important consideration. This is particularly relevant when applying HLFC systems to swept wings with large spans, where placing significant mass near the wingtips could noticeably shift the aircraft's center of gravity. If not properly addressed, such a shift could result in increased trim drag.

Next, 2.3.1 on shielding protection against insect contamination already discussed in detail why the Krueger flap is the optimal choice for a leading-edge high-lift device when applying HLFC to the wing. However, it is also important to highlight why conventional slats are impractical for such applications. The first issue is the rearward-facing step created by a slat in the stored position, which can further enlarge during flight due to the wing's bending motion. This step, inconveniently located in a region highly sensitive to surface disturbances, could lead to early flow transition.

Secondly, slats in the stored position cover a large portion of the leading-edge area where HLFC systems apply most of the suction. Combining slats with HLFC would therefore require the slats to be equipped with a suction system, introducing significant integration challenges due to the limited space inside the slats and the need to transport the extracted air to compressors within the main wing body. Such a complex setup appears impractical for operational use, making conventional slats incompatible with HLFC systems [57].

Finally, a critical influence of an HLFC system on the rest of the aircraft is the electrical power offtakes required to drive the compressors. Similar to the system's mass, power offtakes and the associated increase in fuel burn are essential factors for an accurate assessment of the system's overall benefits. Additionally, understanding the system's power requirements is crucial for sizing the aircraft's electrical system, which must be capable of meeting these demands. For example, in the case of an extensive HLFC system with suction implemented across multiple components, the standard electric generators installed on the engines may not provide sufficient power. such limitation could require resizing the generator, potentially leading to a significant weight penalty, increased manufacturing costs, and other challenges associated with modifying the engine design.

In conclusion, the secondary implications of integrating an HLFC system into an aircraft design must be carefully evaluated, as the resulting trade-offs and design decisions can significantly affect the aircraft's overall performance.

3.2.3. Applicability limits of laminar flow technologies

In the discussion that follows, the term "applicability limits" refers to a set of constraints on flight conditions or component geometry within which laminar flow technologies can sustain a specified extent of laminar flow over the component under consideration. Numerous values for these constraints, derived from previous investigations and experiments, are readily available in the open literature.

For NLF, one of the most widely cited sets of constraints is provided by Schrauf [72], which states that NLF is applicable for leading-edge sweep angles below 23 degrees, Reynolds numbers below 25 million, and Mach numbers below 0.75. Similarly, the work of Holmes et al. [73] uses the same parameters but provides slightly different values: a sweep angle of 27 degrees, a Mach number of 0.7, and a Reynolds number of 30 million. Braslow [6], based on flight tests with an NLF glove on an F-14,

reports a stricter limit for the leading-edge sweep angle of 18 degrees. In contrast, Wilson [57] adopts a limit of 25 degrees. Finally, Joslin [74] states that a sweep angle of 10 degrees allows for 50% of the chord to be laminarized, whereas a 25-degree sweep reduces this potential to only 20%. Some studies also incorporate the assumption of fully turbulent flow below a certain threshold altitude to account for the effects of cloudiness (as discussed in 2.3.2) and free-stream turbulence. This threshold altitude is typically set between flight levels 280 and 350, with examples of its application to both NLF and HLFC available in [49, 59, 61, 75].

This demonstrates that applicability limits are not strict design rules and largely depend on the specific application case. While it is valuable to understand the general limits of the technology, the cited values do not provide insight into how the effectiveness of NLF changes as these limits are approached but not exceeded. Therefore, these values serve as useful guidelines to quickly rule out overly optimistic applications of NLF but should not be treated as absolute limits applicable under all conditions. Additionally, it is crucial to account for the methodologies, setups, and test aircraft used to gather the experimental data from which these constraints were derived.

In the case of HLFC, the information available in the literature regarding its applicability constraints is significantly more limited compared to NLF. This limitation can be attributed to two primary factors. First, the amount of publicly available test data or experimental results for HLFC is considerably lower than that for NLF. Second, the performance of an HLFC system depends heavily on additional design variables, such as the extent of the suction area, the suction intensity, and the variation of suction across different flight conditions. These variables make it challenging to establish a clear set of constraints that would universally apply to all HLFC systems and their applications.

Nevertheless, the most widely accepted consensus is that, with careful design and the avoidance of extreme geometries or flight conditions, HLFC can delay transition up to the point of pressure recovery and the associated shock wave present on the supercritical airfoils used in modern airliners. Although this position varies depending on the specific airfoil design, it is generally located around 60–65% of the chord, which represents the maximum extent of laminar flow achievable by HLFC [57, 65, 66]. However, in real-world operations, these limits may vary with flight conditions, particularly Mach number and lift coefficient, as these factors can cause the shock wave to shift in the chordwise direction [2]. The magnitude of this shift depends on the specific airfoil design and the extent to which the Mach number and lift coefficient vary during the flight. The flow may be also intentionally tripped before reaching the shock wave to prevent laminar separation caused by the interaction between the boundary layer and the shock [65]. In addition to compressibility effects, the extent of laminar flow achievable through the application of HLFC can also be limited by the presence of trailing-edge high-lift devices and their associated surface gaps, which can cause earlier transition.

As a final remark, some publications also provide a visual representation of the discussed applicability limits of the different laminar flow technologies. Example of such plots is provided in Figure 3.6.

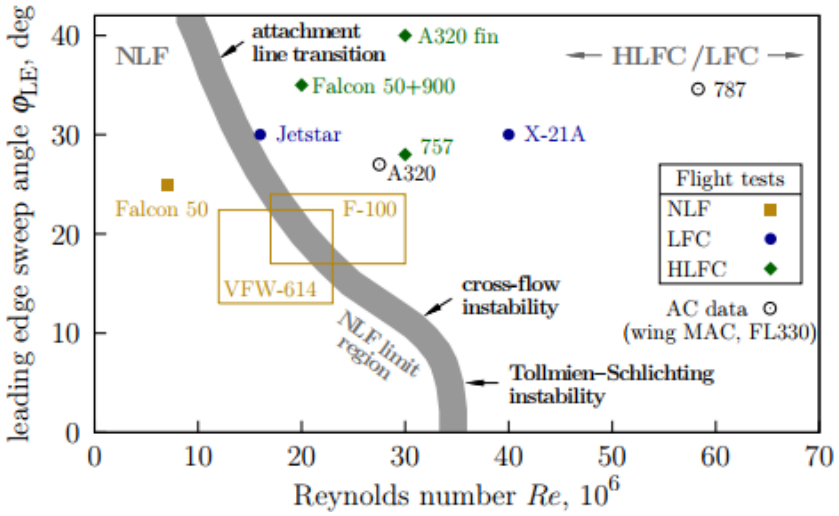

Figure 3.6: Example of plot visualizing applicability limits of the different laminar flow technologies [5]

4 Conclusion

The review of existing literature reveald that the successful development, integration, and operation of an HLFC system within the design process of a new aircraft requires the consideration of three critical disciplines: overall aircraft design, system design, and aerodynamic analysis. The overlaps between these disciplines define the most important factors that must be addressed to capture the critical effects of the HLFC system on the final aircraft. A diagram in Figure 4.1 illustrates these relationships between the disciplines. It is important to note that the diagram highlights only the relationships relevant to implementing an HLFC system, rather than all interactions present between the disciplines in general.

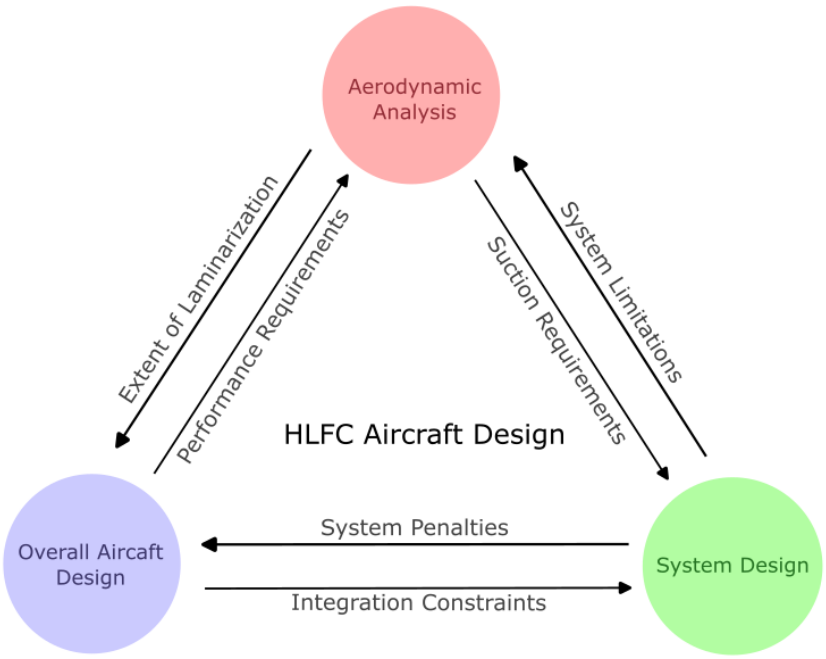

Figure 4.1: Core disciplines for conceptual design of an aircraft equipped with the HLFC system

The connection between aerodynamics and system design can be considered first. Aerodynamic analysis, particularly airfoil and planform design combined with transition analysis, provides the fundamental requirements for the suction system, namely the pressure difference across the suction sheet and the air mass flow through it. These parameters enable the design of the suction system, including the sizing of ducts, compressors, and the electrical motors that drive the compressors. However, system design also influences aerodynamics. For instance, the fraction of the component's surface covered by the suction sheet determines the extent of the surface that can be laminarized, regardless of the level of suction applied.
System design is also influenced by the discipline of overall aircraft design. Integration constraints limit the design and architecture of the HLFC system, as the shape and size of the component to which the system is applied are determined by other disciplines and considerations. For example, the design of a wing planform is primarily determined by the combination of top-level performance requirements and the chosen configuration. Consequently, its general size and shape cannot be significantly altered solely to enhance the performance or integration of the HLFC system, making these factors constraints rather than variables in the HLFC system design process.
However, just as aircraft design influences system design, the reverse is also true. The system impacts the overall aircraft design primarily through its mass and power offtake penalties, though other factors, such as its effect on the center of gravity, are also significant.
The loop then closes through a third connection between aerodynamics and overall aircraft design.

In one direction, the aerodynamic design of various components determines the extent of laminar flow achievable and, consequently, influences the performance of the entire aircraft, which is the primary motivation behind applying any laminar flow technology. In the other direction, aircraft-level requirements, such as the maximum lift coefficient for landing performance, constrain the aerodynamic design, preventing it from focusing solely on maximizing the extent of laminar flow and necessitating trade-offs with other performance requirements.
With this framework, the relationships diagram could be expanded to include additional disciplines when transitioning to more detailed design phases. One such example is operational analysis, which evaluates the aircraft's performance in real-world utilization. This discipline is critical for assessing the practical benefits of new technologies under actual operating conditions. However, it is not essential for the basic implementation of the HLFC system in the conceptual aircraft design process. Therefore, it was omitted from the diagram in Figure 4.1, where the three primary disciplines presented are sufficient for a top-level evaluation of the potential of the HLFC technology.
Finally, the diagram in Figure 4.1 could be modified to represent the implementation of NLF by removing the system sizing discipline, as NLF is a passive technique that does not require additional systems or components. This simplification significantly eases implementation and minimizes the necessary trade-offs, which is then one of the advantages of NLF over HLFC.

4.1. Knowledge gaps in the existing research

The presented literature review showed that a number of previous studies have evaluated the effect of NLF [60, 65–67, 76, 77] and HLFC [57, 58, 78–80] on aircraft design and performance. These studies have employed a variety of methodologies, including retrofitting the technology to an existing aircraft and considering it in the conceptual aircraft design. Nevertheless, there are certain areas of interest with regard that still require further investigation.
First, although previous studies have demonstrated the potential benefits of the individual technologies, there has been no investigation into the feasibility of utilizing them simultaneously on a single aircraft or even a single component. By combining the NLF and HLFC, it may be possible to leverage their respective advantages and enhance the overall benefit on the aircraft level.
A second room for further investigation is a consequence of a common practice observed in the majority of previous works. The design process typically initiates with a set of top-level aircraft requirements (TLARs), which are based on an existing aircraft that the new developed concept is intended to replace in the corresponding market sector. However, as the design progresses, these TLARs are often varied in order to maximize the benefit obtained from the utilization of laminar technologies. To illustrate, the cruise Mach number is frequently reduced in order to permit the use of a wing with a lower sweep angle to postpone transition. Although this approach is justified in academic studies aimed at establishing the maximum potential of the given technology, it is unlikely to be the practice employed by the industry. In the real world, the TLARs are a result of a market analysis, reflecting the customer requirements. If a laminar concept is therefore designed to replace an existing aircraft in a specific market sector, the TLARs are likely to be fixed and not available for variation.
The next difficulty arises from the fact that evaluation of the benefits of any HLFC system when applied to a specific aircraft component relies on the correct estimation of the mass and power offtakes of the suction system. Although, sensitivity analyses were previously conducted ([75, 81]), in which the two values in question were the varied inputs provided to establish a range of potential benefits, such an approach is not applicable in the conceptual aircraft design process, which aims to produce a fully defined aircraft concept.
The most elaborate method for preliminary estimation of the mass and power requirements of HLFC systems was introduced by Pe and Thielecke [82], which was subsequently used in modified forms in additional studies [7, 62]. These studies, however, approached the sizing of the HLFC system for a given component as a standalone problem, rather than integrating the methodology into a larger aircraft design process.
A unique study was conducted by Risse [5], who integrated the aforementioned methodology with aircraft sizing tools and high-fidelity aerodynamic simulations to create an integrated preliminary aircraft sizing process. This process was then used to assess the potential of the HLFC technology when applied to the wing and tail of a long-range passenger aircraft.
Finally, majority of the existing work considered the HLFC only in the context of medium-to-long range

aircraft [5, 78, 81, 83–85]. However, as illustrated in Figure 4.2, more than half of the total CO_2 emissions are currently produced by the short-to-medium aircraft category, with the highest production observed for the short-range category.

Figure 4.2: Share of passenger CO_2 emissions in 2019, by stage length and aircraft class [86]

4.2. Research question

Based on the gaps identified in existing research, the following research question has been formulated:

What fuel savings can be expected from the application of laminar flow technologies to a short-to-medium range aircraft with a fixed set of top-level requirements, when considering a realistic laminar flow system design in the aircraft sizing process?

Furthermore, fully addressing the stated research question requires answering the following sub-questions within the context of the conceptual design of short-to-medium range aircraft:

1. Which laminar flow technologies should be applied to different components to maximize fuel-saving benefits at the aircraft level?
2. What additional fuel benefits can be expected from the combined application of two laminar flow technologies, NLF and HLFC, compared to the utilization of a single technology across all laminarized components?
3. What benefits can be expected from the combined application of NLF and HLFC to a single component, specifically the wing?
4. How are the fuel-saving benefits of HLFC affected by the associated system mass and power offtake penalties?
5. Utilizing the optimal combination of laminar flow technologies across various components, and accounting for secondary effects and penalties, what realistic overall fuel savings can be expected?
6. How do different failure scenarios, including contamination of NLF surfaces and failure of HLFC suction systems, affect the performance of the developed laminar aircraft, and what are the implications for fuel planning strategies?

4.3. General research approach and methodology

To ensure the research question would be fully answered, a preliminary research plan was developed. This plan organizes the research into five fundamental stages: extending the conceptual aircraft design process, calibrating the methodology, verifying and validating the approach, developing a laminar aircraft concept, and analyzing aircraft performance.

1. Extending conceptual aircraft design process

The work in this thesis shall utilize a software toolchain, referred to as the "workflow", previously developed by the German Aerospace Center (DLR) for conceptual aircraft design. This workflow integrates multiple aircraft sizing and performance evaluation tools developed internally by DLR into an iterative design process. It combines low-fidelity handbook methods for overall aircraft design with higher-fidelity methods for mission analysis and low-speed performance evaluation.
The first task of this research will be to adapt the workflow to enable the sizing of aircraft equipped with two laminar flow technologies, NLF and HLFC. The adapted workflow must account for the aerodynamic effects of these technologies, as well as secondary effects such as the additional power offtakes and mass introduced by the HLFC systems. It should also consider the increase in fuel consumption caused by the additional power offtakes and the impact of the added mass on the aircraft's center of gravity.
To estimate the system masses and power offtakes of the considered HLFC systems, the workflow will be also extended with an additional tool. This tool, previously developed by the author, enables the design, sizing, and analysis of HLFC systems for various aircraft components. Within the workflow, it will calculate the power offtakes and masses of the individual HLFC subsystems applied to different components. Additionally, the tool will calculate the amount of wetted area subject to laminar flow on a given component, based on a user-defined transition location.

2. Methodology calibration

After adjusting and extending the workflow, the next step will be its calibration. The laminar aircraft concept developed in this work will not be created from scratch but will be derived from an existing turbulent aircraft concept, referred to as the baseline aircraft. This process will involve applying laminar flow technologies to its components, namely the wing, VTP, and HTP, followed by its full resizing using the described workflow.
As such, if the workflow is provided with the input parameters used to generate the original turbulent aircraft, without applying any laminar flow technologies, it should produce an aircraft concept identical to the turbulent design. However, since the turbulent aircraft was developed using a slightly different version of the original workflow, which did not include the additional HLFC system sizing tool or adaptations for laminar flow technologies, the output is not expected to perfectly match the turbulent aircraft concept. A calibration process will therefore be carried out, during which calibration factors will be applied to the outputs of the various tools implemented in the workflow until the results match the turbulent concept with sufficient accuracy.

3. Verification and validation

The verification and validation of the implemented methodology will follow, focusing on the accurate estimation of the mass and power offtakes of the HLFC systems and the precise evaluation of the impact of increased power offtakes on fuel consumption.

4. Development of laminar aircraft concept

While the first three phases of the research focused on establishing a reliable methodology for the conceptual design of laminar aircraft, the third research phase will gather the data required to address the stated research question and sub-questions. This will be achieved by gradually introducing the two laminar flow technologies to the turbulent baseline aircraft.
First, both NLF and HLFC will be applied to each of the considered components to determine the most suitable laminar flow technology for each one. The components will be laminarized individually, with full aircraft resizing performed to account for secondary effects. Once the most suitable technology for each component has been selected, the turbulent baseline aircraft will be resized with the selected technologies applied simultaneously to all components. Additionally, the same resizing process will be

conducted for aircraft concepts featuring only one of the technologies applied across all the components. Comparing the resulting fuel savings will provide an estimate of the additional fuel savings achievable by combining the two laminar flow technologies on a single aircraft concept.
The next step in the research will involve investigating the potential benefits of combining NLF and HLFC on the wing. If this approach proves to be beneficial, the final laminar aircraft will be developed by incorporating a wing utilizing both technologies, along with the laminar flow technologies selected in the previous step for the VTP and HTP.

5. Analysis of the aircraft performance

In the final stage of the research, the design of the developed laminar aircraft concept will be considered fixed and no longer subject to resizing. This stage will focus on obtaining additional data on aircraft performance using the mission analysis tool previously employed during the sizing process. As part of this analysis, various failure scenarios of the HLFC systems and the loss of laminarity over the NLF surfaces will be evaluated to assess their impact on the performance of the laminar aircraft concept.

Part III

Supporting material

1 Verification

This chapter presents the verification tasks performed to confirm the correct implementation and functionality of the utilized methodology.
First, the validation process of the OpenAD engine model is described, assessing whether the model accurately captures the effect of increased power off-takes on fuel consumption. The second part of the chapter focuses on the verification of the HLFC system sizing tool, ensuring that the masses and power off-takes of HLFC subsystems are correctly calculated based on comparisons with results from previous studies.

1.1. Verification of the engine model

To accurately estimate the block fuel penalties associated with implementing HLFC subsystems in an aircraft design, the utilized engine model must accurately capture the increase in fuel consumption resulting from a given increase in electric power off-takes.
In this study, the engine sizing and performance calculations were facilitated by the OpenAD tool. While these calculations account for the effect of electric power offtakes, they are based on low-fidelity cycle calculations, handbook methods, and fundamental thermodynamic relations. To ensure the accuracy of the results, a verification process was therefore conducted. In this process, the engine of the baseline aircraft was sized for varying levels of additional power offtakes across a range of altitudes and thrust levels. The resulting values for trust-specific fuel consumption (TSFC) under different conditions were then compared to results obtained for the same conditions using a rubber-engine model, representing a higher-fidelity method.
Figure 1.1 compares the thrust-specific fuel consumption (TSFC) obtained from OpenAD and the rubber engine model as a function of thrust and power offtakes at a flight level 370 (FL370). This flight level corresponds to the cruise level observed for the baseline aircraft during both evaluation and design missions. The percentual increase in TSFC was calculated relative to the TSFC of the baseline aircraft with its original cruise power offtakes of 50 kW. For clarity, the figure displays power offtake levels only up to 150 kW, although calculations were performed for values up to 250 kW. Similar calculations were also conducted for FL330 and FL350.

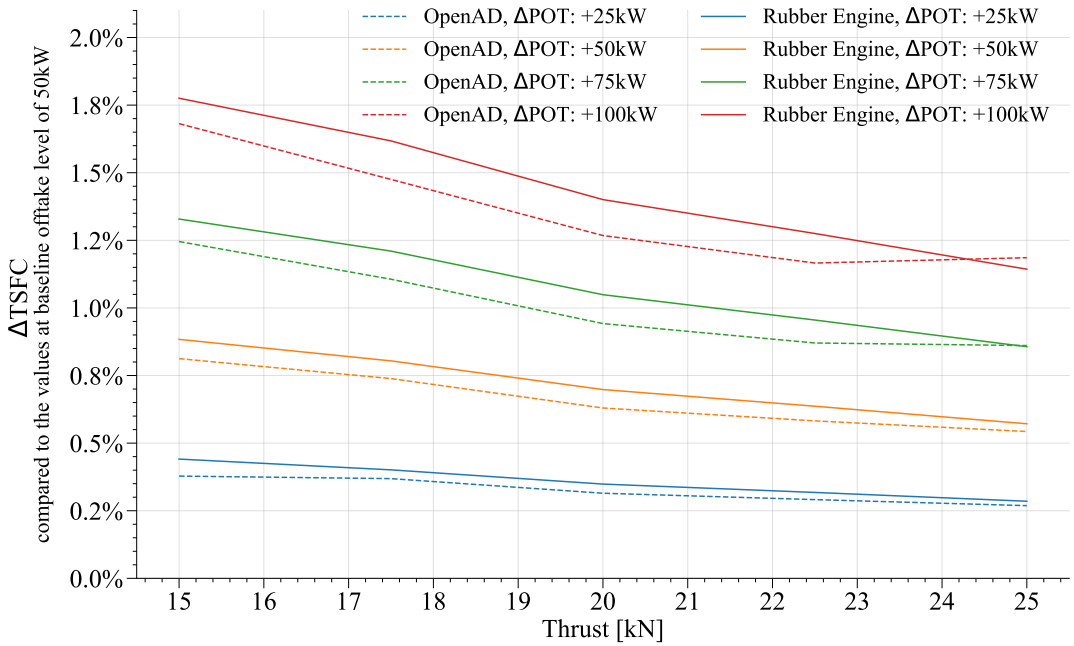

Figure 1.1: Increase in TSFC due to additional power off-takes as predicted by OpenAD and the rubber engine model at FL370

The observed general behavior indicates that the OpenAD model underestimates the effect of power offtakes on fuel consumption, and that the magnitude of this discrepancy increases with the magnitude of the offtakes.
To enable further analysis of the observed differences, Figure 1.2 shows the change in TSFC predicted by both models at a constant thrust of 20 kN as a function of the magnitude of the power offtakes. The chosen thrust level of 20 kN corresponds to the average cruise thrust of the baseline aircraft.

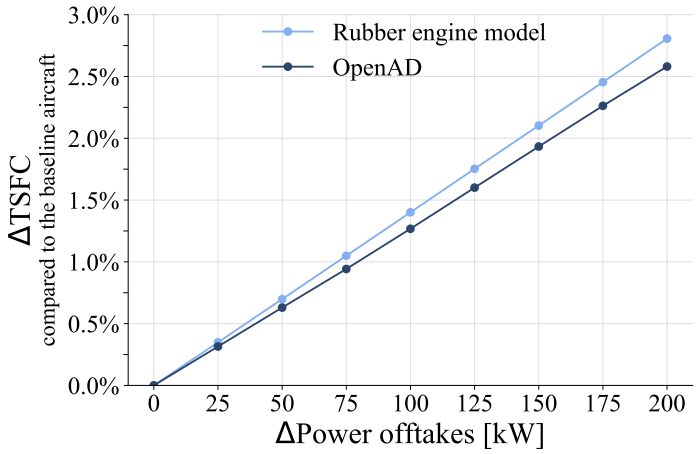

Figure 1.2: TSFC as a function of additional power off-takes predicted by OpenAD and the rubber engine model at FL370 and a thrust level of 20 kN

Figure 1.2 confirms the earlier observation that the discrepancy between the predictions of the two models increases with the magnitude of the power offtakes. However, even at the maximum considered offtake level of 250 kW, the observed difference is only 0.2%.
Given these observations and the marginal discrepancy between the models at the relevant thrust levels, it was concluded that the engine model implemented in OpenAD was sufficiently precise for capturing the effects of increased power off-takes. Consequently, no additional modifications or calibrations were deemed necessary for its use in subsequent calculations. This approach was further justified when the additional power off-takes calculated for all HLFC subsystems were found to be less than 50 kW, where the observed difference in predictions of the two models remains below 0.1%.

1.2. Varification of the HLFC system sizing tool

To verify the implementation of the methodology for calculating the HLFC system's mass and power off-takes within the HLFC system sizing tool, the calculations performed by Krishnan et al. [7], who utilized the same methodology, were replicated. In their work, Krishnan et al. [7] investigated five different architectures for an HLFC subsystem for the VTP of Airbus A320. As previously mentioned, the DLR-F25 featured a VTP of identical geometry to the one of Airbus A320, rendering the results obtained by Krishnan et al. [7] particularly relevant and feasible for replication in this work.
The verification process was executed in two stages. In the initial stage, the system architecture number 1 was modeled based on the the information provided in [7]. This architecture was utilized by Krishnan et al. [7] in his work to determine the pressure ratio to be delivered by the compressor and the overall system power requirements. Krishnan et al. [7] performed this calculation for four different flight levels, using readily available suction performance parameters (air mass flow and plenum pressure), and presented the results, together with numerous intermediate results for various parameters. These results were replicated here using the HLFC system sizing tool, with inputs including the architecture of the HLFC subsystem, the air mass flow, and the plenum pressure and temperature.
As an intermediate step, the lengths of the transfer and exhaust ducts were varied such as to match the pressure losses and the compressor pressure ratio at the design flight level FL310. This step was necessary because Krishnan et al. [7] does not provide details about the dimensions and properties of the individual system elements. Therefore, the system had to be initially modeled based purely on the notional pictures of the system given in [7] combined with the known dimensions of the VTP and the

knowledge of similar systems developed in previous studies for the VTP of Airbus A320. Varying the duct lengths therefore enabled the calibration of the model to account for pressure losses occurring both upstream and downstream of the compressor.
Subsequent to this calibration, the calculation was repeated for the remaining flight levels. The maximum discrepancy in the required power offtakes compared to the results obtained by Krishnan et al. [7] was 1%. The majority of the intermediate results corresponded to the values in [7] with a discrepancy of less than 0.1%. The most significant discrepancy of 9% was observed for the compressor pressure ratio at FL290. While this difference might appear large, the absolute difference was merely 0.11 (PR of 1.163 instead of 1.275 given in [7]), so the resulting power required still differed only by 1% from the value reported in [7]. With these results, Figure 11 from [7], showing the required suction power as function of flight altitude, could be recreated. The comparison is shown in Figure 1.3.

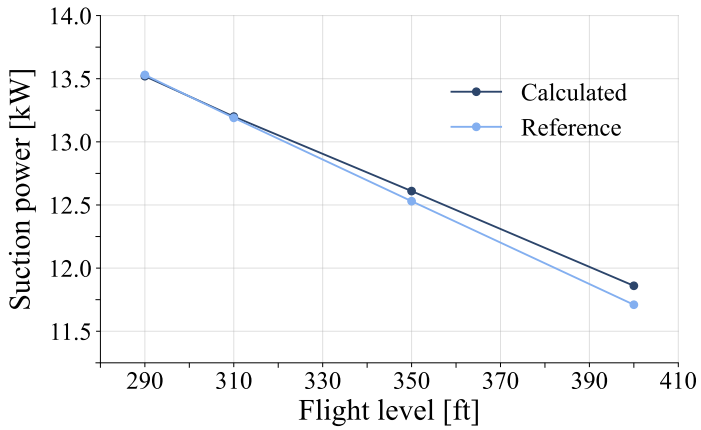

Figure 1.3: Comparison of calculated variation in suction power with altitude to values from Krishnan et al.[7]

Figure 1.3 shows that a good agreement was achieved between the values calculated by the HLFC system sizing tool and the values reported by Krishnan et al. [7]. The minor discrepancy that remained could be attributed to the residual uncertainty in the system dimensions, system architecture, as well as the underlying assumptions and methodological choices. The fact that the calculated and reference values coincide at FL310, with the difference increasing as the altitude deviates further from this level, is a consequence of the ducting length calibration performed for FL310. In hindsight, a more appropriate approach would have been to calibrate with respect to the power off-takes at the cruise altitude of FL350, as this flight level is closer to the cruise level FL370 later observed for the baseline aircraft. However, Figure 1.3 demonstrates that, even with calibration at FL310, the disparity between the obtained results and the reference value at FL370 remains negligible, with a magnitude of 0.2 kW or 0.1%.
The second stage of the verification process addressed the methodology for calculating the mass of HLFC systems and of their individual elements. For this purpose, the remaining four architectures defined by Krishnan et al. [7] were modeled. In developing these models, particular attention was paid to ensuring the consistency of the proportions of the systems, particularly of the duct lengths, with respect to the calibrated duct lengths previously obtained for architecture 1.
Given the absence of detailed data in [7], a number of assumptions had to be made when defining the individual elements. These included, but were not limited to, the utilized materials, the wire mass per unit length, the wall thicknesses of the ducting, and the structural design of the suction chambers (number of ribs, presence of a supporting structure behind the scuton sheet, etc.). The assumptions were made on the basis of prior knowledge of other HLFC systems developed in the past, similar assumptions made in previous studies, and engineering judgment.
The calculated masses of the complete architectures, as well as those of their constituent elements, were compared to the values reported by Krishnan et al. [7]. A visualization of this comparison is provided in Figure 1.4. Note that the sizing of all architectures was performed for altitude of FL310, consistent with the calculations conducted by Krishnan et al.[7].

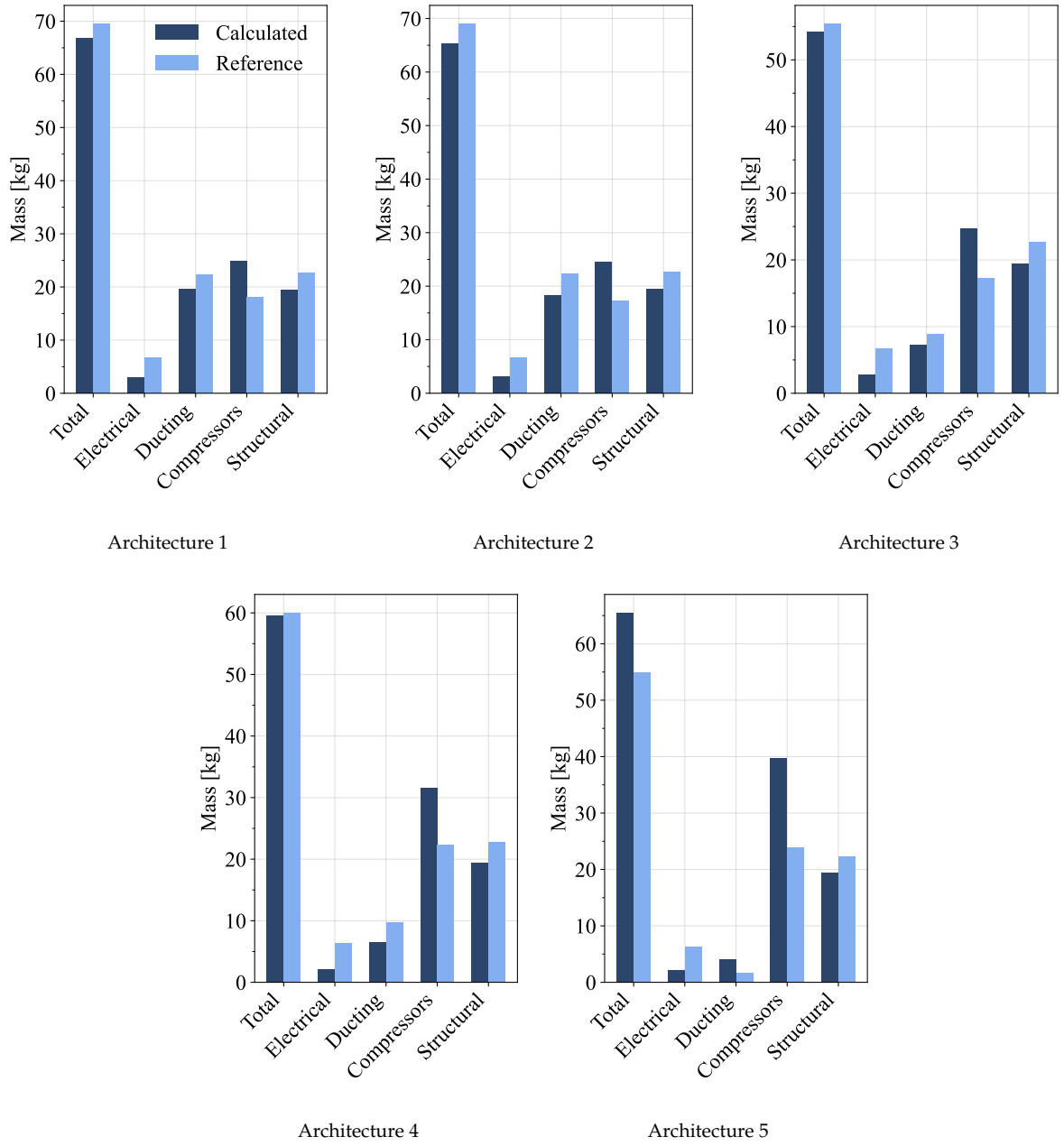

Figure 1.4: Comparison of calculated mass breakdowns for different HLFC system architectures to reference values from Krishnan et al.[7]

As apparent in Figure 1.4, it is evident that, despite the various assumptions and the associated uncertainty, the obtained results exhibited a remarkable agreement with those obtained by Krishnan et al. [7]. Most of the calculated system masses deviated by less than 4 kilograms from the values provided in [7]. The only exception was architecture number 5, where the system mass differed by 10 kilograms. However, within the context of aircraft design, such a minor difference in mass can be still considered negligible.

Figure 1.4 further demonstrates that the calculated distribution of masses across the individual elements were also consistent with the results obtained by Krishnan et al. [7]. However, a notable exception is observed for the compressors, mass of which the HLFC system sizing tool consistently overestimated. This discrepancy is likely due to the limitation of the HLFC sizing tool, which currently allows implementation of only axial compressors, while Krishnan et al. [7] utilized radial compressors in their designs. Furthermore, in their work, Krishnan et al. [7] included the mass of the electric motor drive

within the compressor mass, making it impossible to determine what proportion of this discrepancy is attributable to the compressor sizing and what proportion to the motor drive sizing.
The overestimation of the compressor (and motor) mass is also the primary factor contributing to the significant discrepancy in the mass of Architecture 5. This architecture incorporates three separate compressors, leading to an accumulation of the described error.
In the next step of the verification process, a calibration factor was calculated for each of the system elements (or groups of elements) shown in Figure 1.4. These factors were determined by dividing the individual masses reported for Architecture 1 in [7] by those calculated for the same architecture using the HLFC system sizing tool. The calculated masses of the elements for all architectures were then adjusted by multiplying them by these calibration factors. The calibrated results are presented in Figure 1.5.

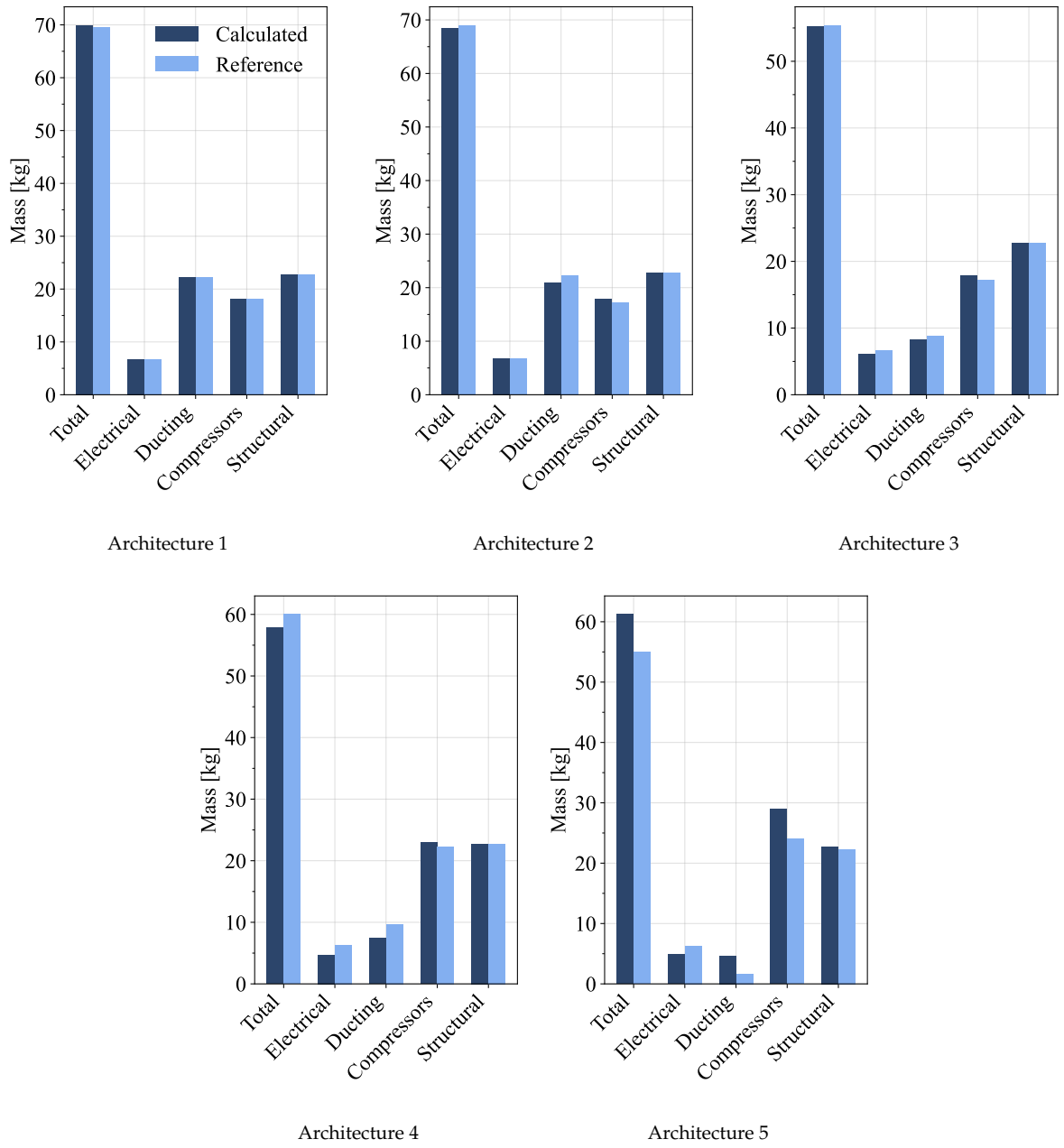

Figure 1.5: Comparison of calibrated mass breakdowns for different HLFC system architectures to reference values from Krishnan et al. [7]

As illustrated in Figure 1.5, the application of calibration factors led to further significant improvements in the agreement between the obtained results and those reported by Krishnan et al. [7]. Architecture 5 continued to show the most substantial difference, however, the magnitude of this difference was also reduced.
In light of these findings, the same calibration factors were employed in all HLFC system mass calculations in this study, with the exception of the factor for structural mass. The structural mass was calibrated by modeling an HLFC wing section prototype developed by DLR, described in detail in [54]. This calibration process involved adjusting the thickness of the carbon fiber support structure until the HLFC sizing tool produced a structural mass matching the value reported in [54].
It must be further noted that the HLFC system configuration for the VTP that was ultimately used in developing the laminar aircraft concept would correspond more accurately to Architecture 2, which also does not feature a transfer duct. Therefore, it would have been more appropriate to derive the calibration factors from Architecture 2 instead of Architecture 1, as was done here. However, the decision to not utilize the transfer duct was made after the verification process described in this chapter was carried out. Additionally, Figure 1.5 illustrates that the error introduced by calibrating the results with respect to Architecture 1 is negligible, as both architectures exhibit virtually identical masses.
Finally, Figure 1.6 presents the calculated variation in the mass of the compressor from Architecture 1, sized for different operational altitudes. The figure compares the values calculated before and after calibration with those obtained by Krishnan et al.[7].

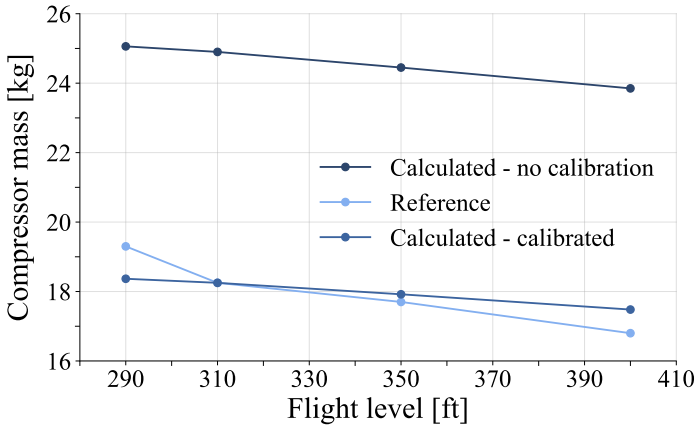

Figure 1.6: Comparison of calculated variation in compressor mass with altitude to values from Krishnan et al.[7]

Figure 1.6 illustrates the initial disparity in the compressor mass and the significant reduction of this error following calibration. Since these results were obtained for Architecture 1 with the ducting length calibrated for FL310, as discussed earlier, the calculated and reference values coincide at this altitude, with the disparity increasing as the flight altitude deviates further from the calibration point. However, even when the compressor was sized for the highest altitude of FL400, the mass was overestimated by less than 1 kg, or approximately 5% of the value reported by Krishnan et al. [7]. At FL370, the cruise altitude of the baseline aircraft, the difference is even smaller, approximately 0.5 kg or 3%.
In conclusion, this verification process demonstrated that the HLFC system sizing tool predicts the masses and power off-takes of HLFC systems with sufficient accuracy and can be reliably used for subsequent calculations.

References

[1] Hermann Schlichting and Klaus Gersten. *Boundary-Layer Theory*. 9th ed. Springer Berlin Heidelberg, 2017. ISBN: 9783662529195. DOI: 10.1007/978-3-662-52919-5.

[2] Roelof Vos and Saeed Farokhi. *Introduction to Transonic Aerodynamics*. Springer Netherlands, 2015. ISBN: 9789401797474. DOI: 10.1007/978-94-017-9747-4.

[3] Daniel P. Raymer. *Aircraft design: a conceptual approach. A conceptual approach*. Sixth edition. AIAA education series. Includes bibliographical references and index. Reston, VA: American Institute of Aeronautics and Astronautics, Inc., 2018. 1062 pp. ISBN: 9781624104909.

[4] John David Anderson. *Fundamentals of aerodynamics*. Sixth edition. McGraw-Hill series in aeronautical and aerospace engineering. Literaturverzeichnis Seite 1111-1116. New York, NY: McGraw-Hill Education, 2017. 1130 pp. ISBN: 9781259129919.

[5] Kristof Risse. "Preliminary overall aircraft design with hybrid laminar flow control". en. PhD Thesis. Technischen Hochschule Aachen, Aug. 2016, Diagramme(2016). DOI: 10.18154/RWTH-2017-00974.

[6] Albert L. Braslow. *A History of Suction-Type Laminar Flow Control with Emphasis on Flight Research*. Monographs in Aerospace History 13. 1999.

[7] Gopalakrishnan Kalarikovilagam Sri and Oliver Bertram. "Assessment of a Chamberless active HLFC system for the vertical tail plane of a mid-range transport aircraft". In: *Deutscher Luft- und Raumfahrtkongress 2017*. 2017. URL: https://elib.dlr.de/113848/.

[8] Bram van de Kamp, Markus Kleineberg, and Andreas Schroder. "Hybrid Laminar Flow Control ready for Series Application". Eng. In: *Aerospace Europe Conference 2023 – 10 EUCASS – 9 CEAS* (2023). DOI: 10.13009/EUCASS2023-647.

[9] T. M. Young, B. Humphreys, and J. P. Fielding. *Investigation of hybrid laminar flow control (HLFC) surfaces*. English. College of Aeronautics, Cranfield University, Cranfield, Beds, MK43OAL, United Kingdom, 2001. DOI: 10.1016/S1369-8869(01)00010-6. URL: https://www.scopus.com/inward/record.uri?eid=2-s2.0-0035355482%5C&doi=10.1016%5C%2fS1369-8869%5C%2801%5C%2900010-6%5C&partnerID=40%5C&md5=5fb0334c35f13817d47bcef52b1ce6b6.

[10] Ronald D. Joslin. *Overview of laminar flow control*. Technical Publication (TP) 19980232017. Langley Research Center, Oct. 1998.

[11] Long P. Yip Bruce J. Holmes Clifford J. Obara. *Natural Laminar Flow Experiments on Modern Airplane Surfaces*. Tech. rep. 2256. NASA, June 1984.

[12] C.-C. Rossow. "Aerodynamics - A discipline swept away?" In: *The Aeronautical Journal* 114.1160 (2010), pp. 599–609. ISSN: 0001-9240. DOI: 10.1017/S0001924000004085. URL: https://www.cambridge.org/core/product/996B3A7DCFD946F823B0AEB18190872B.

[13] Roelof Vos. *Lecture 5 - Pressure distribution about airfoils*. PowerPoint presentation. 2023.

[14] Nick Rogers Tom Gibson Bertrand Soucheleau. "BLADE - Natural Laminar Flow Flight Testing". In: *32nd Congress of the International Council of the Aeronautical Sciences (ICAS)*. Airbus. Sept. 2021.

[15] Géza Schrauf. "On Allowable Step Heights:Lessons Learned from the F100 and ATTAS Flight Tests". In: *6th European Conference on Computational Mechanics* (June 2018).

[16] Horstmann K. et al. "Flight tests with a natural laminar flow glove on a transport aircraft". In: Guidance, Navigation, and Control and Co-located Conferences 0. American Institute of Aeronautics and Astronautics, Sept. 1990. DOI: 10.2514/6.1990-3044. URL: https://doi.org/10.2514/6.1990-3044.

[17] N. Voogt. "Flight testing of a Fokker 100 test aircraft with laminar flow glove". In: *Verhandelingen Natuurkunde* 46 (1996), pp. 39–51. URL: https://dwc.knaw.nl/DL/publications/PU00011208.pdf.

[18] Arne Seitz and Karl-Heinz Horstmann. "Design Studies on NLF and HLFC Applications at DLR". In: *ICAS 2010*. Ed. by Ian Grant. Vol. 27. Conference Proceedings. International Council of the Aeronautical Sciences, Sept. 2010. URL: https://elib.dlr.de/78537/.

[19] Flying Staff. *Fuel Miser*. Online article. Visisted on 25.06.2024. Nov. 2021. URL: https://www.flyingmag.com/pilot-reports-turboprops-fuel-miser/.

[20] Michimasa Fujino. "Design and Development of the HondaJet". In: *Journal of Aircraft* 42.3 (May 2005), pp. 755–764. ISSN: 1533-3868. DOI: 10.2514/1.12268.

[21] Bill Read. "Going with the flow". In: *Royal Aeronautical Society* (Mar. 2021). Visited on 25.06.2024. URL: https://www.aerosociety.com/news/going-with-the-flow/.

[22] Peter Garrison. "The Design of the Celera 500L". In: *Flying Magazine* (2021). Visited on 25.06.2024. URL: https://www.flyingmag.com/technicalities-celera-500l-design/.

[23] Mega Ricos. *Piaggio Aerospace: P.180 Avanti EVO*. Online article. Visited on 26.06.2024. July 2019. URL: https://megaricos.com/2018/02/25/piaggio-aerospace-avanti-evo/.

[24] Niki Britton. *Honda Aircraft, pilots group stand behind HondaJet following runway excursions*. Online article. Visited on 24.06.2024. June 2023. URL: https://www.aopa.org/news-and-media/all-news/2023/june/22/honda-aircraft-pilots-group-stand-behind-hondajet-following-runway-excursions.

[25] Bill Cox. *Cessna 210: High Wing Cruiser*. Online article. Visited on 24.06.2024. Nov. 2015. URL: https://cessnaowner.org/cessna-210-high-wing-cruiser/.

[26] Steve Ells. *Cessna 210: King of the Singles*. Online article. Visited on 25.06.2024. URL: https://www.cessnaflyer.org/cessna-models/cessna-singles/cessna-210/cessna-210-king-of-the-singles.html.

[27] Leroy Cook. "The Marvelous Mooney". In: *Planes and Pilot* (Dec. 2021). Visited on 24.06.2024.

[28] Lancair. *Lancair Legacy History*. Online article. Visited on 25.06.2024. URL: https://lancair.com/lancair-legacy-history/.

[29] GlobalAir.com. *lancair Legacy - Technical specification*. Website. URL: https://www.globalair.com/aircraft-for-sale/specifications?specid=1663.

[30] Aircraft.com. *Mooney M20E Super 21*. Website. Visited on 24.06.2024. URL: https://www.aircraft.com/aircraft/219228295/n79808-1965-mooney-m20e-super-21.

[31] Martin Hepperle. *Turbulators*. Online article. Visited on 26.06.2024. May 2018. URL: https://www.mh-aerotools.de/airfoils/turbulat.htm.

[32] Snorri Gudmundsson. *General Aviation Aircraft Design - Applied Methods and Procedures*. Ed. by Joe Hayton. 1st. Boston: Butterworth-Heinemann, 2014. DOI: 10.1016/B978-0-12-397308-5.00001-5.

[33] Alexander Schleicher Segelflugzeugbau. *AS 33*. Website. Visited on 24.06.2024. URL: https://www.alexander-schleicher.de/en/flugzeuge/as-33/.

[34] Airbus. *European laminar flow research takes a new step with Airbus' BLADE Flight Lab*. Website. Visited on 24.06.2024. Sept. 2017. URL: https://www.airbus.com/en/newsroom/news/2017-09-european-laminar-flow-research-takes-a-new-step-with-airbus-blade-flight-lab.

[35] F. Collier Jr. "An overview of recent subsonic laminar flow control flight experiments". In: Fluid Dynamics and Co-located Conferences 0. American Institute of Aeronautics and Astronautics, July 1993. DOI: 10.2514/6.1993-2987. URL: https://doi.org/10.2514/6.1993-2987.

[36] Gopalakrishnan Kalarikovilagam Sri, Oliver Bertram, and Tobias Simon Ole Seibel. "Review of hybrid laminar flow control systems". In: *Progress in Aerospace Sciences* (July 2017). Ed. by Max Platzer. URL: https://elib.dlr.de/112799/.

[37] *High Reynolds Number Hybrid Laminar Flow Control (HLFC) Flight Experiment IV. Suction System Design and Manufacture*. Tech. rep. CR-1999-209326. Seattle, Washington: Boeing Commercial Airplane Group and NASA, Sept. 1999.

[38] Max Kingsley-Jones. *FARNBOROUGH: Aero secrets of Boeing's new Dreamliner*. Online article. Visited on 24.06.2024. July 2014. URL: https://www.flightglobal.com/farnborough-aero-secrets-of-boeings-new-dreamliner/113955.article.

[39] Rolf Henke. ""A 320 HLF Fin" flight tests completed". In: *Air & Space Europe* 1.2 (1999), pp. 76–79. ISSN: 1290-0958. DOI: 10.1016/S1290-0958(99)80019-7. URL: https://www.sciencedirect.com/science/article/pii/S1290095899800197.

[40] J.-P. Rosenblum. "An overview of flow control activities at Dassault Aviation over the last 25 years". In: *The Aeronautical Journal* 120.1225 (Mar. 2016), pp. 391–414. ISSN: 2059-6464. DOI: 10.1017/aer.2016.9.

[41] DLR. *Dornier DO 228-101 (D-CODE)*. Website. Visited on 25.06.2024. URL: https://www.dlr.de/en/research-and-transfer/research-infrastructure/dornier-228-101-en.

[42] Géza Schrauf and Heiko Frhr. von Geyr. "Simplified hybrid laminar flow control for transport aircraft". In: *ECCOMAS 2012 - European Congress on Computational Methods in Applied Sciences and Engineering, e-Book Full Papers* (Jan. 2012), pp. 3831–3842.

[43] Geza Schrauf and Heiko von Geyr. "Simplified Hybrid Laminar Flow Control for the A320 Fin Aerodynamic and System Design - First Results". In: *AIAA Scitech 2020 Forum*. Jan. 2020. URL: https://elib.dlr.de/133922/.

[44] Geza Schrauf and Heiko von Geyr. "Hybrid Laminar Flow Control on A320 Fin: Retrofit Design and Sample Results". In: *Journal of Aircraft* 58.6 (Nov. 2021), pp. 1272–1280. URL: https://elib.dlr.de/146436/.

[45] Matthias Horn, Arne SEITZ, and Marvin SCHNEIDER. "Novel tailored skin single duct concept for HLFC fin application". In: (2017). DOI: 10.13009/EUCASS2017-44.

[46] *High Reynolds Number Hybrid LaminarFlow Control (HLFC) Flight ExperimentIII. Leading Edge Design, Fabrication, and Installation*. Tech. rep. CR-1999-209325. Seattle, Washington: Boeing Commercial Airplane Group and NASA, Sept. 1999.

[47] T. M. Young and B. Humphreys. "Liquid anti-contamination systems for hybrid laminar flow control aircraft–a review of the critical issues and important experimental results". In: *Proceedings of the Institution of Mechanical Engineers, Part G: Journal of Aerospace Engineering* 218.4 (Apr. 2004), pp. 267–277. ISSN: 0954-4100. DOI: 10.1243/0954410041872825. URL: https://doi.org/10.1243/0954410041872825.

[48] Daniel Reckzeh. "Multifunctional wing moveables: Design of the A350XWB and the way to future concepts". In: *29th Congress of the International Council of the Aeronautical Sciences, ICAS 2014* (Jan. 2014).

[49] Kai Wicke and Volker Gollnick. "System analysis of aircraft with natural laminar flow and forward swept wings". In: *CEAS Aeronautical Journal* 7.2 (2016), pp. 259–274. ISSN: 1869-5590. DOI: 10.1007/s13272-016-0187-2. URL: https://doi.org/10.1007/s13272-016-0187-2.

[50] Yueping Guo, Casey L. Burley, and Russell H. Thomas. "Modeling and Prediction of Krueger Device Noise". In: Aeroacoustics Conferences 0. American Institute of Aeronautics and Astronautics, May 2016. DOI: 10.2514/6.2016-2957. URL: https://doi.org/10.2514/6.2016-2957.

[51] A. A. Pohya et al. "Cloud encounter impact on operational and economical effectiveness of hybrid-laminar-flow-control aircraft". English. In: vol. 56. 4. Air Transportation Systems-Air Transport Infrastructures and Operations, Hamburg University of Technology (TUHH), Blohmstr. 20, Hamburg, 21079, Germany: American Institute of Aeronautics and Astronautics Inc., 2019, pp. 1513–1523. DOI: 10.2514/1.C035205.

[52] W. H. Jasperson et al. "GASP cloud encounter statistics - Implications for laminar flow control flight". In: *Journal of Aircraft* 21.11 (Nov. 1984), pp. 851–857. ISSN: 0021-8669. DOI: 10.2514/3.45054. URL: https://doi.org/10.2514/3.45054.

[53] A. A. Pohya and K. Wicke. "An impact assessment of degrading elements on the overall benefit of aircraft with hybrid laminar flow control". English. In: German Aerospace Center (DLR), Institute of Maintenance, Repair and Overhaul, Department Product Lifecycle Management, Hein-Sa, ß, -Weg 24, Hamburg, 21129, Germany: American Institute of Aeronautics and Astronautics Inc, AIAA, 2019. DOI: 10.2514/6.2019-1589.

[54] Benjamin Fröhler et al. “Performance and Economic Assessment of a Wing-Integrated Hybrid Laminar Flow Control System”. In: *34th Congress of the International Council of the Aeronautical Sciences, ICAS 2024*. 2024.

[55] P. Catalano et al. “Performance Improvements of a Regional Aircraft by Riblets and Natural Laminar Flow”. In: *Journal of Aircraft* 57.1 (Jan. 2020), pp. 29–40. ISSN: 1533-3868. DOI: 10.2514/1.c035445.

[56] C. Atkin. *Performance trade-off studies for a retrofit Hybrid Laminar Flow Control System*. English. Future Systems and Technology Division, Küchemann Building, United States, 2004. URL: https://www.scopus.com/inward/record.uri?eid=2-s2.0-84897806480%5C&partnerID=40%5C&md5=8bcf4a7184b641d092ab2f8cde2e19b7.

[57] R.A.L. Wilson. “The Introduction of Laminar Flow to the Design and Optimisation of Transport Aircraft”. PhD Thesis. Mar. 1997. URL: https://books.google.de/books?id=u66D0AEACAAJ.

[58] Stanislav Karpuk, Rolf Radespiel, and Ali Elham. “Assessment of Future Airframe and Propulsion Technologies on Sustainability of Next-Generation Mid-Range Aircraft”. In: *Aerospace* 9.5 (May 2022), p. 279. ISSN: 2226-4310. DOI: 10.3390/aerospace9050279.

[59] Boeing Comercial Airplane Company. *Natural laminar flow airfoil analysis and trade studies*. Tech. rep. 19820007145. Seattle, WA, USA: Boeing Comercial Airplane Company, May 1979.

[60] Zhouwei Fan et al. “Benefit Assessment of Low-Sweep Transonic Natural Laminar Flow Wing for Commercial Aircraft”. In: *Journal of Aircraft* 58.6 (May 2021), pp. 1294–1301. ISSN: 0021-8669. DOI: 10.2514/1.C036138. URL: https://doi.org/10.2514/1.C036138.

[61] John D. Vachal Robert M. Kulfan. *Application of Laminar Flow Control to Large Subsonic Military Transport Airplanes*. Tech. rep. AFFDL-TR.77-6 5. Seattle , Washington 98124: Boeing CommercialAirplane Company, July 1977.

[62] Gopalakrishnan Kalarikovilagam Sri and Oliver Bertram. “Preliminary Design and System Considerations for an Active Hybrid Laminar Flow Control System”. In: *Aerospace*. Special Issue "Aeronautical Systems for Flow Control" 6.10 (Oct. 2019). Ed. by Michael Sinapius and Rolf Radespiel. URL: https://elib.dlr.de/129642/.

[63] Aerocorner.com. *Bombardier CRJ 1000*. Online article. Visited on 08.07.2024. URL: https://aerocorner.com/aircraft/bombardier-crj-1000/.

[64] Werner Pfenninger. “Long-range LFC Transport”. In: *Research in Natural Laminar Flow and Laminar-Flow Control, Part 1*. 90-12508. NASA, Langley Research Center. Sept. 1987.

[65] M. Kruse, T. Wunderlich, and L. Heinrich. *A conceptual study of a transonic NLF transport aircraft with forward swept wings*. English. DLR Institute of Aerodynamics and Flow Technology, 38108 Braunschweig, Lilienthalplatz 7, Germany, 2012. DOI: 10.2514/6.2012-3208. URL: https://www.scopus.com/inward/record.uri?eid=2-s2.0-84878559661%5C&doi=10.2514%5C%2f6.2012-3208%5C&partnerID=40%5C&md5=3d1ad05ccb4c4d06c77271700d7fb15d.

[66] A. Seitz, A. Hübner, and K. Risse. *The DLR TuLam project: design of a short and medium range transport aircraft with forward swept NLF wing*. English. DLR (German Aerospace Center), Institute of Aerodynamics and Flow Technology, Lilienthalplatz 7, Brunswick, 38108, Germany, 2020. DOI: 10.1007/s13272-019-00421-1. URL: https://www.scopus.com/inward/record.uri?eid=2-s2.0-85073943417%5C&doi=10.1007%5C%2fs13272-019-00421-1%5C&partnerID=40%5C&md5=26a05462c144abc467b5094b34cc40d6.

[67] Jia Xu and Ilan Kroo. “Aircraft Design with Active Load Alleviation and Natural Laminar Flow”. In: *Journal of Aircraft* 51.5 (Sept. 2014), pp. 1532–1545. ISSN: 1533-3868. DOI: 10.2514/1.c032402.

[68] Lucas Kugler. “Design and Assessment of TransonicTruss-Braced Wing Aircraft Concepts”. MA thesis. Universität Stuttgart, Oct. 2023.

[69] FlightGlobal Jon Hemmerdinger. *PICTURE: Boeing unveils trussed wing capable of jet speeds*. Online article. Jan. 2019. URL: https://www.flightglobal.com/airframers/picture-boeing-unveils-trussed-wing-capable-of-jet-speeds/130914.article.

[70] Ohad Gur, † Schetz, and William Mason. “Aerodynamic Considerations in the Design of Truss-Braced-Wing Aircraft”. In: *Journal of Aircraft* 48 (May 2011), pp. 919–939. DOI: 10.2514/1.C031171.

[71] J. Grasmeyer et al. “Multidisciplinary Design Optimization of a Strut-Braced Wing Aircraft with Tip-Mounted Engines”. In: (Jan. 1998).

[72] Géza Schrauf. “Status and perspectives of laminar flow”. In: *Aeronautical Journal* 109 (Dec. 2005), pp. 639–644. DOI: 10.1017/S000192400000097X.

[73] Bruce Holmes et al. “Flight research on natural laminar flow applications”. In: (Dec. 1986).

[74] Ronald D. Joslin. “AIRCRAFT LAMINAR FLOW CONTROL”. In: *Annual Review of Fluid Mechanics* 30.1 (Jan. 1998), pp. 1–29. ISSN: 1545-4479. DOI: 10.1146/annurev.fluid.30.1.1.

[75] T. M. Young. “An investigation into potential fuel savings for 110-130 seat passenger transport aircraft due to the incorporation of natural laminar flow or hybrid laminar flow control on the engine nacelles”. English. In: *Proceedings of the Institution of Mechanical Engineers, Part G: Journal of Aerospace Engineering* 227.8 (2013), pp. 1300–1324. ISSN: 20413025 (ISSN). DOI: 10.1177/0954410012454812. URL: https://www.scopus.com/inward/record.uri?eid=2-s2.0-84883711523%5C&doi=10.1177%5C%2f0954410012454812%5C&partnerID=40%5C&md5=4fff713a7d32f59fad6fc74662b2efbd.

[76] Eric Allison et al. *Aircraft conceptual design with natural laminar flow*. Sept. 2010.

[77] Yuandong Zhao, Haixin Chen, and Yufei Zhang. *An Aircraft Conceptual Design and Optimization Platform and Its Application for Nature Laminar Flow Aircraft Study*. Jan. 2015. DOI: 10.2514/6.2015-0516.

[78] T. Chiba and K. Rinoie. “Integrated conceptual design method considering advanced aircraft systems and aircraft trajectory”. English. In: University of Tokyo, Tokyo, 113-8656, Japan: International Council of the Aeronautical Sciences, 2016. URL: https://www.scopus.com/inward/record.uri?eid=2-s2.0-85013670980%5C&partnerID=40%5C&md5=e63252242ec8058bf7e04e9d96a3caf2.

[79] Tim Effing, Florian Schültke, and Eike Stumpf. “HLFC-optimized retrofit aircraft design of a medium-range reference configuration within the AVACON project”. In: *CEAS Aeronautical Journal* 12.2 (2021), pp. 441–456. ISSN: 1869-5590. DOI: 10.1007/s13272-021-00510-0. URL: https://doi.org/10.1007/s13272-021-00510-0.

[80] T. Effing et al. “Combined Application of Hybrid Laminar Flow Control and Variable Camber in Preliminary Aircraft Design”. English. In: vol. 1. Bauhaus Luftfahrt e.V., Willy-Messerschmitt-Str. 1, Taufkirchen, 82024, Germany: International Council of the Aeronautical Sciences, 2022, pp. 106–126. URL: https://www.scopus.com/inward/record.uri?eid=2-s2.0-85159616916%5C&partnerID=40%5C&md5=f0f365d966a99cc1352d97d935d2e0ff.

[81] T. M. Young. “Fuel sensitivity analyses for active drag reduction systems”. In: *The Aeronautical Journal* 108.1082 (Apr. 2004), pp. 215–221. ISSN: 2059-6464. DOI: 10.1017/s0001924000000129.

[82] F. Thielecke T.Pe. “Synthesis and Topology Study of HLFC System Architecturesin Preliminary Aircraft Design”. In: *3rd CEAS Air&Space Conference, 21st AIDAA Congress*. 2011.

[83] K. Risse and E. Stumpf. “Conceptual aircraft design with hybrid laminar flow control”. English. In: *CEAS Aeronautical Journal* 5.3 (2014), pp. 333–343. ISSN: 18695582 (ISSN). DOI: 10.1007/s13272-014-0111-6. URL: https://www.scopus.com/inward/record.uri?eid=2-s2.0-84921403820%5C&doi=10.1007%5C%2fs13272-014-0111-6%5C&partnerID=40%5C&md5=bf9d38e834b0f8ade1cd8d9907bafc87.

[84] Thomas S. Streit et al. “NLF Potential of Laminar Transonic Long Range Aircraft”. In: *AIAA Aviation 2020 Forum*. American Institute of Aeronautics and Astronautics, June 2020. DOI: 10.2514/6.2020-2748.

[85] P. C. Arcara, D. W. Bartlett, and L. A. McCullers. “Analysis for the Application of Hybrid Laminar Flow Control to a Long-Range Subsonic Transport Aircraft”. In: *SAE Technical Paper Series*. AEROTECH. SAE International, Sept. 1991. DOI: 10.4271/912113.

[86] Brandon Graver, Dan Rutherford, and Sola Zheng. *CO2 Emissions from Commercial Aviation - 2013, 2018, and 2019*. Tech. rep. The International Council on Clean Aviation, 2020.